205

205

Atmospheric Sciences Section
Illinois State Water Survey
Urbana, Illinois 61801

VARIATIONAL INITIALIZATION FOR AN INSTANCE OF STRONG CYCLOGENESIS

by

Gary L. Achtemeier

FINAL REPORT

Contract: NSF ATM76-16683
for
National Science Foundation

October 1978

Atmospheric Sciences Section
Illinois State Water Survey
Urbana, Illinois 61801

VARIATIONAL INITIALIZATION FOR AN INSTANCE OF STRONG CYCLOGENESIS

by

Gary L. Achtemeier

FINAL REPORT

Contract: NSF ATM76-16683
for
National Science Foundation

October 1978

TABLE OF CONTENTS

Page

ABSTRACT v

1. Introduction 1

2. A Variational Initialization Method 4

3. Case Description 15

4. Alternate Formulation for the Hydrostatic Constraint 23

5. Results: Convergence Test 25

   a. Satisfaction of Dynamical Constraints 27
   b. Adjustment Departures from Observed Fields 32

6. Results: Pattern Recognition 35

   a. Prefrontal Squall Line Vertical Motions 41
   b. Vertical Velocity Near the Major Cyclone 44

7. Results: Tendency Term Formulation 63

8. The Moisture Parameterization for Large Scale Stable Precipitation . 78

9. Additional Tests 83

   a. Reweighted Precision Moduli 83
   b. Specific Volume Correction 84

10. Vertical Velocity History for the Developing Storm: 00 GMT 12 April - 00 GMT 13 April 1964 84

11. Summary of the Performance of the Variational Model 94

APPENDIX: Variational Objective Analysis 96

1. Introduction 96

2. The Two Analysis Method 97

3. A Variational Method 104

4. Concluding Remarks 112

12. References 113

LIST OF FIGURES

Page

Figure 1. The smoothed surface topography that forms the lower boundary of the variational model. Heights are in departures from a reference value of 425 m 17

Figure 2. Sigma surface level meteorological partition pressures reduced to sea level. Date is 12 GMT 13 April 1964 19

Figure 3. 500 mb heights for 12 GMT 13 April 1964 20

Figure 4. Isotachs (m s^{-1}) and streamlines of the surface wind field. Date is 12 GMT 13 April 1964 21

Figure 5. Isotachs (m s^{-1}) of wind speed at 500 mb 12 GMT 13 April 1964 22

Figure 6. Map of analysis area showing positions of fronts, pressure centers, and precipitation for the 12 h period centered about 12 GMT 13 April 1964. Values in parentheses are for the 6 h period after 12 GMT; other values are for the 6 h period prior to 12 GMT 24

Figure 7. Areas (shaded) where the quasi-geostrophic approximation is violated in the tendencies of u, v, a. Date is 12 GMT 13 April 1964 26

Figure 8. Root mean square residuals for the five adjustable sigma levels as a function of cycle for the five constraints 28

Figure 9. Differences between the root mean square residuals for the adjusted minus observed fields and the standard error of observation for the energy equation at level 6 and cycle 7 .. 31

Figure 10. Differences between the root mean square residuals for the adjusted minus observed fields and the standard errors of observation for u, v, □ , a as a function of cycle 33

Figure 11. 500 mb vertical velocity (cm s^{-1}) from the Krishnamurti (1968) 12 forcing function balance omega equation solved on a 2.5 degree grid. Date is 12 GMT 13 April 1964 38

Figure 12. Sigma level 5 (455 mb) vertical velocity (cm s^{-1}) from the primitive equation constrained variational analysis. Date is 12 GMT 13 April 1964 40

Page

Figure 13. Map of analysis area showing positions of fronts, pressure centers, and precipitation for the 12 h period centered about 12 GMT 13 April 1964. Values in parentheses are for the 6 h period after 12 GMT; other values are for the 6 h period prior to 12 GMT 42

Figure 14. Vertical cross section of variational vertical velocity (cm s^{-1}) from the northern Gulf of Mexico to Nevada. Date is 12 GMT 13 April 1964 43

Figure 15. Vertical cross section of variational vertical velocity (cm s^{-1}) from the Gulf of Mexico along the cold front to the Minnesota low thence westward to Montana. The 12 h rainfall centered about 12 GMT 13 April 1964 along the cross section is also shown 45

Figure 16. Illustration of the convergence pattern surrounding a strong wind maximum (jet maximum) embedded within a mid level trough 48

Figure 17. Vertical velocity (cm s^{-1}) measured along the axis of a jet stream simulated by rotating tank experiments (from Reiter, 1961) 50

Figure 18. Illustration of magnitude and direction of vertical velocities along the axis of a jet stream that flows through a large scale ridge-trough pattern 51

Figure 19. Variational vertical motions along the axis of the mid tropospheric jet stream on 12 GMT 13 April 1964 52

Figure 20. Vertical velocity (dashed lines) in cm s^{-1} and horizontal velocity (solid lines) in m s^{-1} along a vertical cross section constructed from Montana to Ohio through the mid tropospheric jet stream 54

Figure 21. Same as in figure 20 except the cross section was constructed from Texas to Canada 55

Figure 22. Vertical velocity (dashed lines) in cm s^{-1} and relative humidity along a vertical cross section constructed along a line approximately 200 km ahead of the cold front from Minnesota to the Gulf of Mexico 58

Figure 23. Relative humidity at 750 mb for 12 GMT 13 April 1964 60

Figure 24. Relative humidity at 600 mb for 12 GMT 13 April 1964 61

Page

Figure 25. The level 5 $\partial v/\partial t$ Method 1 observed tendencies for 12 GMT 13 April 1964 70

Figure 26. The level 5 $\partial v/\partial t$ Method 1 variational tendencies for 12 GMT 13 April 1964 71

Figure 27. The level 5 $\partial v/\partial t$ Method 2 variational tendencies for 12 GMT 13 April 1964 75

Figure 28. The level 5 $\partial v/\partial t$ Method 3 variational tendencies for 12 GMT 13 April 1964 79

Figure 29. Sigma level 5 (455 mb) vertical velocity (cm s^{-1}) from the variational analysis with tendencies determined by Method 3 . 80

Figure 30. Summary of variational vertical velocity patterns, precipitation patterns (shaded) and the positions of low pressure centers and fronts for 00 GMT 12 April 1964 86

Figure 31. Same as in figure 29 except for 12 GMT 12 April 1964 88

Figure 32. Same as in figure 30 except for 00 GMT 13 April 1964 89

Figure 33. Fronts, pressure centers and 6 h rainfall for 00 GMT 13 April 1964 91

Figure 34. Fronts, pressure centers and 6 h rainfall for 06 GMT 13 April 1964 92

APPENDIX FIGURE CAPTIONS

Figure 1. a) SC streamlines and isotachs, b) SC divergence, c) SC vorticity, d) LI streamlines and isotachs, e) LI divergence, and f) LI vorticity for the St. Louis area at 1600 m MSL, 1600 CST, 26 July 1973. Units are m sec^{-1} for isotachs and 10^{-6} sec^{-1} for divergence and vorticity 102

Figure 2. Distribution of the space function g(x,y) that weighted the SC and LI methods in the variational analysis 109

Figure 3. The variational analysis: a) streamlines and isotachs, b) SC minus variational u-component, c) divergence, and d) vorticity for the case of figure 1. Units are m sec^{-1} for wind speed and 10^{-6} sec^{-1} for divergence and vorticity 110

VARIATIONAL INITIALIZATION FOR AN INSTANCE OF STRONG CYCLOGENESIS

Gary L. Achtemeier

ABSTRACT

This report presents the results of the application of the Achtemeier (1975) variational initialization model to an instance of strong cyclogenesis on 12-13 April 1964. Three important problem areas addressed were: 1) Would the model converge to a solution under conditions of rapid cyclogenesis that would cause the quasi-geostrophic approximation to be invalidated over large areas? 2) Would the model detect net vertical mass transports associated with convective subsynoptic and mesoscale weather systems? 3) How does the tendency term subsidiary variational formulation influence the final outcome of the variational fields?

The answers to the first two questions were very encouraging. With one exception, the rms residuals for the constraining equations either decreased to truncation levels or stabilized after significant residual decreases. The variational method resolved vertical motions associated with a strong prefrontal squall line and with the mid-tropospheric jet stream.

The answer to the third question was not encouraging. The subsidiary tendency term formulations that gave realistic vertical motion fields also gave unrealistically large tendencies. The formulation that gave smaller tendencies also gave physically unrealistic vertical motion fields. Further investigation is necessary to determine why these problems persist and whether they are symptomatic of uncorrectible flaws in the variational model.

1. Introduction

The guiding principle that has stimulated developments in numerical weather prediction is that the atmosphere is a deterministic system governed by macroscale physical laws. As a consequence, much effort has been expended on the development of mathematical models of the atmosphere and the associated initial and boundary conditions. Larger and faster computing systems have made possible the routine and research multi-level primitive equation models that include the complex physics of various boundary layer, cumulus scale, precipitation and radiative interactions. However, the ability to describe complex physical processes has not led to fully accurate forecasts.

The need for increased forecast accuracy has stimulated investigations directed toward improving the methods of model initialization. One general approach has been to find improved observational techniques and/or objective analyses with the view that a more accurate presentation of the state of the atmosphere will lead to increasingly accurate forecasts. This method, based on the principle of determinism, finds support in studies of the error growth and predictability of the atmosphere for various time scales. Lorenz (1969) showed that small differences between two analogous atmospheric systems at one time can lead to large differences at later times.

Another approach involves treating initialization consistently within the physical and mathematical framework of the model to be utilized for integration. The initial state for a crude model may not be a very accurate reproduction of the actual state of the atmosphere. However, as the model physics are improved, the model initial state should converge toward the optimal analysis of the observations. The extent to which this convergence occurs is not yet fully known.

The building of an initial state by forcing a compatibility with the model dynamical equations is known as dynamic initialization. Most dynamic initialization schemes involve the cyclic forward and backward integration of the model equations about the initial time to force the variables into a mutual balance and to use the differencing scheme to selectively damp out unwanted high frequency oscillations. Introduced into numerical weather prediction by Miyakoda and Moyer (1968) and Nitta and Hovermale (1969), dynamic initialization has been widely used because of its simplicity. The model equations in their finite difference forms are already available for use. The method is also flexibile. It is possible, if desired, to force the wind field to adjust to the mass field by restoring the mass field after each iteration or vice versa. One can also leave the variables to adjust freely.

The dynamic initialization method also has some disadvantages. In general, many iterations are necessary to obtain a satisfactory balance. A scheme proposed by Okamura (Nitta, 1969) has helped speed convergence. The removal of internal gravity waves by a dynamic initialization scheme or by any damping scheme is difficult, because some internal gravity waves have frequencies very close to Rossby wave frequencies (Temperton, 1976). Further, the forward-backward integration principle becomes dubious when irreversible processes such as diffusion and friction are incorporated into the models. Finally, forced adjustment with a certain variable imples that that variable has been correctly observed and gridded. Temperton (1976) shows that mutual adjustment is generally preferred to forced adjustment. However, there is often little control over how the observed fields are to be mutually adjusted. Methods to provide greater control over the mutual adjustment include "nudging" (Hoke and Anthes, 1976) and variational matching (Sasaki, 1958).

Several comparative forecast studies involving different initializations are still inconclusive but indicate that the forecasts may be insensitive to the method of initialization. The presence or absence of divergent meteorological and inertial modes seems to have little impact on the quality of the forecasts (Houghton et al., 1971; Dey and McPherson, 1977; Temperton, 1976) at least for hemispheric and global models. However, similar insensitivity was reported for a fine-mesh limited-area model (Temperton, 1976).

Most of these forecast comparisons were made with "model data" extracted from the numerical models at a period well into a long range forecast when gravitational energies had dissipated. This approach has been criticized by Hayden (1973) who has found that dynamic initialization with real data were not as promising as experiments with model data.

Although the inclusion of divergent modes in numerical models that predict large scale motions has not had much impact on forecast accuracy, there is reason for concern that neglect of divergent modes when they are the same order of magnitude as nondivergent modes may degrade forecasts obtained from mesoscale numerical models (Kreitzberg, 1976). Here the mass field should be in mutual balance with the wind field initially. Hoke and Anthes (1976) found large errors when the wind field was forced to balance with the mass field. Warner (1976) has found that the mass field can be obtained from the wind field but the wind field is apparently unable to dissipate its errors through partitioning the error-energy into gravity-inertia modes in the dynamic adjustment process.

These problems demonstrate the need for a method that can provide the numerical models, particularly mesoscale numerical models, with initial fields that 1) satisfy the model equations and 2) are mutually balanced according to

the observation and analysis accuracies of each variable. It would appear that the variational method (Sasaki, 1958) is capable of accomplishing this.

2. A Variational Initialization Model

At present, the variational approach has not been widely received by modelers, as many are unfamiliar with the method. The method complicates initialization by increasing the number of equations to be solved; the increase being equal to the number of strong constraints. (The strong constraints are the model dynamic equations which are required to be satisfied exactly.) Further, the number of strong constraints permitted must be one fewer than the number of variables to be adjusted. This means that, unless some alternative method is found, one of the model equations may not be satisfied by the initial state. Achtemeier (1975) has presented a method to obtain variational balance for all equations of his primitive equation initialization model.

The variational approach to initialization may interface with numerical weather prediction models in several ways. First, the variational constraints may be written in exactly the same difference form as they appear in the prediction model. This insures that the model equations will be satisfied exactly. A second approach is to write the constraints in easier centered differences thereby treating the variational initialization as an objective analysis and to use dynamic initialization to obtain the final balance. It is presumed that if an objective analysis nearly satisfies the model equations, it will require less time for the dynamical initialization to converge to a divergent initial state. Further, the variational method makes optimum use of data from several sources. This tends to minimize errors and mis-analyses that could contaminate any one data set analyzed independently and would provide a "good" set of initial fields for the dynamical initialization step.

The second approach is used in this study. The variational model becomes an objective analysis model. The resulting constrained meteorological fields are investigated for mathematical and physical realism according to several prescribed criteria. These are 1) satisfaction of dynamical constraints, 2) extent of departure of adjusted from observed fields, and 3) physical realism as determined from pattern recognition techniques.

The Achtemeier (1975) variational model is derived from "strong constraint" variational formulas. The five primitive equations: the horizontal momentum equations sans friction terms the adiabatic energy equation, the hydrostatic equation and the continuity equation form the strong constraints which are to be satisfied exactly by modifying the observations in a least squares variational formulation. Diabatic effects are omitted as a matter of convenience. The solution method is a technique that incorporates previously adjusted fields into the nonlinear terms of the equations and cycles through the adjustment set to a specified convergence criteria. Explicit local tendencies are included through a subsidiary variational formulation that is easily included in the cycle's adjustment sequence.

The method was first applied to real data for an instance of cyclogenesis over the midwestern United States on 12 December 1965. The three criteria used to evaluate the adjusted initial fields were a) the extent of agreement with dynamical constraints, b) whether the minimum adjustment from the observed fields was within the range of estimates for observational error, and c) whether the adjusted synoptic patterns were realistic as could be judged from subjective pattern recognition.

The variational analysis satisfied the 3 criteria for the 12 December 1965 case. However, the case was characterized by very slow development, slow movement, and generally weak circulation patterns. It remained unclear whether

the variational method would perform well for an instance of intense cyclogenesis. Specifically, the major questions to be answered by the present study are:

1) Will the analysis converge to a solution if the Rossby number approaches or exceeds unity over large areas?

2) Can the variational method resolve the net mass vertical displacements associated with mesoscale weather systems?

3) How does the divergence-tendency term subsidiary variational formulation contribute to the final solution under conditions of rapid cyclogenesis?

Although formulated in detail in the 1975 paper, the general theory of the variational model is reproduced here to provide easy reference for the analysis aimed at answering the questions listed above.

The equations are written in contravariant form (Stephens, 1965) in the polar stereographic map-image frame. The vertical sigma coordinate varies with terrain in a manner similar to the development by Phillips (1957).

To simplify the theoretical development and to present relative weights accorded observations in an easier-to-interpret form, the dynamical constraints are non-dimensionalized and magnitudes of individual terms are expressed in powers of the Rossby and Froude numbers. Charney (1948, 1962), Phillips (1963), Ogura (1962), Haltiner (1968) and others have presented various extensions of quasi-geostrophic scale theory. Achtemeier (1972) extended scale theory to the equations of constraint expressed in sigma coordinates as specifically adapted to variational initialization. By this method, non-dimensionalized thermodynamic variables are partitioned into reference, terrain, and meteorological perturbation atmospheres and orders of magnitudes deduced. Separate treatment of the orographic contribution allowed determination of characteristic terrain scales consistent with quasi-geostrophic scale theory.

Once determined, the reference and terrain atmospheres were not altered. However, this explicitly required these partitions to be in mutual hydrostatic balance initially.

With the Coriolis and map scale parameters included in the form of a Taylor series, the constraining equations are truncated after the second order. These take the form:

$$M_1 = R_0 \left(\frac{\partial u}{\partial t} + u\frac{\partial u}{\partial x} + v\frac{\partial u}{\partial y} + \dot{\sigma}\frac{\partial u}{\partial \sigma}\right) - v(1 + R_2C_0 + R_2^2C_1) + (1 + R_2K)^2 \left[\frac{\partial}{\partial x}(\phi + \phi_T)\right.$$

$$\left. + \sigma(\alpha_r + R_1\alpha_T + R_0^2\alpha)\frac{\partial}{\partial x}(p_s + p_{sT})\right] + R_0R_2\varepsilon(v^2 - u^2) - 2R_0R_2\delta uv = 0, \quad (1)$$

$$M_2 = R_0 \left(\frac{\partial v}{\partial t} + u\frac{\partial v}{\partial x} + v\frac{\partial v}{\partial y} + \dot{\sigma}\frac{\partial v}{\partial \sigma}\right) + u(1 + R_2C_0 + R_2^2C_1) + (1 + R_2K)^2\left[\frac{\partial}{\partial y}(\phi + \phi_T)\right.$$

$$\left. + \sigma(\alpha_r + R_1\alpha_T + R_0^2\alpha)\frac{\partial}{\partial y}(p_s + p_{sT})\right] - R_0R_2\delta(v^2 - u^2) - 2R_0R_2\varepsilon uv = 0, \quad (2)$$

$$M_3 = R_0\left(\frac{\partial \alpha}{\partial t} + u\frac{\partial \alpha}{\partial x} + v\frac{\partial \alpha}{\partial y}\right) + R_1\left(u\frac{\partial \alpha_T}{\partial x} + v\frac{\partial \alpha_T}{\partial y}\right) - \dot{\sigma}\left[\sigma_\sigma - R_0\left(\frac{\partial \alpha}{\partial \sigma} + \alpha\frac{p_s - p_u}{\gamma p}\right)\right] +$$

$$R_0\frac{\sigma\alpha_r\omega_s}{\gamma p} + R_0R_2\frac{\sigma\alpha_T\omega_s}{\gamma p} = 0, \quad (3)$$

$$M_4 = \frac{\partial u}{\partial x} + \frac{\partial v}{\partial y} + \frac{\partial \dot{\sigma}}{\partial \sigma} + R_0^2\frac{\omega_s}{p_s - p_u} - 2R_2(\varepsilon u + \delta v) = 0, \quad (4)$$

$$M_5 = \frac{\partial \phi}{\partial \sigma} + \alpha_r p_s + \alpha(p_s - p_u) = 0. \quad (5)$$

The quantities u, v, a, ø are non-dimensionalized meteorological variables in standard notation and are of order unity. The $\dot{\sigma}$ is vertical velocity.[1]

---

[1] $\dot{\sigma}$ is treated as of order unity; however, the zero-order (R_0^0) approximation yields $\dot{\sigma}_0 = 0$ as per the geostrophic approximation.

Subscripts r, T, s refer to reference and terrain atmosphere partitions and surface quantities, respectively.

The following also hold:

f' = $f/f_0 = 1 + R_2C_0 + R_2^2C_1$, series expansion of Coriolis parameter

m' = $m/m_0 = 1 + R_0K$, series expansion of map scale factor

F = C^2/gH, Froude number

R_0 = C/f_0L, Rossby number

R_1 = $R_0^2/F\ hL/Hl$, "Rossby" number for the terrain atmosphere partition

f Coriolis parameter

f_0 constant Coriolis parameter (10^{-4} s^{-1})

L characteristic length scale (10^6 m)

H scale height for homogeneous atmosphere (10^4 m)

g gravitational acceleration at earth's surface (10 m s^{-2})

h characteristic terrain height scale (10^3 m)

φ characteristic terrain length scale (L/R_0)

C_0, C_1, K Taylor series expansions for Coriolis and map scale parameters (10)

ε,6 Map projection parameters (10^0) (Achtemeier, 1972)

γ = C_p/C_v, ratio of specific heats at constant pressure and volume

σ_σ static stability (10°)

σ = $(p-p_u)/(p_s-p_u)$, vertical coordinate (Phillips, 1957)

p_s surface pressure

p pressure at upper reference level

R_2 = 0.1

The observations to be modified are meshed with the dynamic constraints through a generalization of Sasaki's (1970a) variational formulation. The adjustment functional is

$$F = \int_t \int_v \{\Pi_1 (u-u^o)^2 + \Pi_1(v-v^o)^2 + \Pi_2(\dot{\sigma} - \dot{\sigma}^o)^2 + \Pi_3 (\alpha - \alpha^o)^2 + \Pi_4(\frac{\partial \phi}{\partial x} - \frac{\partial \phi^o}{\partial x})^2$$

$$+ \Pi_4 (\frac{\partial \phi}{\partial y} - \frac{\partial \phi}{\partial y})^2 + \Gamma M_4^2 + \lambda_1 M_1 + \lambda_2 M_2 + \lambda_3 M_3 + \lambda_4 M_5\} \, dVdt, \qquad (6)$$

where the weights, Π_i, $i = 1, 4$ are Gauss' precision moduli (Whittaker and Robinson, 1926). The "observed" quantities $(u^o, v^o, \alpha^o, \dot{\sigma}^o, \phi^o)$ to be adjusted enter in a least squares formulation and receive precision modulus weights according to their relative observation accuracies. Specific volume is obtained from temperature and pressure through the State equation. Vertical velocity is not observed, therefore in application, $\dot{\sigma}^o$ in the third term of the integrand of (6) is set equal to zero. This is tractable since synoptic scale vertical velocities are small (Charney, 1948). The geopotential gradient appears in the horizontal momentum equations. Therefore adjustments are preferred with respect to its gradient rather than its magnitude. Table 1 lists precision moduli and standard observation errors for wind components and height (Hovermale, 1962) and specific volume (Achtemeier, 1972) used for the five adjustable levels.

Strong constraints, to be satisfied exactly (to within truncation) are introduced through the Lagrangian multipliers, λ_i, $i = 1, 4$. The continuity equation (M_4) is chosen as a weak constraint in (6) because of the restriction that these be one strong constraint less than the number of variables to be adjusted. Thus, at this stage of the development of the variational model, there is no guarantee that the continuity equation will be satisfied by the final adjusted fields. The continuity equation will become a strong constraint

Table 1. Standard errors of observations and precision moduli weights used to obtain the primitive equation variational balance. All values are non-dimensionalized. To obtain wind error (m s^{-1}) and height error (m) multiply the σ_u by 10 and the σ_H by 100.

	Standard observation error			Precision moduli			
Level*	σ_u	σ_α	σ_H	$\Pi_1(u,v)$	$\Pi_2(\dot{\sigma})$	$\Pi_3(\alpha)$	$\Pi_4(\phi)$
2(829)	0.23	0.44	0.07	9.4	0.34	2.60	5.1
3(703)	0.28	0.45	0.08	6.4	0.23	2.50	3.9
4(577)	0.30	0.65	0.10	5.6	0.20	1.20	2.8
5(452)	0.33	1.04	0.12	4.6	0.17	0.46	1.5
6(325)	0.40	2.01	0.15	3.1	0.11	0.11	1.1

*Values in parentheses give approximate pressure level.

through the divergence-tendency term subsidiary variational formulation that follows.

Objectively modified meteorological variables (f_i) are determined by requiring the first variation on F to vanish. A necessary condition for the existence of a stationary set is that the functions are determined from the domain of admissible functions as solutions of the Euler-Lagrange equations,

$$- \frac{\partial}{\partial x_j} \left\{ \frac{\partial}{\partial \left[\frac{\partial f_i}{\partial x_j} \right]} \right\} + \frac{\partial I}{\partial f_i} = 0, \tag{7}$$

for each variable, i. The Lagrangian density I is the integrand of (6). Repeated indices, j, imply summation. That the Euler-Lagrange equations constitute a minimum is implied from the least squares formulation for the Lagrangian density and verified by the results.

Subjecting the integrand of (6) to the operations specified by (7) yields the variations on u, v, α, ϕ, $\dot{\sigma}$. These are:

$$2\Pi_1 (u - u^o) + \lambda_2(1 + R_2C_0 + R_2{}^2C_1) - 2\Gamma \frac{\partial M_4}{\partial x} + \{-4R_0\epsilon\Gamma M_4 - R_0(\frac{\partial \lambda_1}{\partial t} + u \frac{\partial \lambda_1}{\partial x}$$
$$+ v \frac{\partial \lambda_1}{\partial y} + \dot{\sigma}\frac{\partial \lambda_1}{\partial \sigma}) - R_0\lambda_1 (\frac{\partial u}{\partial x} + \frac{\partial v}{\partial y} + \frac{\partial \dot{\sigma}}{\partial \sigma}) + R_0(\lambda_1 \frac{\partial u}{\partial x} + \lambda_2\frac{\partial v}{\partial x} + \lambda_3 \frac{\partial \alpha}{\partial x})$$
$$+ R_1 \lambda_3 \frac{\partial \alpha_T}{\partial x} + \frac{2R_0{}^2}{m'} (-u\epsilon\lambda_1 - v\delta\lambda_1 + u\delta\lambda_2 - v\epsilon\lambda_2)\} = 0. \tag{8}$$

$$2\Pi_1 (v - v^o) - \lambda_1(1 + R_2C_0 + R_2{}^2C_1) - 2\Gamma \frac{\partial M_4}{\partial y} + \{-4R_0\delta\Gamma M_4 - R_0(\frac{\partial \lambda_2}{\partial t} + u\frac{\partial \lambda_2}{\partial x}$$
$$+ v\frac{\partial \lambda_2}{\partial y} + \dot{\sigma}\frac{\partial \lambda_2}{\partial \sigma}) - R_0\lambda_2 (\frac{\partial u}{\partial x} + \frac{\partial v}{\partial y} + \frac{\partial \dot{\sigma}}{\partial \sigma}) + R_0(\lambda_1\frac{\partial u}{\partial y} + \lambda_2 \frac{\partial v}{\partial y} + \lambda_3 \frac{\partial \alpha}{\partial y})$$
$$+ R_1\lambda_3 \frac{\partial \alpha_T}{\partial y} + \frac{2R_0{}^2}{m'} (v\epsilon\lambda_1 - u\delta\lambda_1 - v\delta\lambda_2 - u\epsilon\lambda_2)\} = 0, \tag{9}$$

$$2\Pi_2 (\dot{\sigma} - \dot{\sigma}^{\circ}) - \lambda_3 \sigma_{\sigma} - 2\Gamma \frac{\partial M_4}{\partial \sigma} + \{R_0(\lambda_1 \frac{\partial u}{\partial \sigma} + \lambda_2 \frac{\partial v}{\partial \sigma} + \lambda_3 \frac{\partial \alpha}{\partial \sigma} + \lambda_3 \alpha (\frac{p_s - p_u}{\gamma p})$$

$$\} = 0. \tag{10}$$

$$2\Pi_3 (\alpha - \alpha^{\circ}) + \lambda_4 (p_s - p_u) + \{-R_0(\frac{\partial \lambda_3}{\partial t} + u \frac{\partial \lambda_3}{\partial x} + v \frac{\partial \lambda_3}{\partial y} + \dot{\sigma} \frac{\partial \lambda_3}{\partial \sigma})$$

$$-R_0 \lambda_3 (\frac{\partial u}{\partial x} + \frac{\partial v}{\partial y} + \frac{\partial \dot{\sigma}}{\partial \sigma}) + \sigma m^2 R_0^2 [\lambda_1 \frac{\partial}{\partial x} (p_s + p_{sT}) + \lambda_2 \frac{\partial}{\partial y} (p_s + p_{sT})]$$

$$+ R_0 \lambda_3 \dot{\sigma} \frac{p_s - p_u}{\gamma p} \} = 0, \tag{11}$$

$$2\Pi_4 (\nabla^2 \phi - \nabla^2 \phi^{\circ}) + \frac{\partial \lambda_1}{\partial x} + \frac{\partial \lambda_2}{\partial y} + \frac{\partial \lambda_4}{\partial \sigma} + \{\frac{\partial}{\partial x} (m^2 - 1) \lambda_1 + \frac{\partial}{\partial y} (m^2 - 1) \lambda_2$$

$$\} = 0, \tag{12}$$

Variation on the multipliers restores the four strong constraints.

The Euler-Lagrange set comprises nine complicated nonlinear equations. Solutions are difficult to obtain by direct convectional methods. Therefore, an indirect iterative solution method is proposed whereby, at the first iteration level, terms multiplied by R_0, R_1, or R_2 are approximated by observed values and, at subsequent iterations, are approximated by previously adjusted variables. Then at any particular solution level these terms are specified and can be treated as forcing functions, F_i $(i = 1, 9)$. Following this argument (8) - (12) reduce to

$$\lambda_2 = -2\Pi_1 (u - u^{\circ}) + 2\Gamma \frac{\partial M_4}{\partial x} - F_1 \tag{13}$$

$$\lambda_1 = 2\Pi_1 (v - v^{\circ}) - 2\Gamma \frac{\partial M_4}{\partial y} + F_2 \tag{14}$$

$$\lambda_3 = \frac{1}{\sigma_\sigma}\left[2\Pi_2(\dot{\sigma} - \dot{\sigma}^o) - 2\Gamma\frac{\partial M_4}{\partial \sigma} + F_3\right] \tag{15}$$

$$\lambda_4 = \frac{1}{p_s - p_u}\left[-2\Pi_3(\alpha - \alpha^o) - F_4\right] \tag{16}$$

$$2\Pi_4(\nabla^2\phi - \nabla^2\phi^o) + \frac{\partial \lambda_1}{\partial x} + \frac{\partial \lambda_2}{\partial y} + \frac{\partial \lambda_4}{\partial \sigma} + F_5 = 0 \tag{17}$$

Similarly, the constraints become

$$v = \frac{\partial \phi}{\partial x} + F_6 \tag{18}$$

$$u = \frac{-\partial \phi}{\partial y} - F_7 \tag{19}$$

$$\dot{\sigma} = \frac{F_8}{\sigma_\sigma} \tag{20}$$

$$\alpha = \frac{1}{p_s - p_u}\left[-\frac{\partial \phi}{\partial \sigma} - F_9\right] \tag{21}$$

Now the nine nonlinear equations take the form of a closed set of simple algebraic or linear partial differential equations. Variables may be easily eliminated to reduce the number of equations. Equations (13), (14), and (18), (19) formulated as vorticity expressions are combined with (17) eliminating variables u, v, λ_1, λ_2. Equations (16) and (21) combined with (17) eliminate λ_4 and a leaving a three-dimensional second-order elliptic partial differential equation in Ø:

$$\nabla^2\phi + a_1\frac{\partial^2\phi}{\partial\sigma^2} + a_2\frac{\partial\phi}{\partial\sigma} + H = 0 \tag{22}$$

where, for ease of notation the symbols

$$a_1 = \frac{\Pi_3}{\Pi_1 + \Pi_4} \left(\frac{1}{p_s - p_u}\right)^2,$$

$$a_2 = \frac{1}{\Pi_1 + \Pi_4} \left(\frac{1}{p_s - p_u}\right)^2 \frac{\partial \Pi_3}{\partial \sigma}, \tag{23}$$

are introduced. Further,

$$H = \frac{1}{2(\Pi_1 + \Pi_4)} \left\{ 2\Pi_1 \left(\frac{\partial F_6}{\partial x} + \frac{\partial F_7}{\partial y}\right) - \frac{\partial F_1}{\partial y} + \frac{\partial F_2}{\partial x} + \Gamma_5 \right.$$

$$\left. + \frac{1}{p_s - p_u} \frac{\partial}{\partial \sigma} \left[-F_4 + \frac{2\Pi_3}{p_s - p_u} F_9\right] \right\} . \tag{24}$$

Achtemeier (1972) has shown convergence for (22) for the homogeneous case.

Equations (13) - (16) and (18) - (22) comprise the first stage or primary variational model. Once the forcing functions are evaluated the adjusted geopotential is obtained through (22). The variables u, v, $\dot{\sigma}$, α may be easily found from (18) - (21). Then the Lagrangian multiplier adjustments can be found through (13) - (17). Given the adjusted variables, the tendencies can be modified through the divergence-tendency term subsidiary variational formulation which will be discussed in relation to the tendency term analysis in Section 7.

Once new estimates for all dependent variables are available, the forcing functions must be recomputed and the cycles repeated as necessary until variables have stabilized or a prescribed set of convergence criteria have been met.

The observed geopotential provides the boundary conditions for (22). Prescribed boundary conditions are not necessary for the other variables. Where needed, boundary values are extrapolated (Achtemeier, 1975).

3. Case Description

An instance of intense cyclogenesis over the midwestern United States on 12-13 April 1964 was used to test the variational method. This case was analyzed by Krishnamurti (1968), Stuart and Krishnamurti (1970), and Stuart (1971). Their work provides a standard of pattern comparison for the variational model. The case, one of rapid cyclogenesis, is ideal for testing the convergence of the variational analysis and the contribution of the divergence-tendency term subsidiary formulation. Verification data such as observed 3 hour tendencies necessary to accurately assess the subsidiary formulation do not exist for this case. Nevertheless, given the 12 hour progression of synoptic events, it is possible to establish limits upon what can be considered as realistic for the tendencies. Finally, the 13 April 1964 case includes a large intense prefrontal squall line. The variational method's ability to resolve the net mass vertical displacements associated with mesoscale weather systems can be demonstrated. Thus, apart from some limitations in evaluating the subsidiary formulation, all 3 major questions can be addressed by the analysis of the 12-13 April 1964 case.

The data grid for this experiment was a 24 x 20 point regular mesh with a 190 km horizontal grid interval. The grid was bounded by the Sierra ranges on the west and the Atlantic coast on the east. The northern and southern boundaries were located through central Canada and along the United States-Mexican border, respectively. Vertical resolution was provided by 5 sigma

levels sandwiched between the 200 mb level and a smoothed surface topography shown in figure 1. The terrain heights are given as departures from a mean value of 425 m. Thus, the maximum height over western Colorado is more than 1600 m.

The data for this study consisted of rawinsonde observations of height, temperature, and relative humidity at significant pressure levels to 200 mb and winds at standard rawind height levels in meters. The data at significant levels was interpolated log-linearly in pressure to 50 mb pressure levels. The wind data was interpolated linearly in height to the 50 mb pressure levels. Then the observations were interpolated to points of the regular mesh by an objective analysis similar to the exponential method developed by Barnes (1964). Once at the grid points, data values were log-linearly interpolated directly to the sigma-surfaces. Variables were non-dimensionalized and the specific volume calculated.

The non-dimensionalized sigma-level data were partitioned into the reference, terrain, and meteorological variables (Achtemeier, 1972). The reference heights and pressures were obtained at each level by finding the average values at each level. Then the reference specific volume was found from the reference height and reference pressure through the hypsometric equation.

The first level terrain height is the height of the lower coordinate surface. The terrain specific volume for that level was obtained by linear interpolation from the reference specific volume profile. Then the terrain pressure was found from the hydrostatic equation. The terrain pressure at all levels was found from the definition of the sigma coordinate once the level 1 terrain pressure was known. Then the terrain height along the reference height

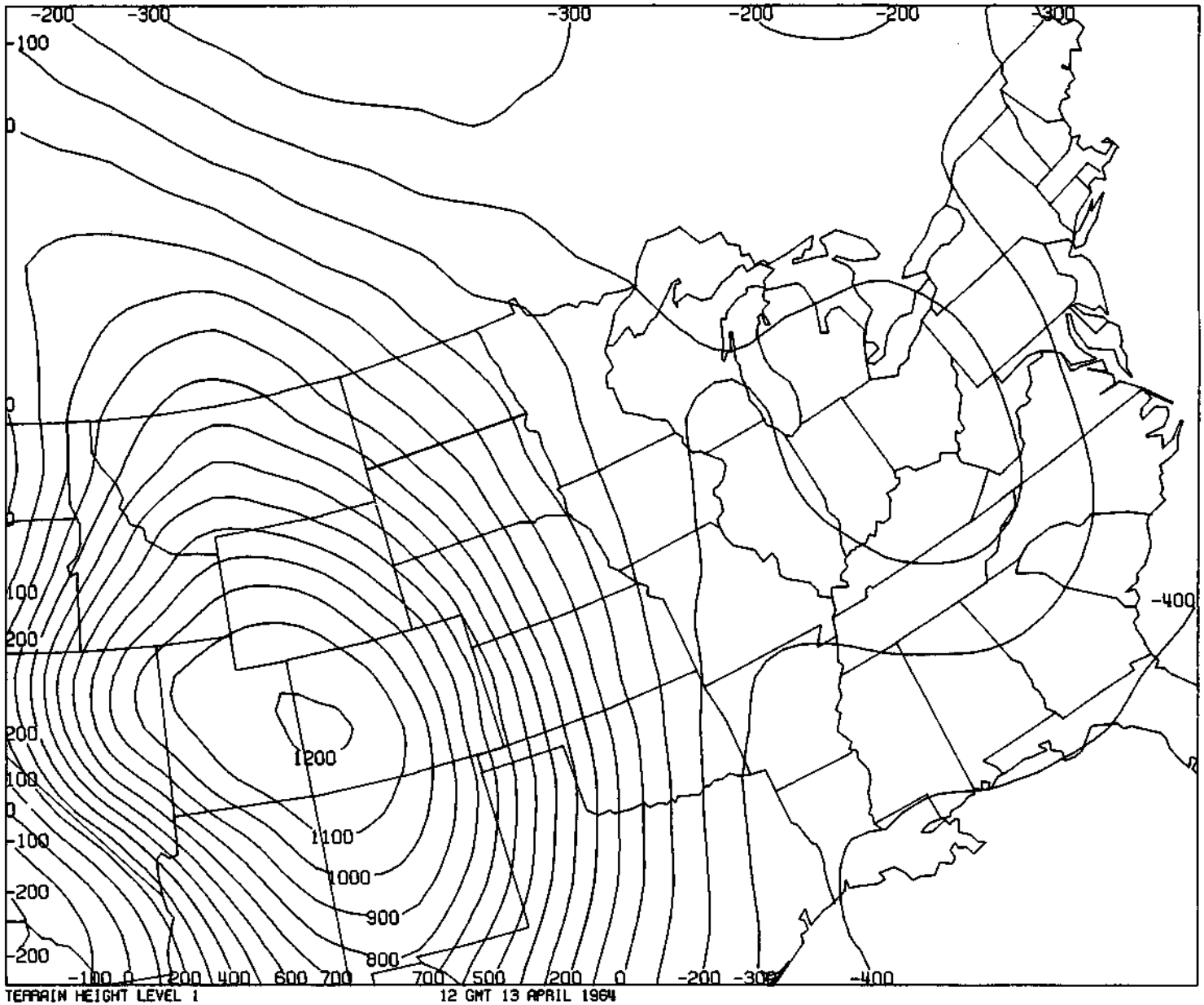

Figure 1. The smoothed surface topography that forms the lower boundary of the variational model. Heights are in departures from a reference value of 425 m.

profile was derived from log-linear interpolation. The terrain specific volume at the remaining levels was found from the hydrostatic equation.

The meteorological partition was computed as the residual between the total and the sum of the reference and terrain values.

Fronts and objectively analyzed sea level pressure patterns obtained from rawinsonde surface data for the 13 April 1964 storm are shown in figure 2. At 12 GMT 974 mb intense cyclone was located over Minnesota. This rapidly deepening low had moved northward from near the Nebraska-Iowa border, absorbed a weak disturbance in southern Canada, and by 12 GMT was drawing part of a strong Canadian airmass into its circulation. A polar cold front extended eastward from the storm center to Indiana and thence southwestward through the lower Mississippi valley region. A ridge of high pressure extended from Nevada into Texas. Detailed analyses with dense surface network data revealed that the ridge was interupted by a weak low pressure area located over eastern New Mexico. An intense prefrontal squall line produced copious amounts of precipitation from Kentucky to Louisiana.

The 500 mb height pattern (fig. 3) shows the surface low in the southeast quadrant of a deep long wave trough. A circulation center had developed over North Dakota.

Isotachs and streamlines of the surface windfield (fig. 4) show two areas of strong convergence: 1) strong inflow into the storm center over Minnesota and 2) strong convergence over Mississippi near the southern end of the prefrontal squall line. At 500 mb (fig. 5), a jet stream extended from Idaho through Kansas and northward from Missouri through Wisconsin and into Canada. Maximum winds that exceeded 30 m s^{-1} were found within the mid-level trough over Missouri.

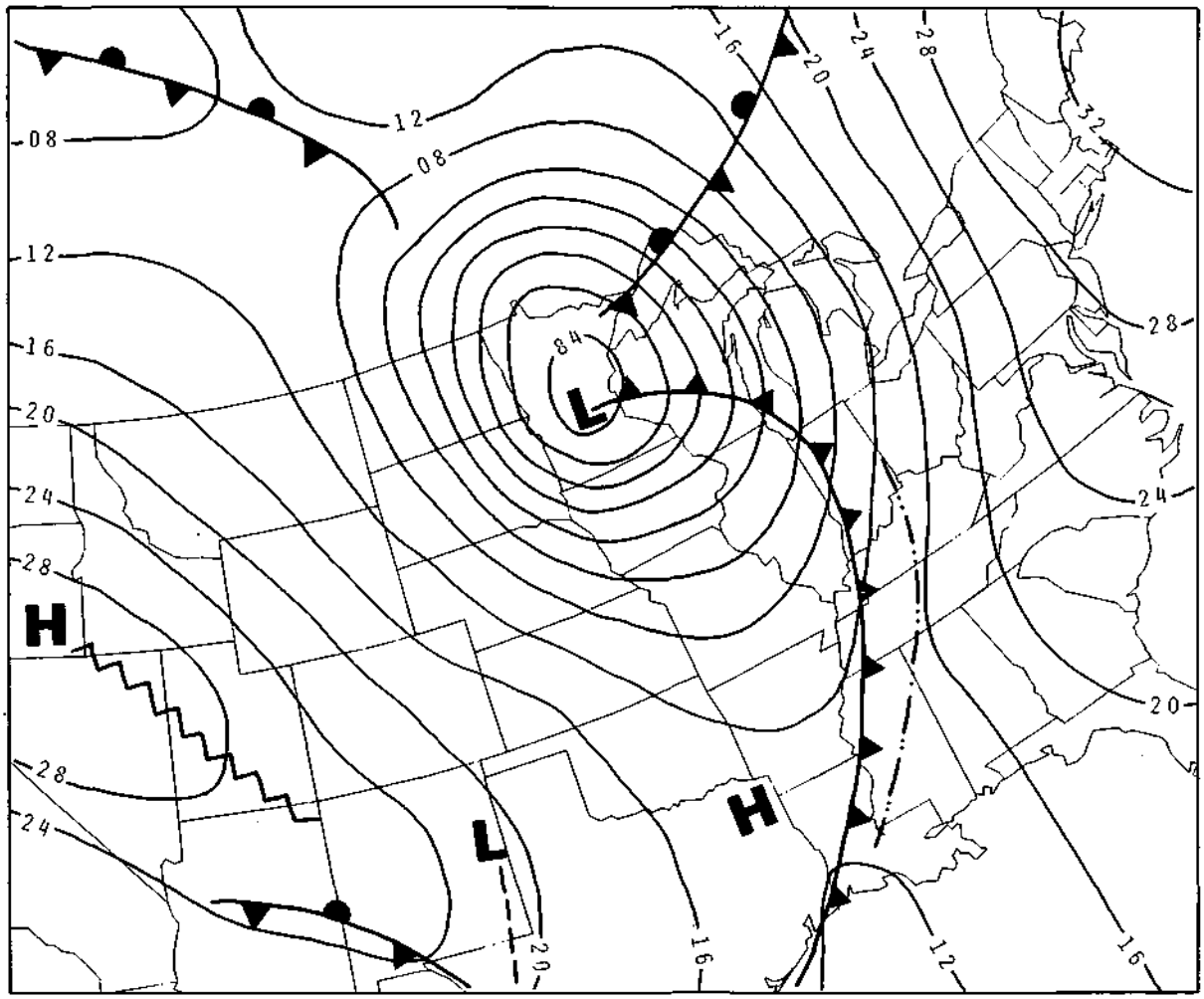

Figure 2. Sigma surface level meteorological partition pressures reduced to sea level. Date is 12 GMT 13 April 1964.

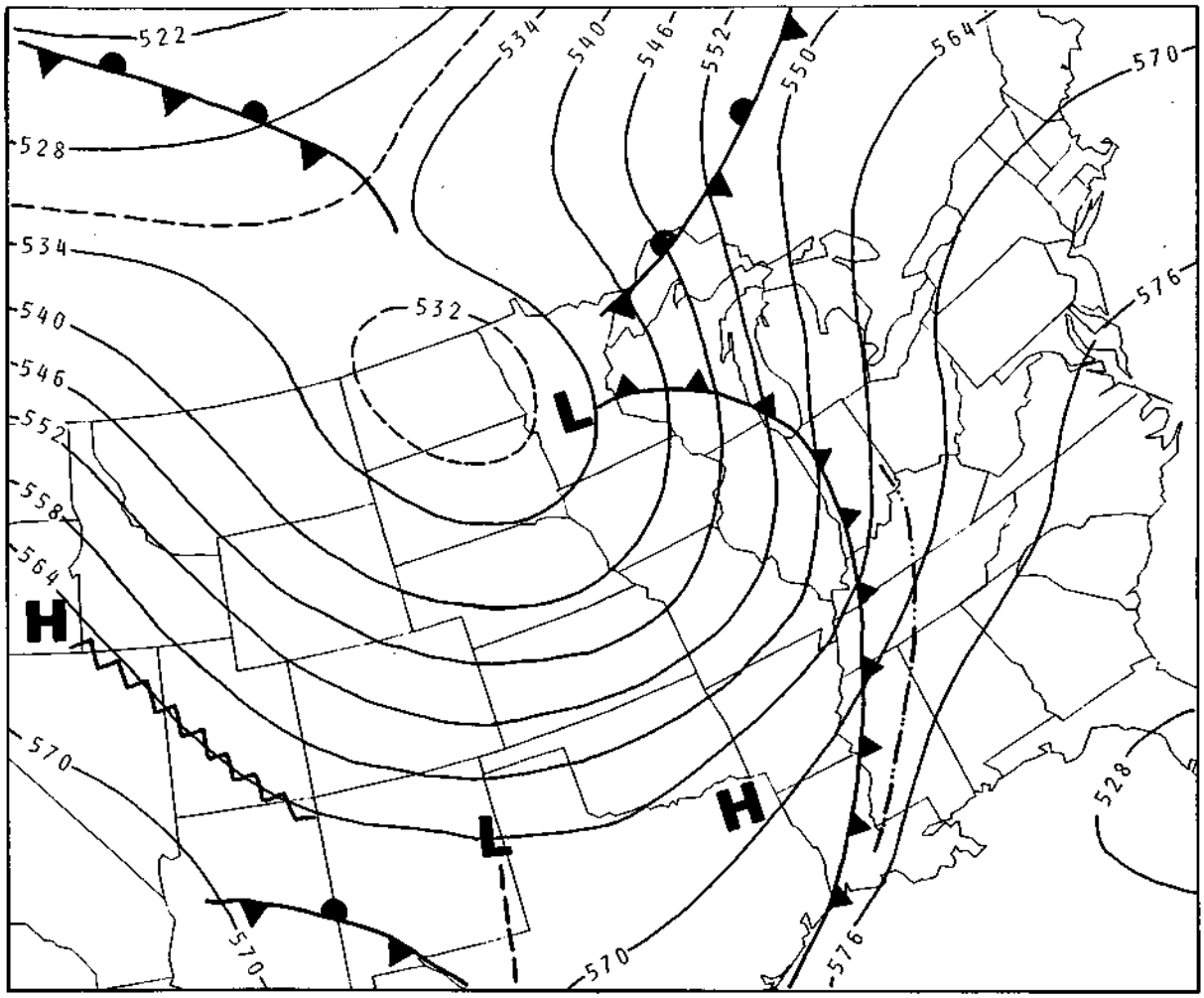

Figure 3. 500 mb heights for 12 GMT 13 April 1964.

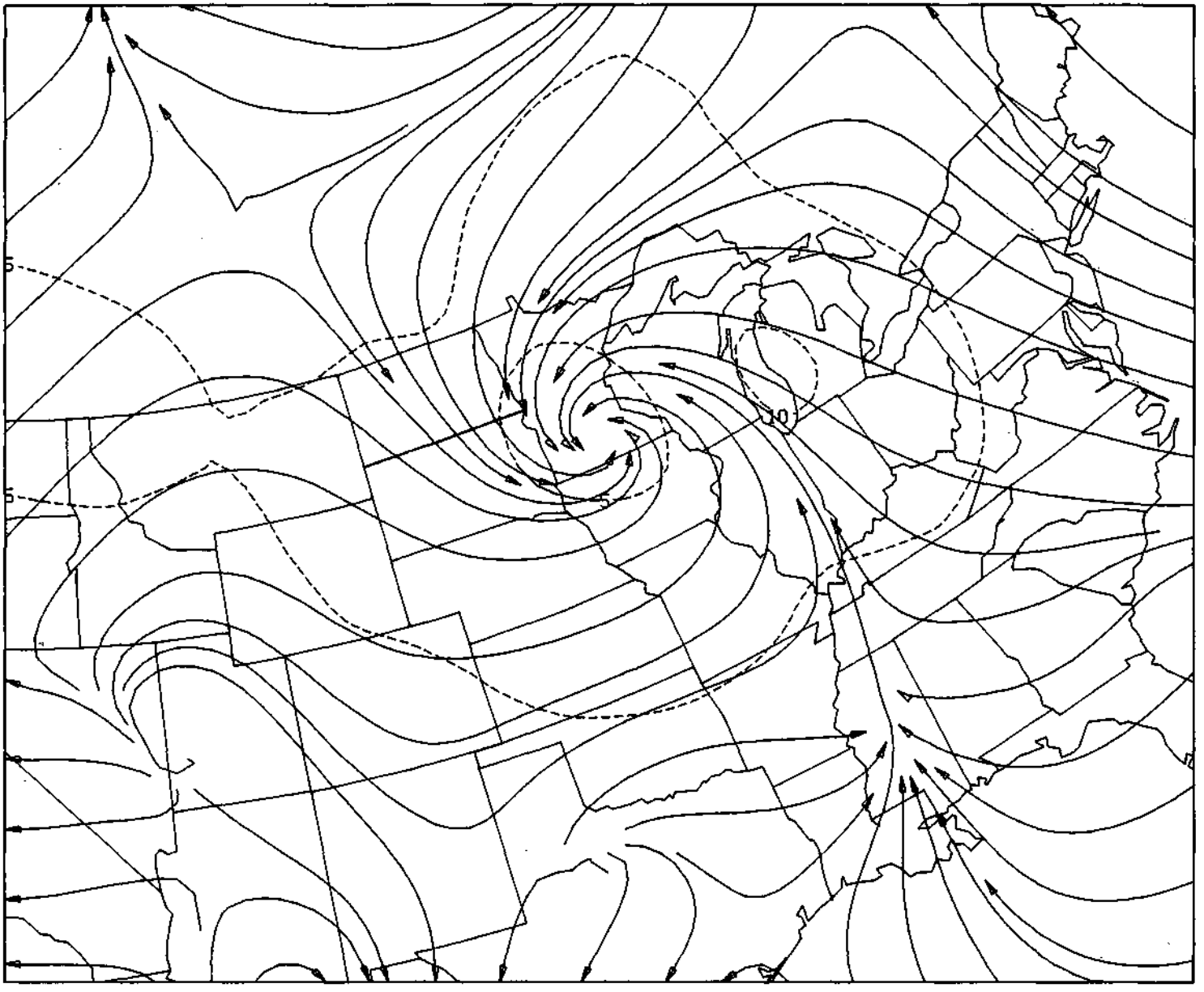

Figure 4. Isotachs (m s^{-1}) and streamlines of the surface wind field. Date is 12 GMT 13 April 1964.

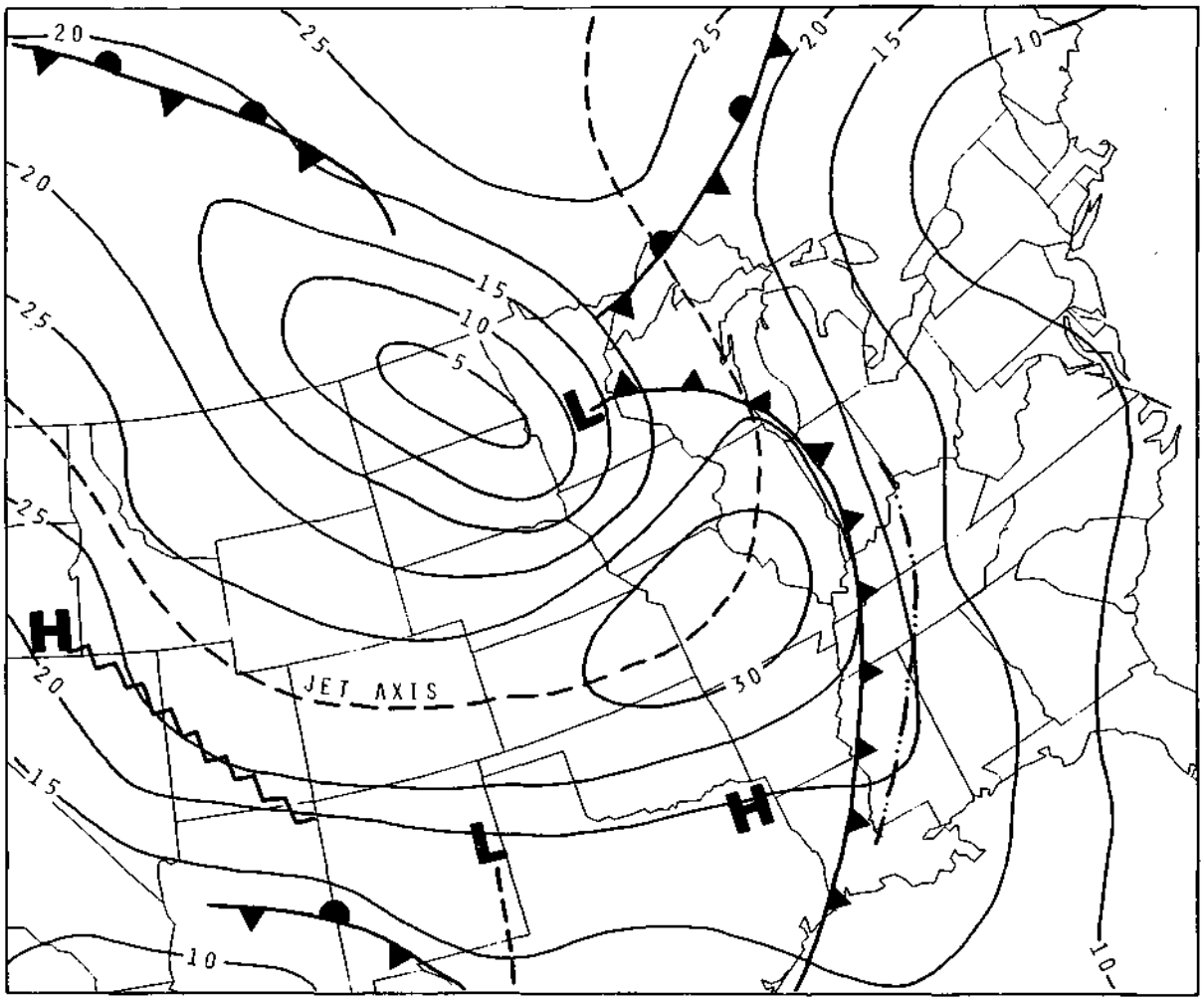

Figure 5. Isotachs (m s^{-1}) of wind speed at 500 mb 12 GMT 13 April 1964.

Figure 6 locates pressure centers, fronts, and precipitation distributions for 12 GMT 13 April 1964. There were two rainfall centers, one associated with the major cyclone over Minnesota and the other associated with a prefrontal squall line that extends from Kentucky to Louisiana. The rainfall centers are connected by a broad area of light rainfall with 12 hour amounts generally less than 0.10 inch.

4. Alternate Formulation for the Hydrostatic Constraint

The variational formulation calls for the mutual adjustment of observed variables subject to the satisfaction of a set of prescribed constraints, namely the primitive equations. One of these constraints is the hydrostatic equation which carries the balance between the specific volume and the geopotential height. There is some lack of initial independence between these two variables because the heights are deduced from pressures and temperatures in the reduction of raw rawinsonde data. The actual relationship between the pressure and height is log-linear as expressed by the hypsometric equation.

The hydrostatic equation is a valid pressure-height relationship only for shallow layers. The sigma-layers, separated by 125 mb, are hardly shallow layers. The variational adjustment for the case described by the 1975 paper included the hydrostatic equation directly. Why the use of this constraint did not cause a major misanalysis for that case is a mystery. An unacceptable analysis was obtained for the 13 April 1964 case.

The breakdown in the April case was quickly traced to the hydrostatic constraint which had forced anomalously warm temperatures into all levels, but particularly into the upper levels where the lapse rate changed from conditionally unstable to stable near the tropopause. These warm thickness

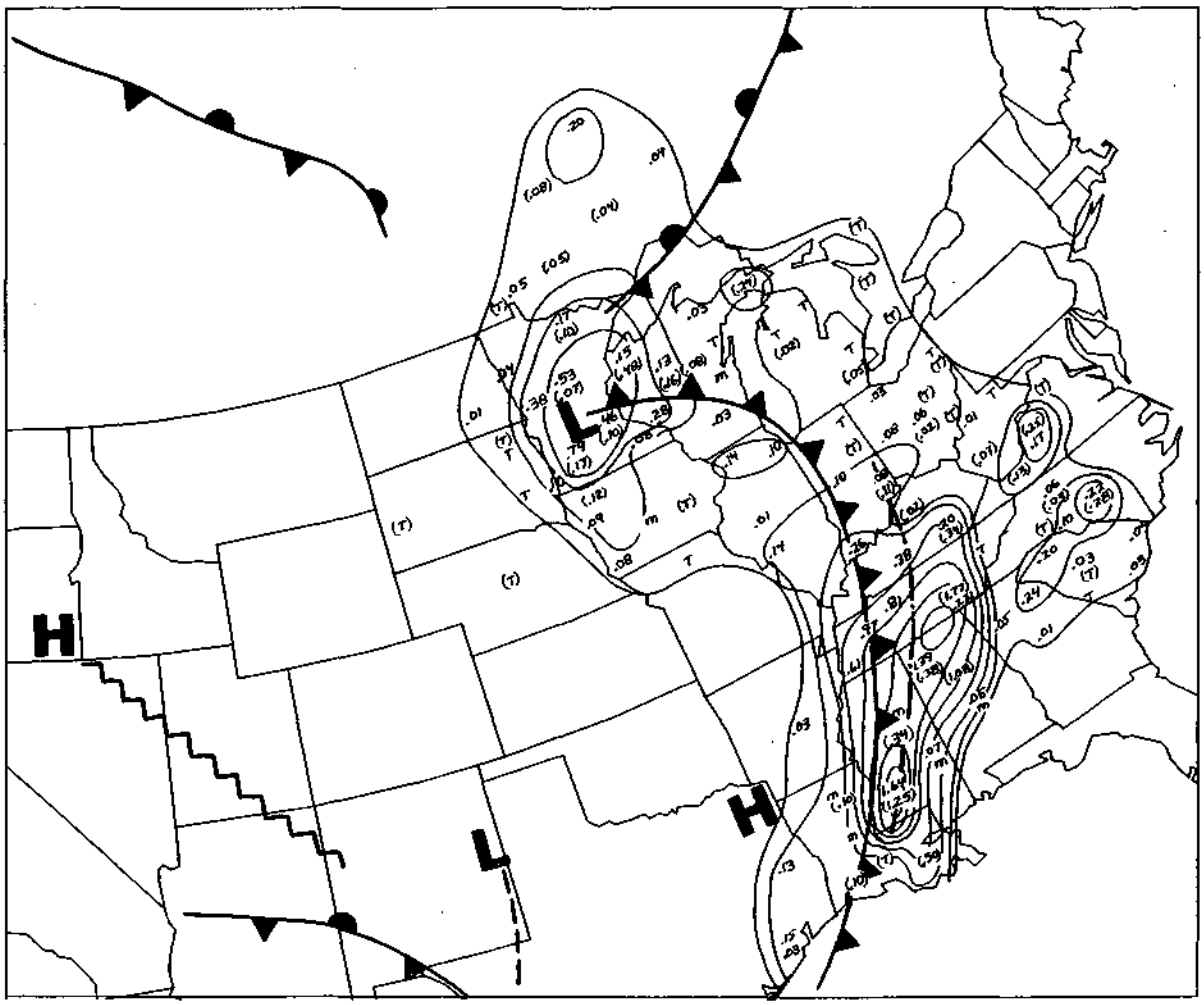

Figure 6. Map of analysis area showing positions of fronts, pressure centers, and precipitation for the 12 h period centered about 12 GMT 13 April 1964. Values in parentheses are for the 6 h period after 12 GMT; other values are for the 6 h period prior to 12 GMT.

combined with the fixed 200 mb upper boundary and caused the upper level trough to deepen extensively. The jet stream was increased from the observed 30 m s^{-1} to greater than 100 m s^{-1}.

The problems associated with linear vertical differencing in hydrostatic numerical weather prediction models are not new. One solution (Gerrity, 1977), is to discard the observed temperatures in favor of new temperatures constructed directly and hydrostatically from the height fields. This approach is not tenable with the variational model which requires the specific volume to be an observed variable. The hydrostatic equation cannot be replaced with the hypsometric equation in sigma-coordinates because the logarithm of sigma at the upper pressure level (a = 0) is undefined.

Several approaches to improving the temperature-height relationship were tried. Finally the hydrostatic equation for the reference atmosphere was transformed back into pressure coordinates and the balance obtained from the hypsometric equation. This reference partition is not adjusted in the variational model and thus, must be in balance initially. The hydrostatic constraint was retained for the meteorological partition. This alternate formulation reduced the root-mean-square temperature error from 11.2°C for the original formulation to 4.8°C for the alternate formulation.

5. Results: Convergence Test

The first major question addressed by this project is whether the variational method would, for an instance of intense cyclogenesis, converge to a solution when the Rossby number approached or exceeded unity over large areas. The 13 April 1964 case is characterized by violations of quasi-geostrophy as is demonstrated with the aid of figure 7. The shaded areas identify where the wind component or

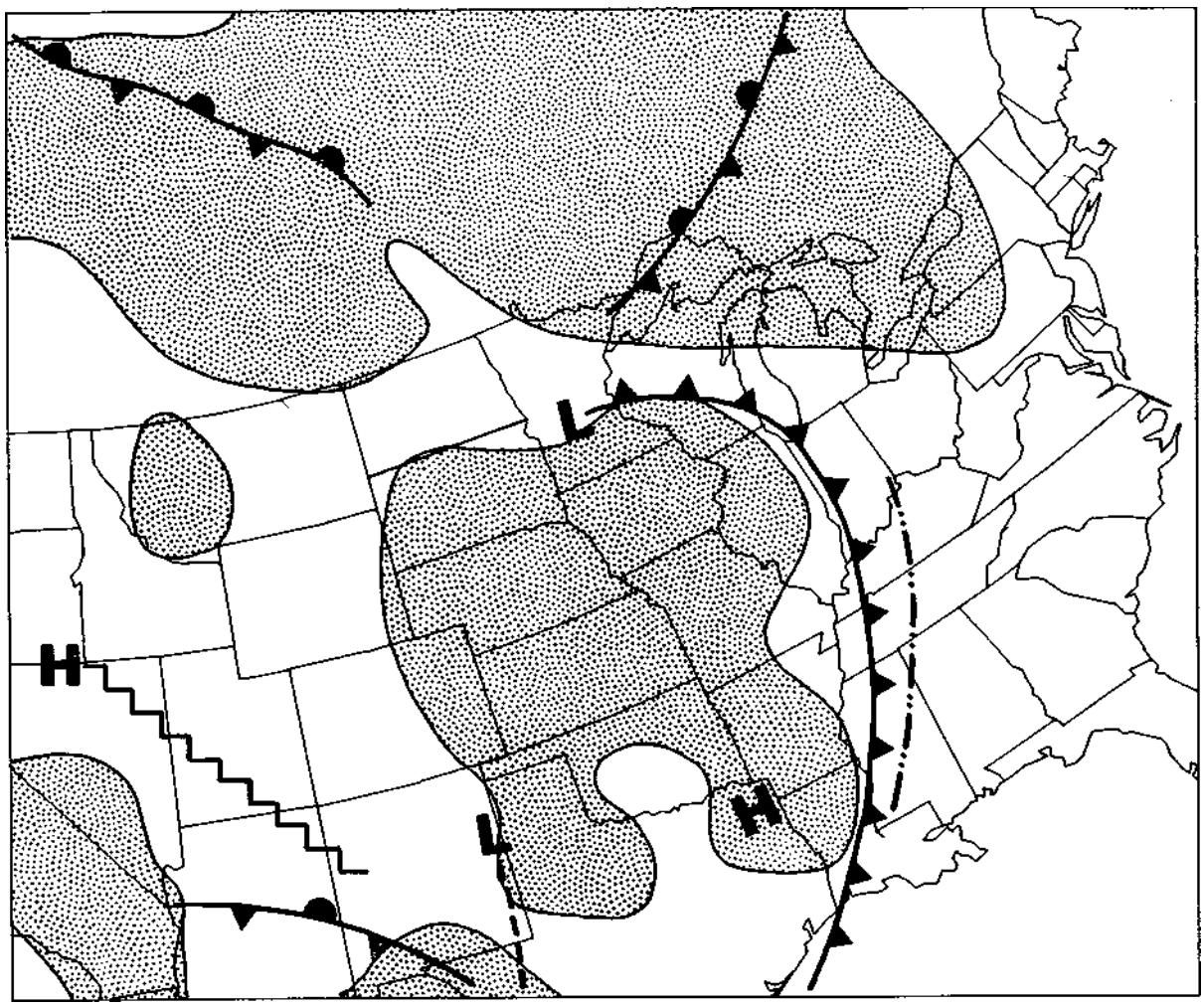

Figure 7. Area (shaded) where the quasi-geostrophic approximation is violated in the tendencies of u, v, a. Date is 12 GMT 13 April 1964.

specific volume tendency magnitudes exceed 5.0, i.e., the tendencies become an order-of-magnitude larger than predicted by quasi-geotrophic scale theory. Calculations of the advective terms in selected areas of strong wind speed gradients also reveal violations of quasi-geostrophy. Most violations occur along the jet stream, in the sharp curvature and strong wind shear regions around the storm center and in regions of strong cold advection behind the cold front.

a. *Satisfaction of Dynamical Constraints*

One of the requirements for the variational model to converge to a solution is that the dynamical constraints should be satisfied. The adjusted variables at two successive cycles were averaged and reintroduced into the constraints. Residuals were computed as remainders of algebraic sums of individual terms of each constraint. The rms error (Glahn and Lowry, 1972) for each level was then found. Residuals vanished (constraint satisfaction) when variables at two successive cycles were unchanged. In some instances, the residuals decreased during the first few cycles and then leveled off at some value other than zero. This happens when the analysis trends unformly towards or oscillates about some solution.

Rms residuals as functions of cycle for the five dynamic equations behave as shown in figure 8. The residuals for the u and v component horizontal momentum equations are zero initially because the tendencies have been set equal to the sum of the remaining terms as a first guess for the divergence-tendency term subsidiary solution which will be discussed in more detail in Section 7. The mutually adjusted wind components at cycle 1 differ from the observed wind components and the residuals become nonzero. By cycle 13, the solution at all 5 levels has converged to near zero, i.e., the horizontal

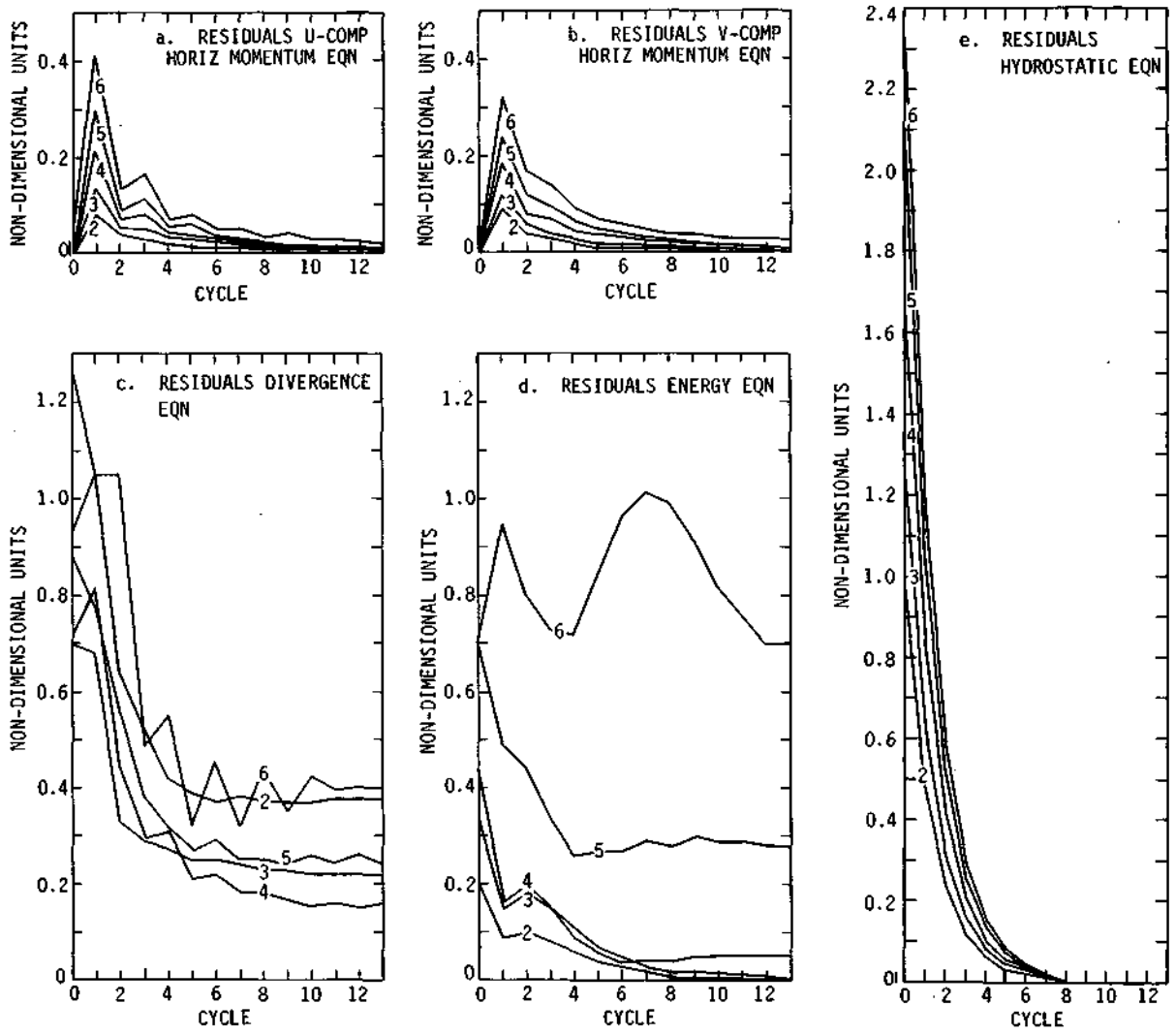

Figure 8. Root mean square residuals for the five adjustable sigma levels as a function of cycle for the five constraints.

momentum equations are satisfied nearly exactly. Table 2 gives the percent residual reduction (to within truncation) after 13 cycles for the five constraints: hydrostatic equation, u anv v-horizontal momentum equations, energy equation and divergence equation. The reductions are calculated from the initial (zero cycle) residuals except for the horizontal momentum equations where the reductions are taken from the first cycle. There is found 100% constraint satisfaction at levels 2 and 3 for both u and v equations. The u-component reductions are greater than 95% and the v-component reductions are greater than 91% at the three upper levels.

Table 2. Percent residual reductions for the five primitive equation constraints after 13 cycles.

Level	u-comp	v-comp	Divergence	Energy	Hydrostatic
2	100	100	70	100	100
3	100	100	69	97	100
4	95	94	79	89	100
5	97	96	70	61	100
6	95	91	58	01	100

The divergence equation residuals for cycle 0 (fig. 8) were obtained from the divergence equation solved with the observed horizontal wind components and with $\dot{\sigma} = 0$. At cycle 1, the input variables were the adjusted u and v components and the a calculated from the energy equation with $\partial\alpha/\partial t = 0$. Figure 8 shows that the residuals increase at levels 4 and 6 during this cycle. After cycle 1 the u, v, and $\dot{\sigma}$ are mutually adjusted through the subsidiary variational formulation that treats the divergence theorem as a strong constraint.

The residuals at all levels decrease through cycle 6 and then level off. The coupled variational method does not satisfy this constraint exactly. (There were similar findings for the 12 December 1965 case study). Table 2 shows that the percent residual reductions for the levels 2-5 were near 70%. The adjustment was less complete at level 6 where the residual reduction was 58%.

The behavior of the energy equation residuals (fig. 8) shows a general decrease in the residuals with increasing cycle for levels 2-5. Variance reductions ranged from 100% at level 2 to 89% at level 4. Level 5 (61%) seemed to be a transition level between an improved analysis at the lower levels and a questionable analysis at level 6. At level 6 the solution initially diverged to reach maximum residuals at cycle 7. Thereafter to cycle 13 the residuals were decreased to approximately the same magnitude as the initial level 6 residuals.

The source of the questionable analysis awaits a term by term study of the energy equation. However, the total solution and the residual pattern are informative. The cycle 7 residual pattern for level 6 (fig. 9), reveals an area of large negative residuals along the prefrontal squall line. If the residuals greater than 2.0 in magnitude were removed from the variance computation, the level 6 variance reduction would have been 47% by cycle 7. These large residuals show that the model was having difficulty reaching a solution in an area of strong upward vertical (as will be shown later) over the squall line. This is an area where the dry version of the variational model did not provide for upper level warming as a consequence of vertical heat transport by deep convective elements. After cycle 7 the residuals were spread with reduced magnitude throughout level 6. This accounted for the reduced variance from cycles 8-13.

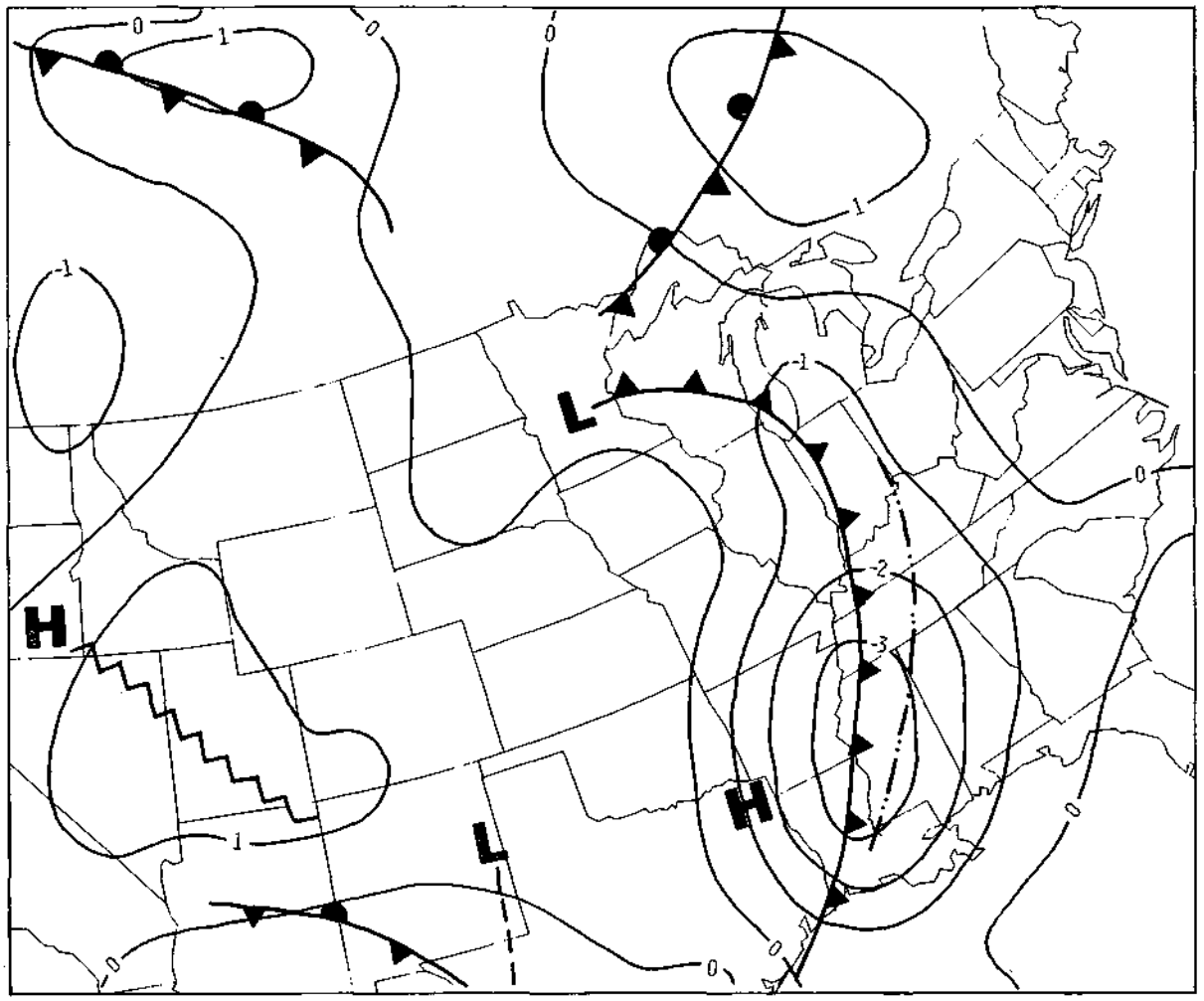

Figure 9. Differences between the root mean square residuals for the adjusted minus observed fields and the standard error of observation for the energy equation at level 6 and cycle 7.

The residual history for the hydrostatic equation is dominated by the large initial height-specific volume residuals discussed in Section 4. The variational analysis reduced the residuals monotonically to zero by cycle 8. Table 2 shows 100% variance reduction for all levels.

b. Adjustment Departures from Observed Fields

Initialization as treated in this paper is a two-step process. Grid point values are found by some interpolative method and then the interpolated fields are adjusted to effect a mutual balance subject to a prescribed set of constraints. No direct information from the original observations is carried into the second analysis step, so the variational method treats the unadjusted initial fields as observed.

Efforts to satisfy the dynamical constraints are made by adjusting initial fields. However, it is presumed that these fields correctly carry the phenomena described by the observations. This assumption allows the statement that the net adjustment from the initial fields should not exceed the standard errors of observation as built into the precision moduli.

Standard errors of observation for wind components, specific volume, and heights for the five adjustable levels are listed in Table 1. This list provides the standard by which rmas residuals between adjusted and initial fields are compared. When a rms value at a particular level substantially exceeded its respective standard observational error, the adjusted fields were examined.

Ems residuals expressing the mean departure of the adjusted fields from the observed fields were constructed for the observed variables (u, v, Ø, α) for each level. These are expressed in figure 10 with the abscissa giving the cycle number and the ordinate giving differences between rms values

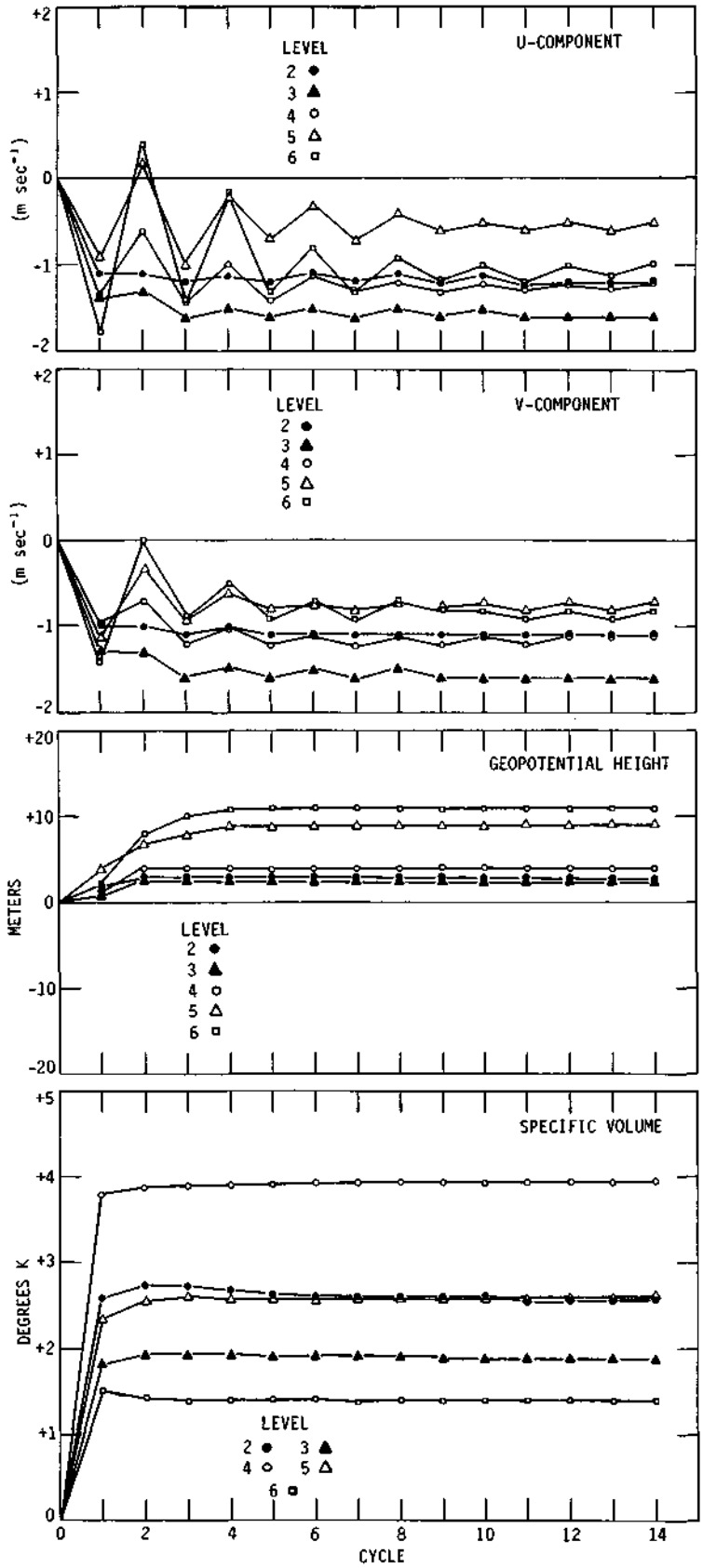

Figure 10. Differences between the root mean square residuals for the adjusted minus observed fields and the standard errors of observation for u, v, Ø, α as a function of cycle.

and the respective standard errors of observation. Values exceeding zero occur whenever adjustments necessary to achieve the primitive equation balance exceed the standard observation error.

Figure 10 shows that the wind field adjustment on the whole did not exceed the standard errors of observation. From Table 1 the greatest precision modulus weighting (II_1) was given to the observed winds. This forced the adjusted fields to converge more toward the observed winds than to the height or the specific volume. Most of the wind field rms departures can be explained by significant smoothing of the wind field along the jet stream by the filter used to control the buildup of noise caused by taking derivatives of derivatives in certain terms of the adjustment equations. The smoothing can be partly eliminated by decreasing the grid spacing currently in use.

Geopotential height adjustments exceeded the standard observational errors at all levels. The over-adjustment at levels 5 and 6, approximately 10 m, could be partly explained by the influence of the specific volume on the adjustment. Heights were on the average lowered; a result of anomalously cold thicknesses brought about by the use of the observed specific volume in the linear hydrostatic constraint. The specific volume residuals are presented in temperature equivalents to allow an appreciation of the magnitude of the adjustment. Specific volume was accorded small relative weights and most of the error introduced by using the linear hydrostatic constraint was returned to the adjusted specific volume.

Finally, as seen in figure 10, the rms adjustments for the specific volume were largely determined at the first cycle. The geopotential height residuals showed little change after the fourth cycle. By contrast, the u and v component departures oscillated through the thirteenth cycle. These oscillations are

fairly pronounced at levels 5 and 6 out through the ninth cycle. This indicates the momentum field's extreme sensitivity to small variation in the mass field; this is in spite of greater relative weight given to the wind field.

The variational analysis appears to have stabilized by the 13th cycle. Significant variance reductions have been realized for all levels and for all constraints with the exception of the energy equation at level 6. The mass field (specific volume and geopotential height) stabilized after the 4th cycle. Small oscillations in the wind field at some levels persisted but there was no evidence for their amplification. On the contrary, the oscillations had been dampled successively in the first cycles and had stabilized or continued to decrease slightly during the later cycles.

6. Results: Pattern Recognition

Pattern recognition techniques have been used for many years for the evaluation of objective with subjective analyses and for objective analysis intercomparisons. (For the results of a recent pattern recognition study, see Otto-Bliesner et al., 1977). Pattern comparisons that reveal similarities, shifts, and magnitude changes between initial and adjusted fields are useful in evaluating the ability of the variational initialization to generate realistic adjusted fields. In this section, pattern recognition techniques are used to answer the question of whether the variational model can detect the net mass vertical transports associated with a prefrontal squall line.

Comparisons between variational analyses that differed by the relative magnitudes of precision modulus weights assigned to the initial variables revealed small geopotential differences which were largely masked by the magnitude

of the overall patterns. Therefore the pattern recognition was directed toward the wind fields which are sensitive to rather minor height adjustments. The criteria used to judge the adjusted fields were 1) the adjustments from the observed fields (u and v) should not be excessive with regard to pattern shifts and magnitudes of changes, and 2) the adjusted patterns must be physically consistent with circulations associated with known weather systems. Vertical velocity patterns were closely scrutinized for correspondence with pressure systems, fronts, etc. in a physically consistent manner. Further, small scale "noise" oscillations introduced through the variational adjustment or the divergence-tendency term adjustment were expected to feed back into the vertical motion fields. Thus the vertical motion field pattern recognition served a dual role; to reveal the vertical motion pattern associated with weather systems and to reveal the magnitude of model generated noise.

One of the reasons for selecting the 13 April 1964 case is that vertical motion fields calculated from different algorithms are available for comparison with the variational vertical motion fields. Stuart (1971) calculated quasi-geostrophic omega vertical velocities on a 160 km grid. Vertical velocities on an 2.5 degree grid (approximately 250 km) from the more general balance omega equation model (Krishnamurti, 1968) were compared with the variational vertical motions.

Pressure surfaces may depart significantly from height surface in the vicinity of intense cyclones. Therefore the conversion from omega (pressure) to vertical velocity (height) is derived from the total derivative of omega, viz.,

$$w = \frac{\alpha}{g} \left[\frac{\partial p}{\partial t} + u \frac{\partial p}{\partial x} + v \frac{\partial p}{\partial y} - \omega\right] \qquad (25)$$

Nondimensionalization of the right-hand of (25) leads to

$$w = \frac{HC}{L} \alpha' \left[\frac{F}{R_o} \left(\frac{\partial p''}{\partial t'} + u' \frac{\partial p''}{\partial x'} + v' \frac{\partial p''}{\partial y'}\right) - R_o \omega'\right] \qquad (26)$$

where H, C, L, F, R_0 are, respectively, the scale height (10 km), scale wind (10 m s^{-1}), scale length (10^6 m), Froude number (10^{-3}), and Rossby number (10^{-1}). The primed and double primed numbers are of order 1. Equation (26) shows that the pressure tendency and the horizontal advection terms are generally an order of magnitude smaller than the vertical motion (omega) and can be neglected. That this can be done for the 13 April 1964 cyclogensis is shown as follows. The maximum observed pressure gradient was approximately 5 mb over 200 km. With a wind of 10 m s^{-1}, the nondimensional pressure advection term of (26) equals 2.5. Multipled by the ratio of the Froude number and the Rossby number the advection term magnitude is 0.025, an order of magnitude smaller than the vertical motion term. Thus, the conversion from omega to vertical velocity (w) reduces to

$$w \simeq \frac{\alpha}{g} \omega \quad . \qquad (27)$$

The vertical velocity (cm s^{-1}) at 500 mb (Krishnamurti, 1968) for the 13 April 1964 storm (fig. 11) shows a general zone of ascending motion along and ahead of the cold front from Minnesota to Louisiana and from the low center into Canada north of Minnesota. Maximum vertical velocities in excess of 8 cm s^{-1} are found just north of Minnesota. Krishnamurti found that his moist latent heat release parameterization contributed about 50% of this vertical velocity. Therefore, it is inferred that the dry vertical motions were slightly in excess of 4 cm s^{-1}. Significant vertical motions extend southeastward with decreasing magnitude in a tongue that stretches from the vertical motion center to Ohio.

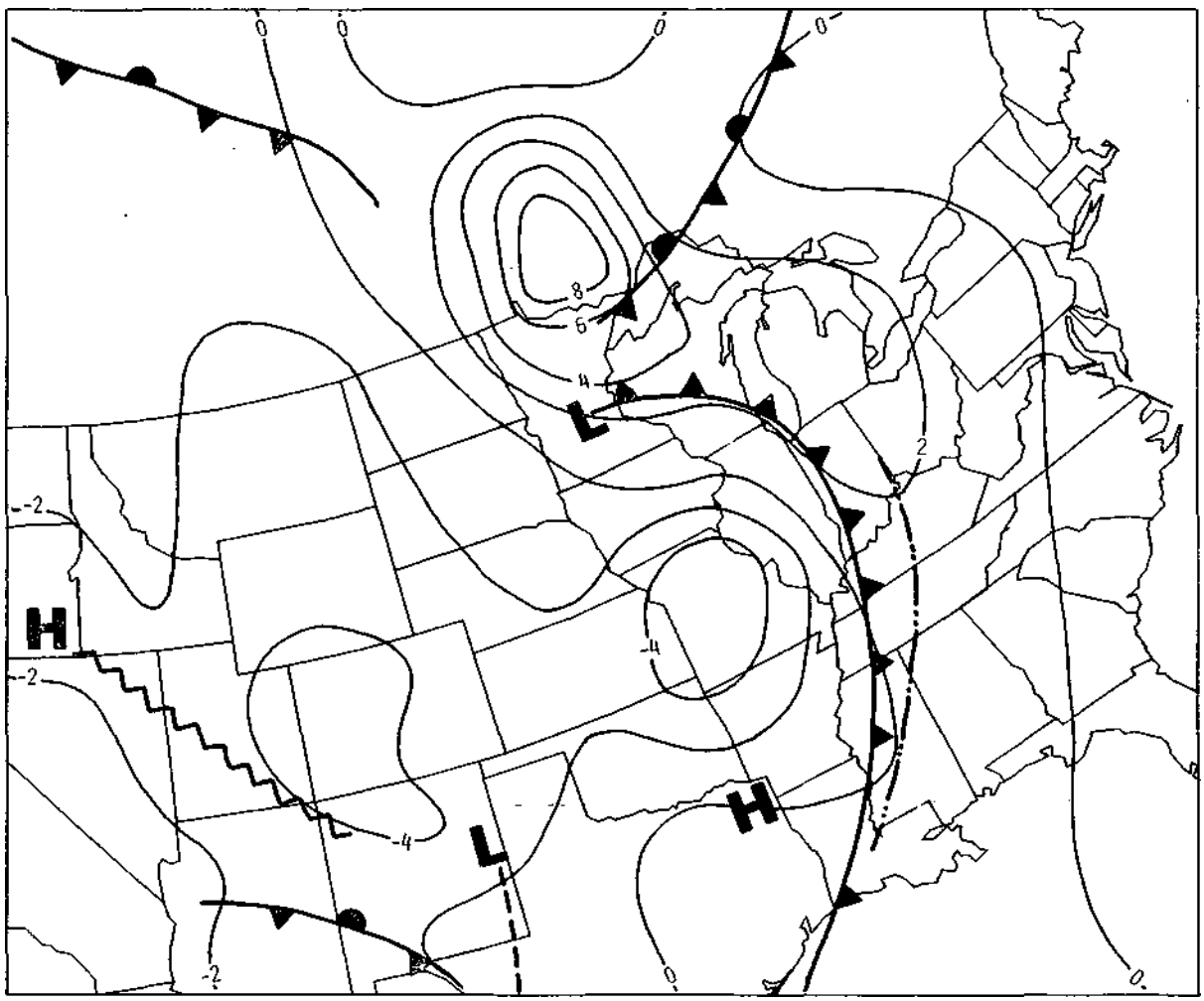

Figure 11. 500 mb vertical velocity (cm s^{-1}) from the Krishnamurti (1968) 12 forcing function balance omega equation solved on a 2.5 degree grid. Date is 12 GMT 13 April 1964.

Subsidence centers of about -4 cm s^{-1} found over Missouri and Colorado are connected by general subsidence over the region behind the low and to the west of the cold front.

No specific center of ascending motions is associated with the weak low over New Mexico.

It is clear that Krishnamurti's balance equation initialization model does not detect the net vertical mass transports associated with the prefrontal squall line. Stuart and Krishnamurti (1970), initiated an intensive study with several static initialization schemes to detect these vertical motions. These efforts were largely unsuccessful. In the variational initialization model, the divergence is included as a dynamical constraint and the observed winds are accorded greatest relative weight in the adjustment. Thus it is expected that the net mass vertical transports, if any, would be represented variationally by a second center of rising motion located along the prefrontal squall line.

Figure 12 shows the level 5 (455 mb) dry vertical velocities (cm s^{-1}) calculated from the variational model. The pattern reveals a center of strong rising motion (6 cm s^{-1}) associated with the prefrontal squall line. However, the dissimilarities between the variational analysis and Krishnamurti's balance equation analysis near the major cyclone center are such as to raise the possibility that the variational model has introduced small scale oscillations into the vertical velocity fields. Major differences between the two initializations include the prefrontal squall line rise center, the placement of a secondary rise center in the vicinity of the New Mexico low, the introduction of a large area of subsidence that extends across the cold front through Wisconsin, Michigan, and into southeastern Canada, and the shifting of the rise center from a position northeast of the Minnesota low center to a position

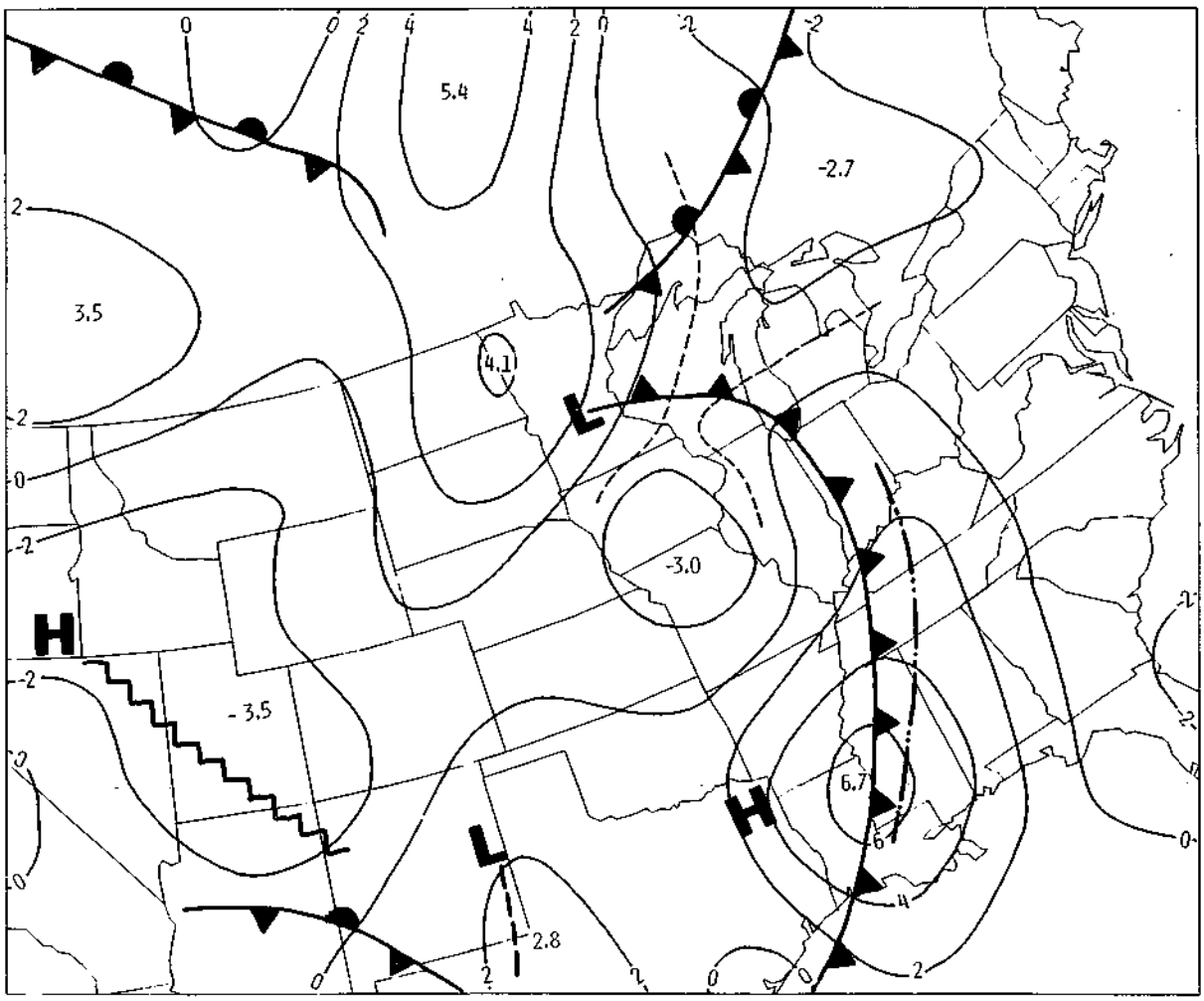

Figure 12. Sigma level 5 (455 mb) vertical velocity (cm s^{-1}) from the primitive equation constrained variational analysis. Date is 12 GMT 13 April 1964.

to the northwest of the center. Elsewhere, the subsidence patterns over Missouri and the regions to the west are essentially identical.

a. Prefrontal Squall Line Vertical Motions

The vertical velocity patterns are compared with the 12 h precipitation centered about 12 GMT 13 April 1964 (fig. 13). Values in parentheses are for the 6 h period after 12 GMT. Other values are for the 6 h period prior to 12 GMT. The precipitation patterns reveal two rainfall centers, one associated with the major cyclone and the other associated with the squall line that extends from Kentucky to Louisiana. Between these two centers is found light precipitation with amounts ranging generally from a trace to less than 0.10 inch. The area of light amounts from central Illinois northward to central Wisconsin and thence eastward corresponds almost exactly with the variational subsidence pattern shown in the same area (fig. 12). This supporting evidence is by no means conclusive proof that the variational pattern is correct because the horizontal distribution of moisture is not taken into consideration and subsident vertical motion patterns are not required to explain light precipitation amounts.

A series of cross sections provide a more complete description of the structure of the variational vertical motion fields relative to fronts, pressure centers, and precipitation patterns. Figure 14 is a vertical cross section that was constructed along a line extending roughly from Nevada to the northeastern Gulf of Mexico; the cross section passed through the center of rising motion located over Mississippi (fig. 12). The letters H, L, and R identify the weak high pressure center behind the front, the weak low over New Mexico, and the high pressure ridge over Utah as seen in the previous figures. The squall line is shown schematically over Mississippi, and the above ground positions of the cold front were determined from vertical cross

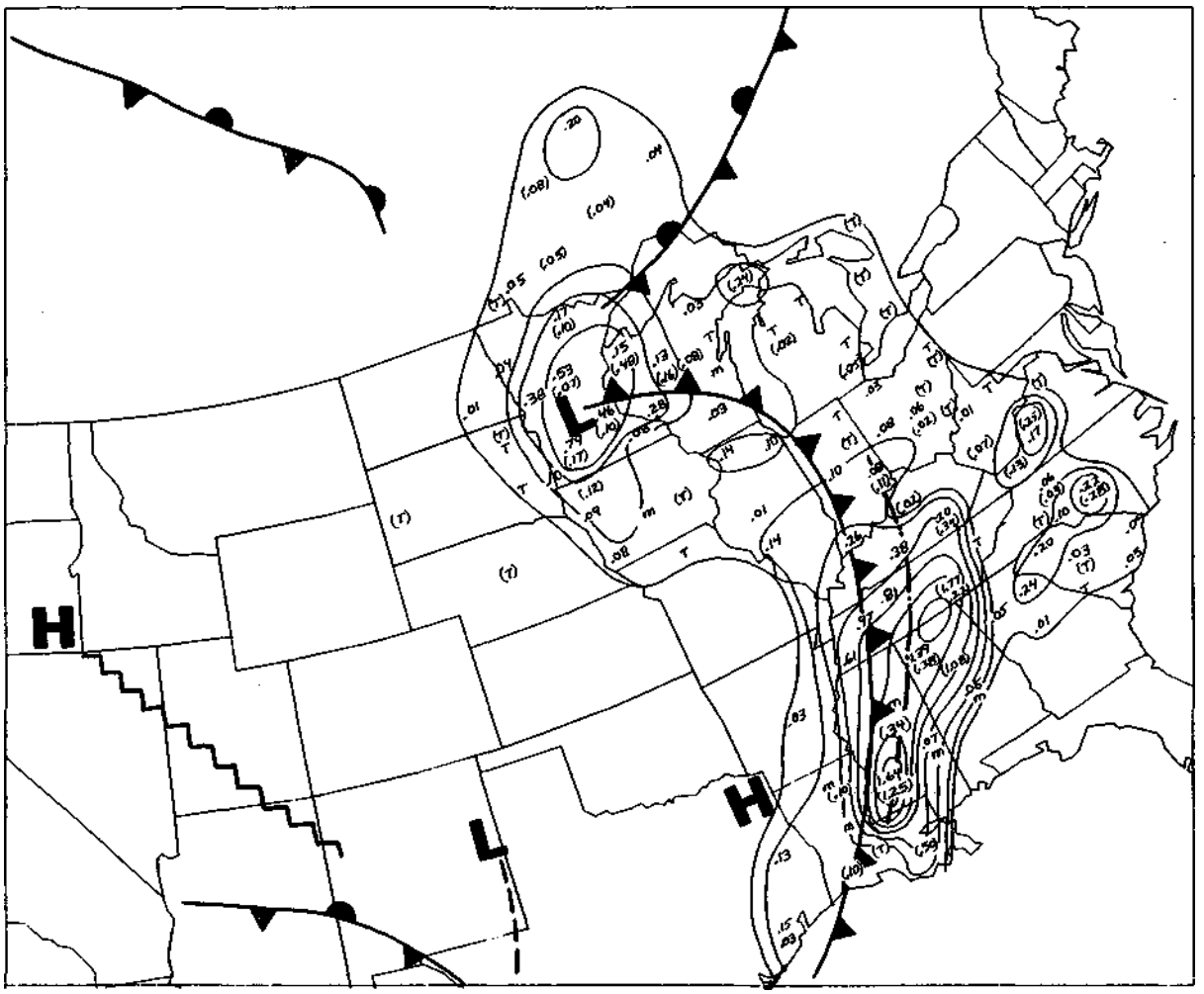

Figure 13. Map of analysis area showing positions of fronts, pressure centers, and precipitation for the 12 h period centered about 12 GMT 13 April 1964. Values in parentheses are for the 6 h period after 12 GMT; other values are for the 6 h period prior to 12 GMT.

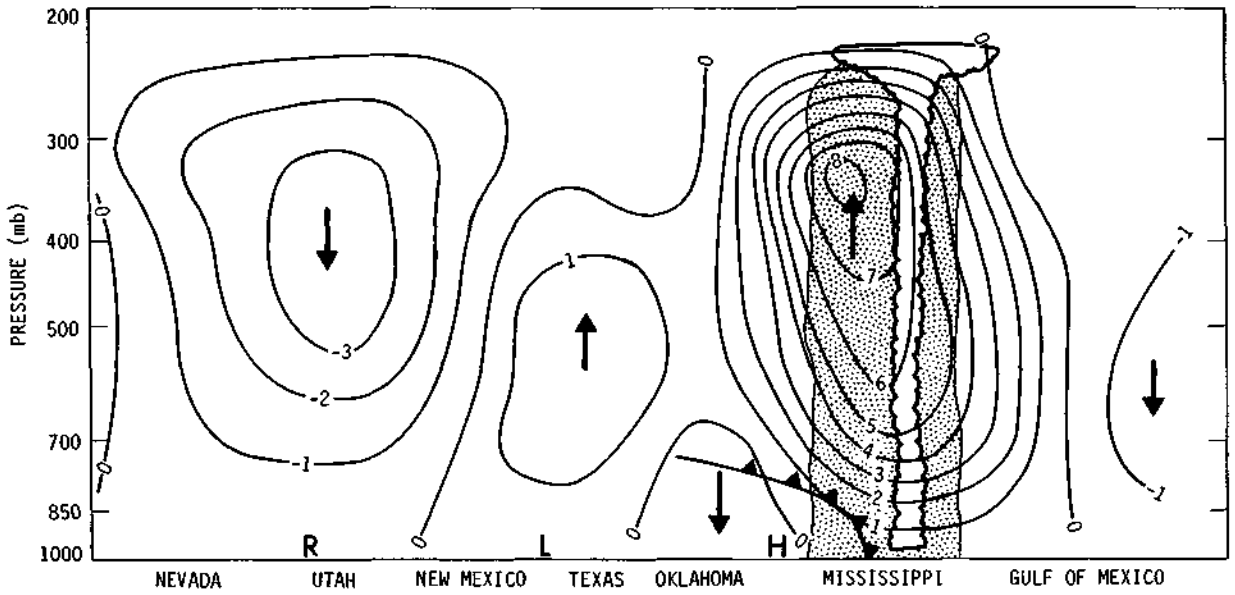

Figure 14. Vertical cross section of variational vertical velocity (cm s^{-1}) from the northern Gulf of Mexico to Nevada. Date is 12 GMT 13 April 1964.

sections. The stippled area is the zone of precipitation shown in figure 13. The patterns are in agreement with the expected vertical motions in relationship with known meteorological disturbances. A narrow zone of strong rising motion (8 cm s^{-1}) accompanies the squall line. This is representative of the net vertical mass displacement by the squall-meso system on the scale of the synoptic observations. A secondary rise center is over the New Mexico surface low. Subsidence is found over the ridge in Utah and behind and beneath the cold front over Oklahoma.

The vertical motion patterns reveal no definite "level of non-divergence." The shallow layer of subsidence below 700 mb over Oklahoma degrades into rising motion in the middle troposphere. The reverse is found for the New Mexico low where, ascending motions in the low and middle troposphere are replaced by subsidence in the layer above 300 mb.

The correspondence between the vertical motion patterns and the meteorological features as presented by the figure 14 cross section is, from pattern recognition, as good as can be expected considering the horizontal and vertical grid resolution. It is puzzeling, therefore, that the vertical velocity patterns for the northern areas could be so poorly related to weather systems because nothing inherent in the variational model could produce a latitudinal bias in the results. Thus we depart from the view that the subsidence ahead of the front is anomalous noise and begin a search for a possible meteorological cause.

b. Vertical Velocity Near the Major Cyclone

A second cross section (fig. 15) was made along the front from the Gulf of Mexico to the Minnesota low and then westward into Montana. It reveals the distribution of vertical motion along the squall line, the position and

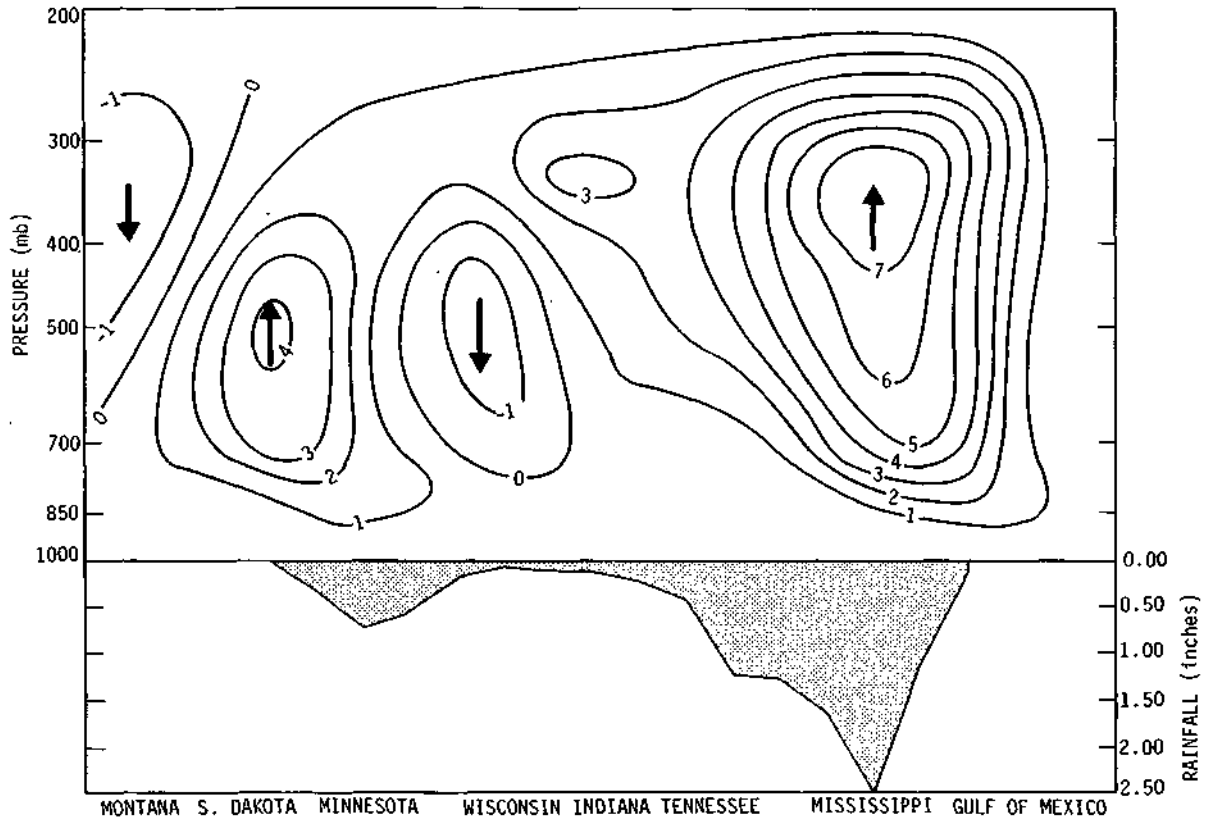

Figure 15. Vertical cross section of variational vertical velocity (cm s^{-1}) from the Gulf of Mexico along the cold front to the Minnesota low thence westward to Montana. The 12 h rainfall centered about 12 GMT 13 April 1964 along the cross section is also shown.

intensity of the subsidence center over Wisconsin and the structure of the rise center associated with the major cyclone. A cross section of the 12 h rainfall centered about 12 GMT 13 April 1964 reveals the rainfall maxima associated with the squall line, the major cyclone and the rainfall minimum beneath the subsidence center.

The subsidence over Wisconsin was found to be a small scale feature of limited vertical extent embedded within a much larger field of upward vertical motion. Sinking was confined to between 700 and 400 mb. Maximum subsidence was slightly in excess of 1 cm s^{-1}. Vertical motions above the subsidence center were positive upward in excess of 1 cm s^{-1} .

Vertical motion fields calculated adiabatically from (3) with the assumption that $\partial\alpha/\partial t = 0$ and kinematically from (4) revealed that the subsidence area was introduced into the variational analysis through the observed wind field. It went undetected in the adiabatic vertical motion calculation. From figure 12, it is seen that the subsidence ahead of the front was an extension of a continuous belt of subsidence that extended from the northwest United States southeastward over Colorado, eastward above Kansas, Missouri, and Iowa, and then northeastward over Wisconsin, the upper Great Lakes, and into southern Canada. This subsidence zone roughly followed the axis of the mid and upper tropospheric jet stream (fig. 5) which dipped southeastward over Idaho, Colorado, and Kansas and then recurved northward above Missouri, Illinois, Wisconsin and Lake Superior. Embedded within this high speed current was a strong subsynoptic scale jet max with speeds greater than 30 m s^{-1} located at the base of the upper level trough over Missouri. The jet max was nearly coincident with the -3 cm s^{-1} subsidence center (fig. 12).

The apparent association of the prefrontal subsidence with the mid-tropospheric jet stream suggests that subsynoptic scale vertical motion fields associated with the jet stream have become superimposed upon the synoptic scale vertical motion fields associated with the major cyclone. Although jet stream scale vertical motion fields are known to exist (Riehl, 1952; Endlich and McLean, 1965), their overall relationship with the larger scale motion patterns has not been clearly established. In an effert to determine if the jet stream was the physical mechanism that caused the subsidence, known and modeled vertical motions for an intense, localized jet maximum buried within an upper level trough gleaned from the literature were compared with the variational vertical velocity patterns.

Riehl (1952) modeled the vertical motion patterns surrounding synoptic scale jet streams under the assumption of conservation of potential vorticity. Air moving toward higher absolute vorticity converges and air moving toward lower absolute vorticity diverges. Variations in the convergence field for a jet maximum embedded within a mid-level trough such as shown schematically in figure 16 can be deduced empirically by considering the contributions of wind shear and flow curvature. North of the jet axis, shear and curvature combine to produce convergence west of the trough axis and divergence east of the trough axis. South of the jet axis, the contributions of shear and curvature are opposed and the sign of the divergence becomes dependent upon the relative magnitudes of the individual contributants. If the shear term is the dominate term, the flow is divergent west of the trough and convergent east of the trough. Since divergence in the mid and upper troposphere is compensated by the upward transport of mass from the lower troposphere, the pattern of vertical motion would be upward on the left forward and right rear quadrants of the jet maximum and downward on the right forward and left rear quadrants of the jet maximum.

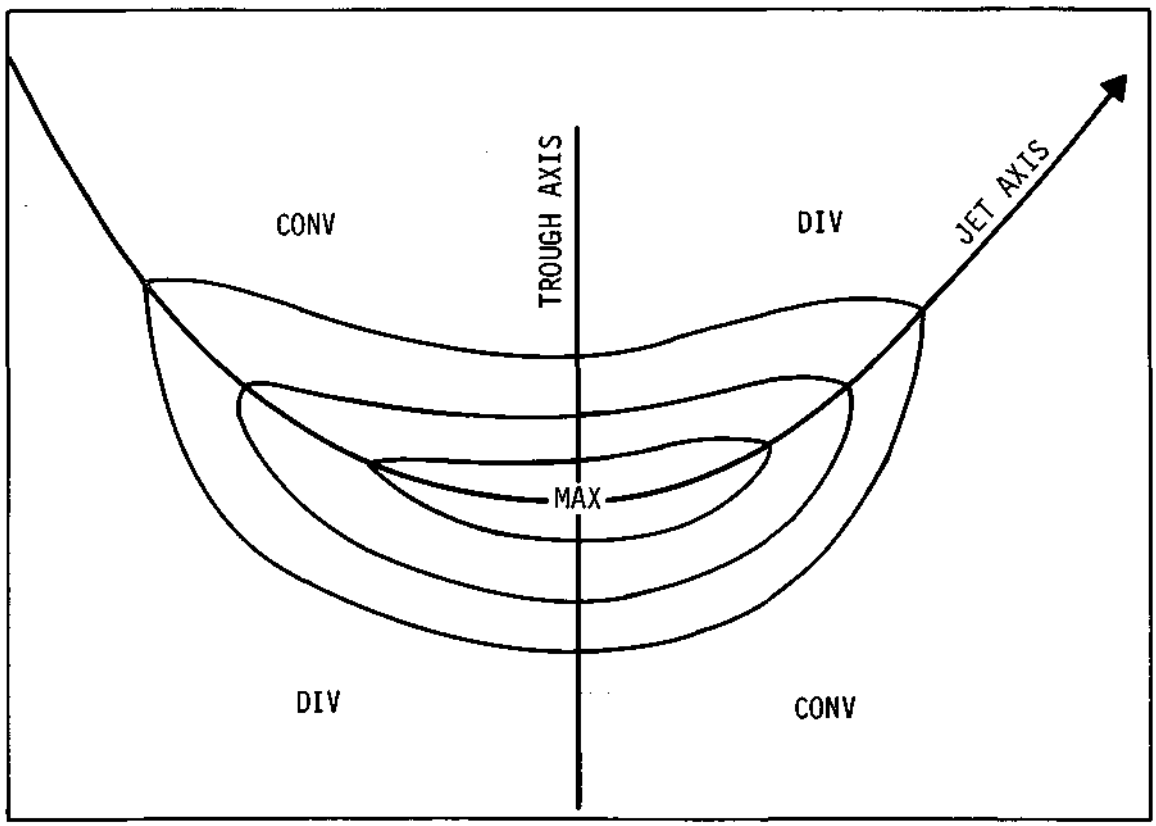

Figure 16. Illustration of the convergence pattern surrounding a strong wind maximum (jet maximum) embedded within a mid level trough.

Estimates of the sign and magnitude of the vertical velocity along the jet stream axis are also needed. Figure 17 shows the vertical velocity profile along the axis of a uniform speed jet stream measured in rotating tank experiments (Reiter, 1961). Maximum vertical motions of the order of 6 cm s^{-1} were found at the 2 cm level - below the level of maximum flow velocity (at 3-4 cm). The rotating tank experiments show that maximum rising motion occurs just upwind of the ridge and maximum sinking motion occurs just upwind of the trough. This is shown schematically in figure 18. Sinking occurs along the jet axis wherever the flow path is cyclonically curved. Ascending motion is found where the flow path curves anticyclonically.

When the schematic flows of figures 16 and 18 are combined, the overall vertical motion pattern surrounding the jet stream becomes one of a general area of subsidence with two isolated centers of rising motion embedded therein. The flow along the jet stream follows a cyclonically curved path (fig. 5) over most of the analysis area, hence subsidence is expected along the jet axis. This is verified by the variational vertical motion cross section (fig. 19) which shows subsidence along all of the cycloncially curved part of the jet axis. Two centers of subsidence with magnitudes of -2.5 cm s^{-1} and -3.5 cm s^{-1} are found along and upwind of the trough axis. These subsidences were approximately an order of magnitude smaller than sinking motions found in the mid tropospheric polar frontal zones of 22 jet streams (Endlich and McLean, 1965). However, caution must be exercised in comparing the magnitudes of the variational vertical motions and with the vertical velocities measured by Endlich and McLean. Variational vertical velocities are presented on a 190 km grid. Further, small scale features of the scale of 400 km are filtered from the variational model.

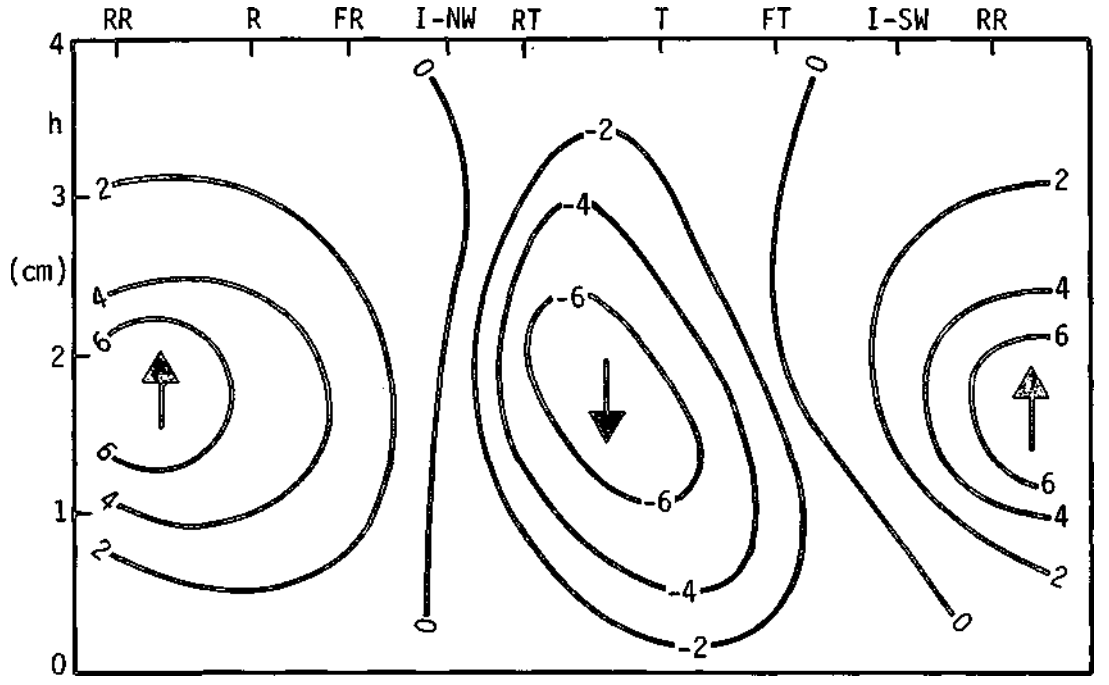

Figure 17. Vertical velocity (cm s^{-1}) measured along the axis of a jet stream simulated by rotating tank experiments (from Reiter, 1961).

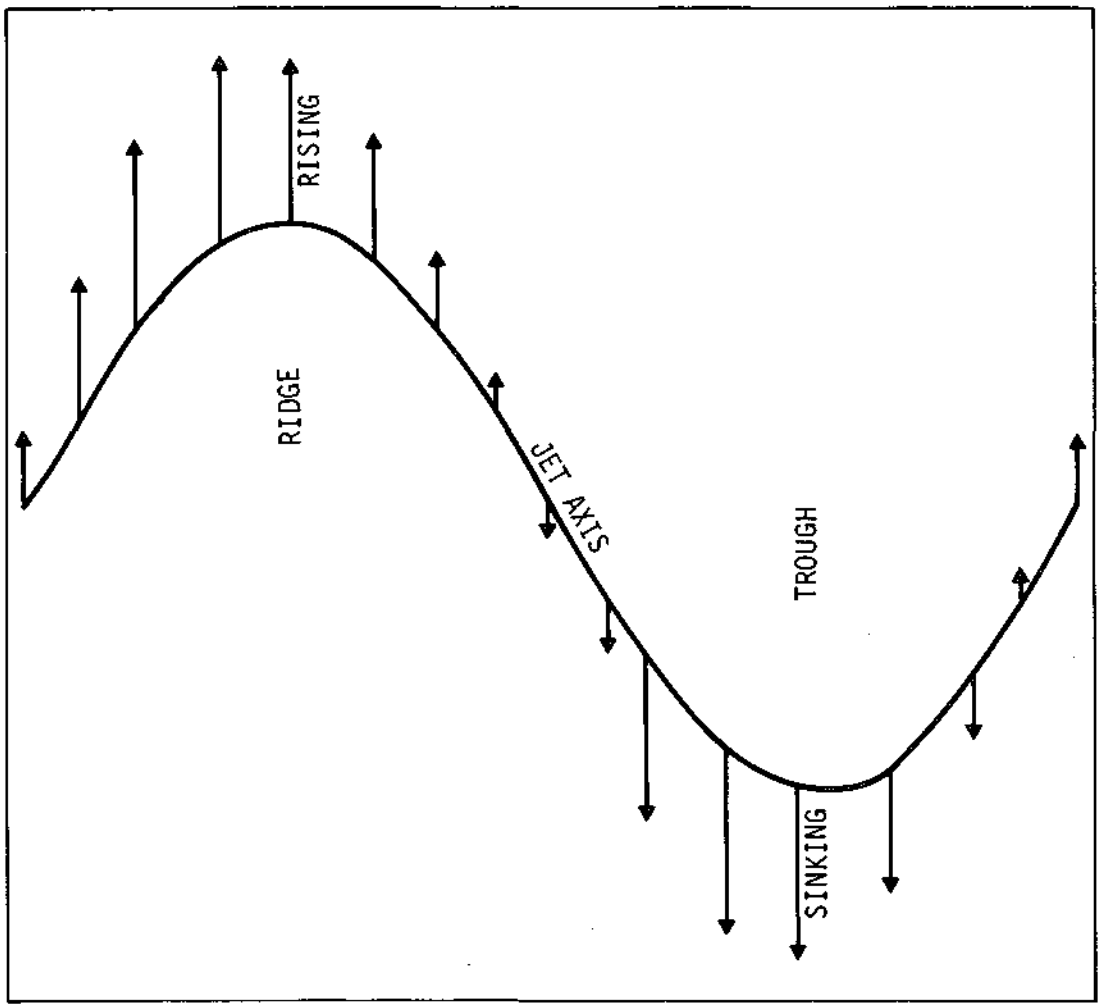

Figure 18. Illustration of magnitude and direction of vertical velocities along the axis of a jet stream that flows through a large scale ridge-trough pattern.

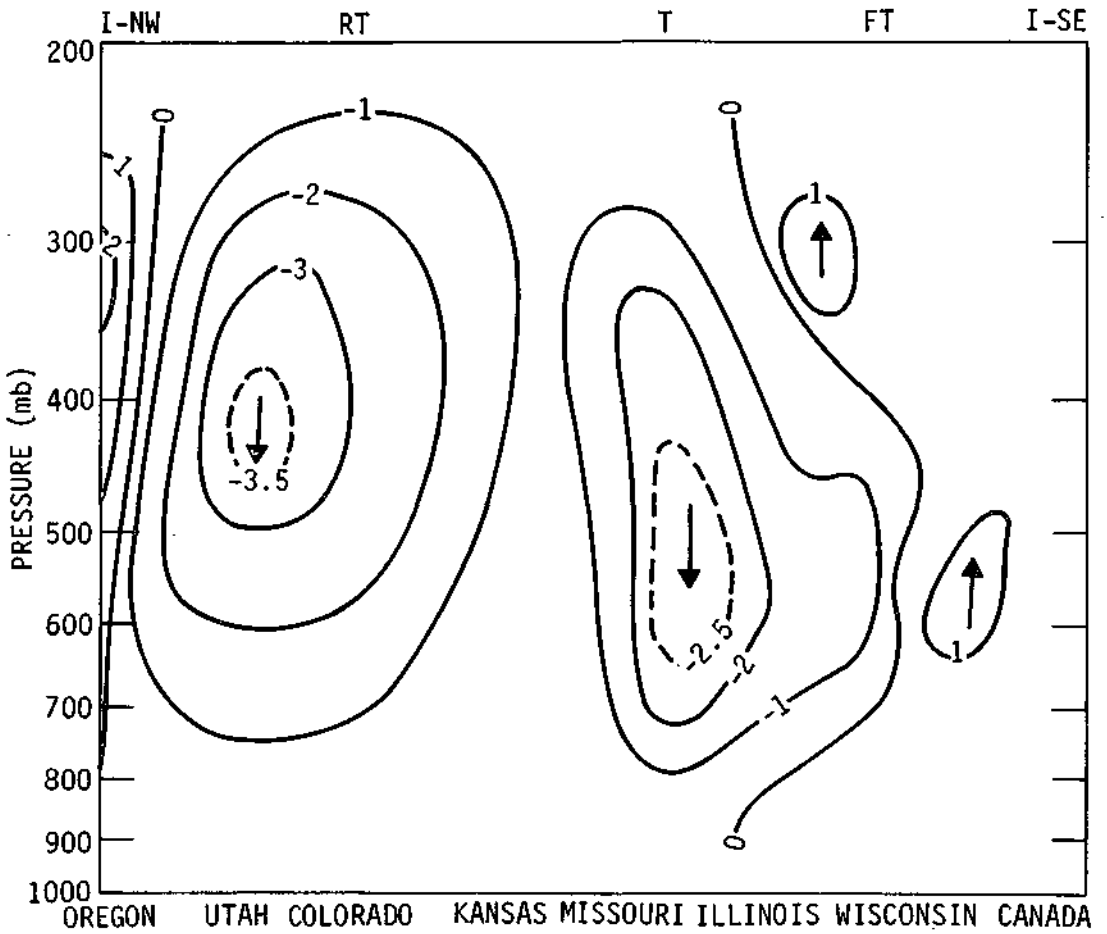

Figure 19. Variational vertical motions along the axis of the mid tropospheric jet stream on 12 GMT 13 April 1964.

Hence, the variational model is presenting only the subsynoptic scale and larger motions associated with the wind field.

According to the schematic jet stream model, the two centers of rising motion should be found along the right forward and left rear flanks of the jet stream. Cyclonic wind shear combines with cyclonic curvature to produce large absolute vorticity to the left (north) of the jet axis over Minnesota (see fig. 5). Air flowing through the left forward flank of the jet maximum moves through strong negative vorticity gradients. This area of expected strong upward motions is located over the position of the surface low pressure center and its associated precipitation. Variational "dry" upward motions are approximately 4 cm s^{-1} (fig. 12). Further verification is provided by a vertical cross section (fig. 20) that was constructed from Ohio to Montana through the jet axis ahead of the jet maximum located over Missouri. The cross section is viewed looking downwind from the jet max. Mid tropospheric subsidence is found beneath and to the right (anticyclonic shear side) of the jet axis. Sinking motions within the jet axis are slightly less than -1.0 cm s^{-1} at 500 mb. Rising motions that exceed 4 cm s^{-1} are embedded within the strong cyclonic shear on the left side of the jet axis. The vertical velocity patterns revealed by figure 20 are in qualitative agreement with the motion fields predicted by the schematic jet stream model.

The second center of rising motion is expected to be located along the upwind anticyclonic shear side of the jet axis. Here, strong anticyclonic shear opposes weak cyclonic curvature to produce an area where flow is directed toward decreasing absolute vorticity. Another vertical cross section through the jet stream (fig. 21) constructed from west Texas through western Minnesota reveals the vertical distribution of vertical motions on the upwind side of

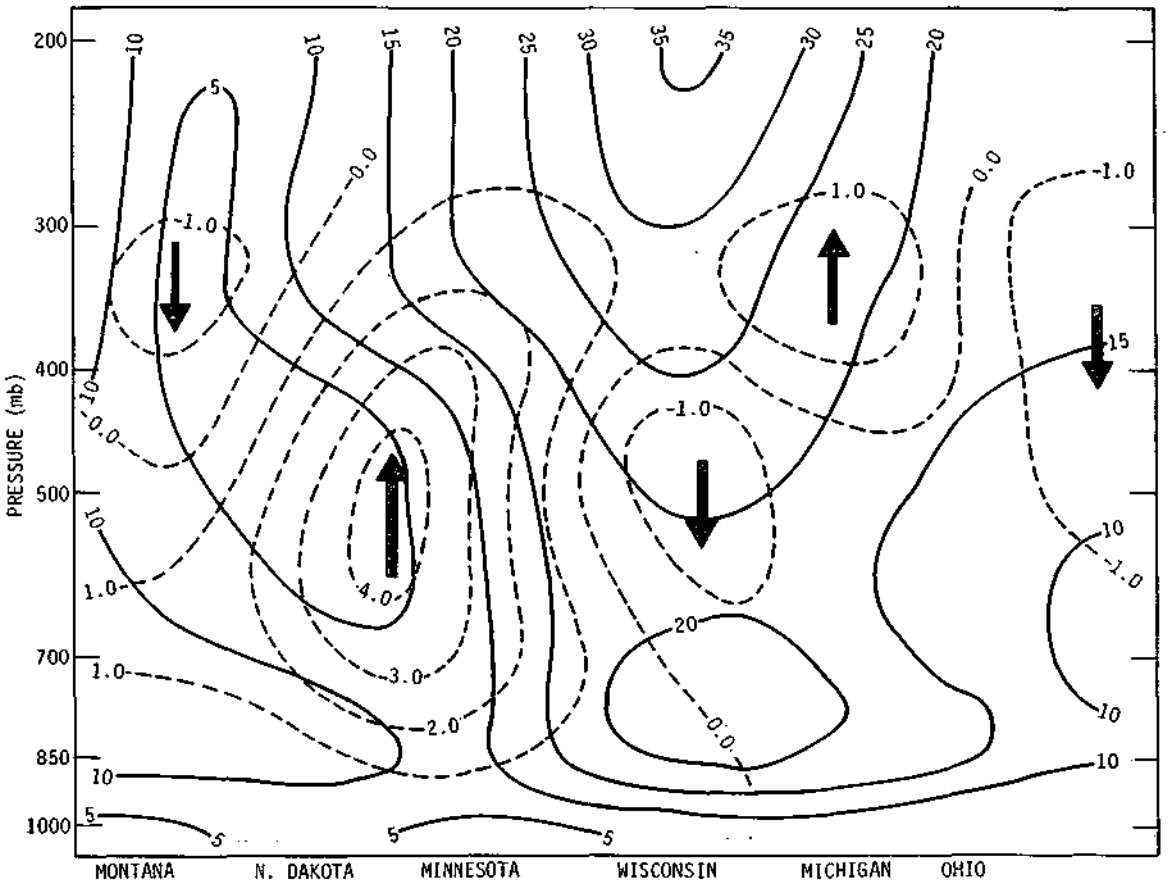

Figure 20. Vertical velocity (dashed lines) in cm s^{-1} and horizontal velocity (solid lines) in m s^{-1} along a vertical cross section constructed from Montana to Ohio through the mid tropospheric jet stream.

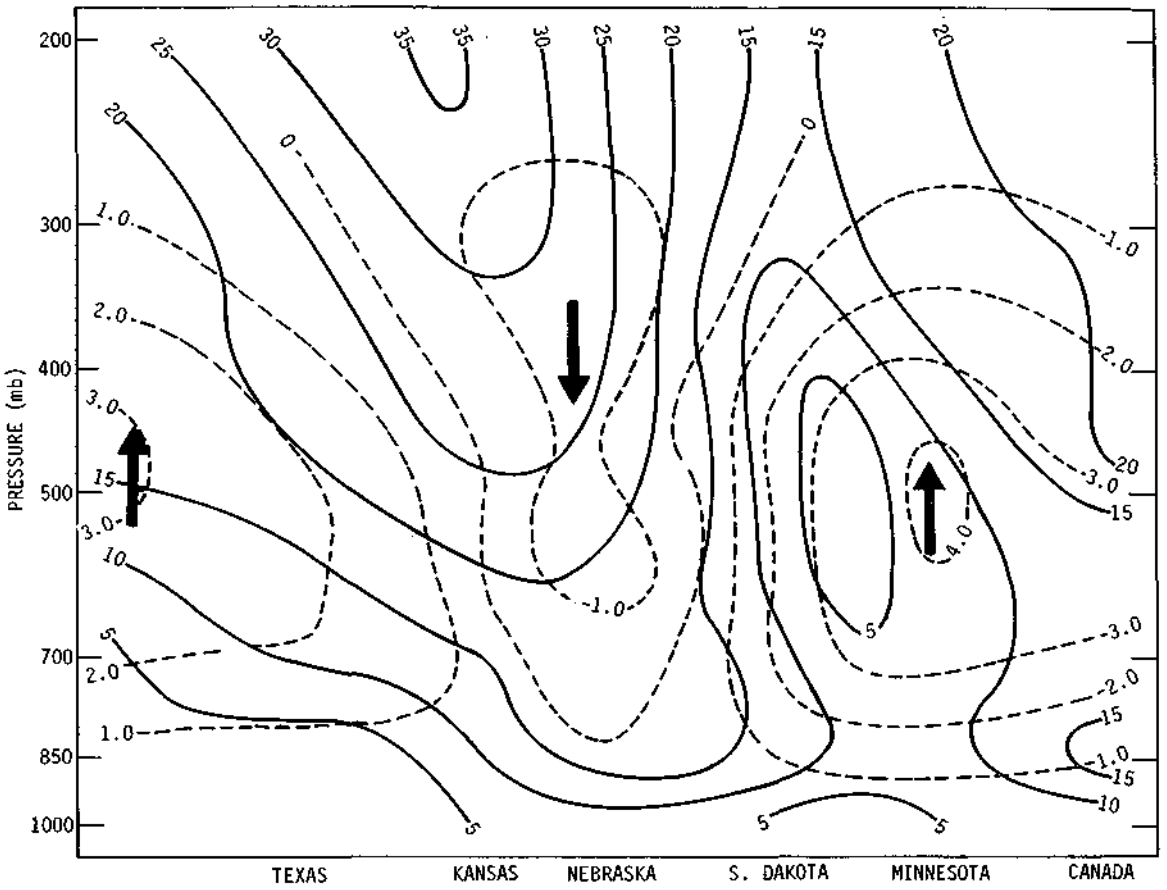

Figure 21. Same as in figure 20 except the cross section was constructed from Texas to Canada.

the Missouri jet maximum. The cross section is viewed looking upwind. Rising motions in excess of 2 cm s^{-1} are found over Texas near the location of the New Mexico surface low (fig. 5). These rising motions are on the anticyclonic shear side of the jet. Sinking motions are found over Kansas and Nebraska along and immediately to the right of the jet axis. The rising motions over North Dakota and Minnesota identify the rise center discussed in the previous paragraph. The jet stream over Kansas (fig. 21) passes out of the cross section toward the viewer as it flows eastward and passes back into the cross section over Canada as it flows northwestward. Part of the cyclonic shear side of the jet is visible at the extreme right side of the cross section.

Detailed wind analysis with the aid of vertical cross sections of the variational wind field has revealed that the variational vertical velocity patterns in the vicinity of the mid-tropospheric jet stream are in qualitative agreement with vertical motion patterns predicted by a schematic jet stream model. These findings support the hypothesis that the unexpected patterns of prefrontal subsidence over Wisconsin and Michigan (fig. 12) were associated with mid-level jet stream motion fields. These findings are by no means conclusive, however. There remains the possibility that the agreement between the model and the analysis is coincidental. Further, it is still possible that the variational vertical motions are not associated with any physical mechanism and are spurious. A verification that the variational vertical velocities are associated with some physical mechanism which is most likely the mid-tropospheric jet stream is provided by relative humidity fields obtained independently from the variational analysis. Vourela (1957) demonstrated that vertical velocities in jet streams could be estimated from the signs and magnitudes of the relative humidity tendencies following the air parcels.

In the absence of precipitation, and mixing, the moisture content of an airmass remains constant. Any change in the relative humidity of the airmass is brought about by a change in its temperature. Subsidence brings about warming and an increase in the saturation mixing ratio. This decreases the relative humidity.

The coarse 12 h sampling frequency for rawinsonde data and the widely spaced observation sites were reasons for not attempting a Lagrangian approach to determine relative humidity tendencies. Instead, the relative humidity patterns were examined for features that could be associated with the jet stream. It was found that a narrow tongue of low relative humidities extended along the jet stream from Missouri through Wisconsin and Michigan. This of course, is the same area where the variational model developed subsidence. Local advection of dry air from the west along the jet core and/or subsidence within the jet core could have produced these low relative humidities. A vertical cross section of relative humidity (fig. 22) was constructed approximately 200 km ahead of and parallel to the cold front. This cross . section cuts through centers of high relative humidity associated with the prefrontal squall line and with the major cyclone. Included in the cross section are the vertical distribution of relative humidity (solid lines) and the distribution of vertical velocity (dashed lines). The jet axis is shown by a thick dashed line. Familiar features are the centers of rising motion associated with the prefrontal squall line and the major cyclone. The subsidence over Wisconsin and Michigan is approximately -2 cm s^{-1}.

The cross section shows moderate levels of relative humidity along the prefrontal squall line. The values are not as high as could be expected because most vertical moisture transport was confined within the convective

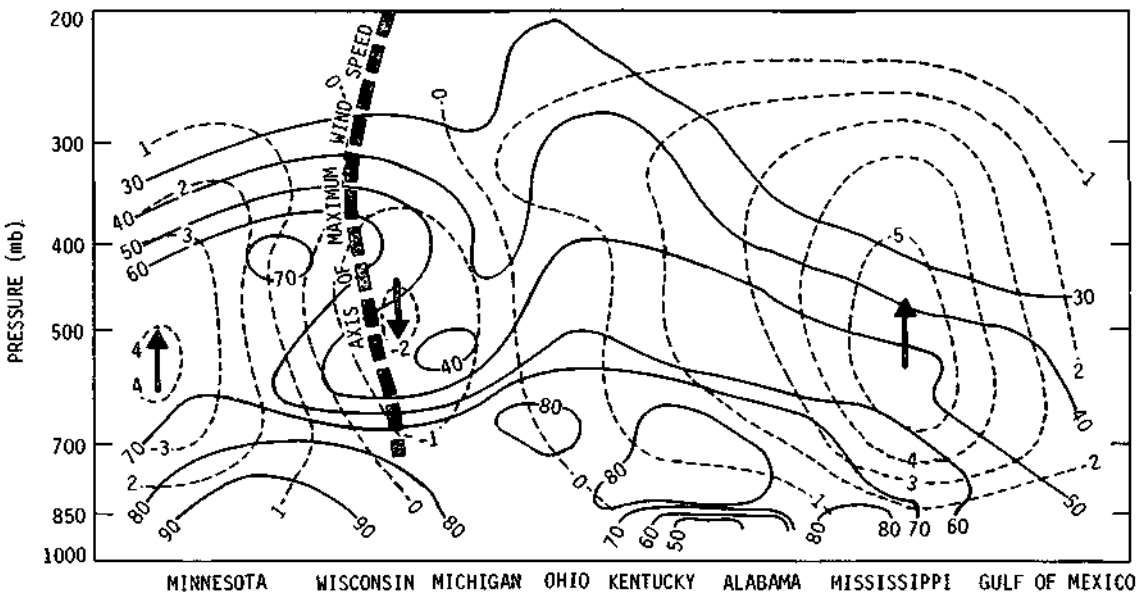

Figure 22. Vertical velocity (dashed lines) in cm s^{-1} and relative humidity along a vertical cross section constructed along a line approximately 200 km ahead of the cold front from Minnesota to the Gulf of Mexico.

towers of the squall line and the objective analysis tended to reduce the centers of relative humidity extremes. Also shown is a deep layer of moderately high relative humidities over Minnesota that has been smoothed somewhat by the objective analysis. Between these two moisture centers lies an area of low relative humidities that is nearly coincident with the subsidence along and on the anticyclonic shear side of the mid-troposphere jet stream. This is precisely the vertical distribution of relatively humidity expected if the variational vertical motion patterns are correct.

It is also especially noteworthy that the relative humidity distribution below 700 mb is essentially uniform along the entirety of the cross section from Minnesota to Mississippi. Both figures 15 and 22 show that the prefrontal subsidence is confined to levels above 700 mb. Figures 23 and 24 are included to show the spatial relative humidity distributions over the areas of discussion at 750 mb (below the subsidence area) and at 600 mb (within the subsidence area) as produced by detailed objective analysis. Figure 23 shows a comma-shaped high relative humidity pattern typical of the late development stages of intense cyclones. The high moisture areas are found along and ahead of the frontal system. Low relative humidities are found in the subsidence region located behind the front. At 600 mb (fig. 23) above Wisconsin and Michigan the comma-shaped high relative humidity pattern has been interrupted by a narrow intrusion of dry air. This intrusion is located along and on the anticyclonic shear side of the mid-tropospheric jet stream.

The conclusion drawn from the jet stream and relative humidity analyses is that vertical circulations associated with the mid-tropospheric jet stream produced subsidence that reduced the relative humidity and increased the stability of the airmass over Wisconsin and Michigan. The development of

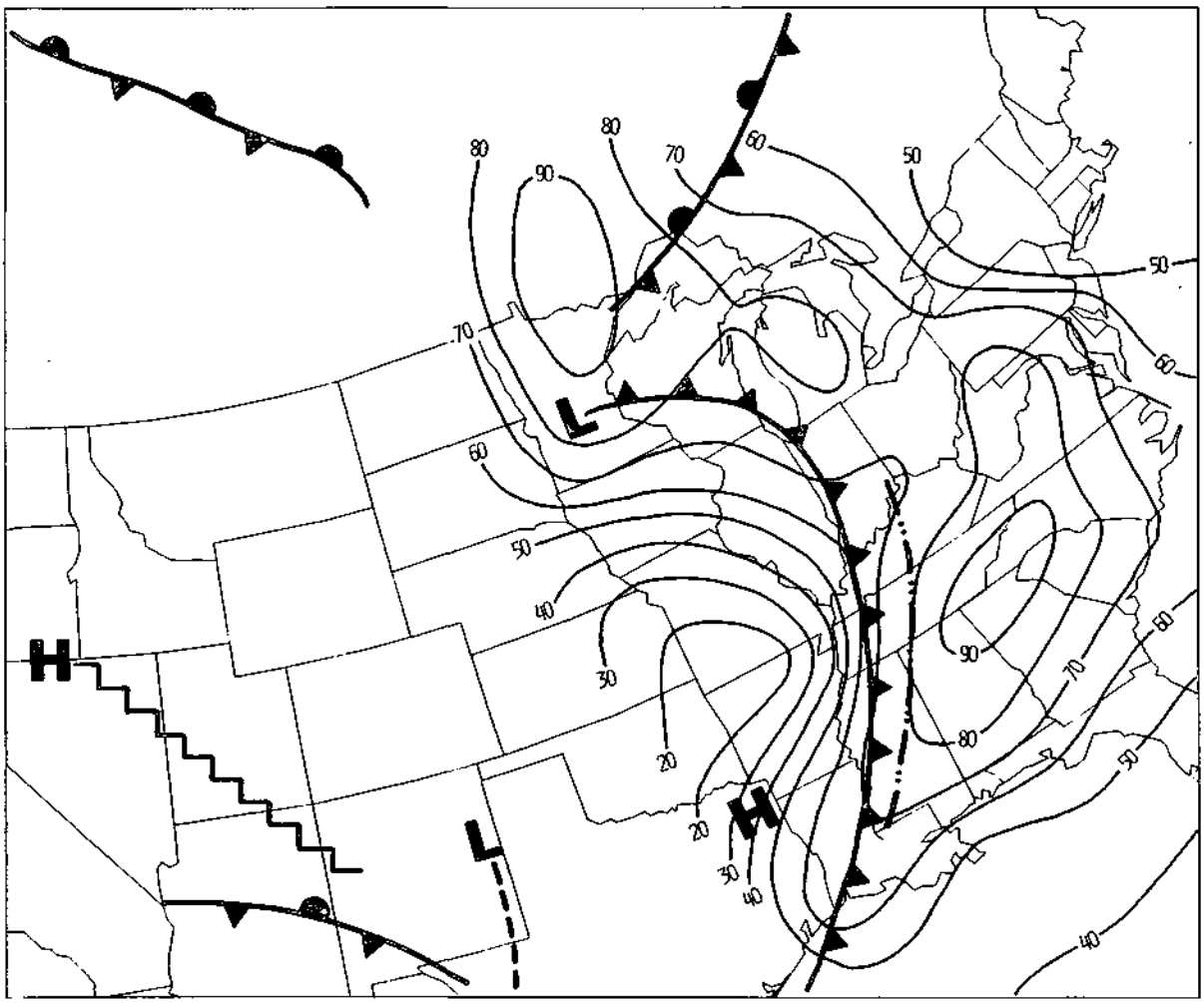

Figure 23. Relative humidity at 750 mb for 12 GMT 13 April 1964.

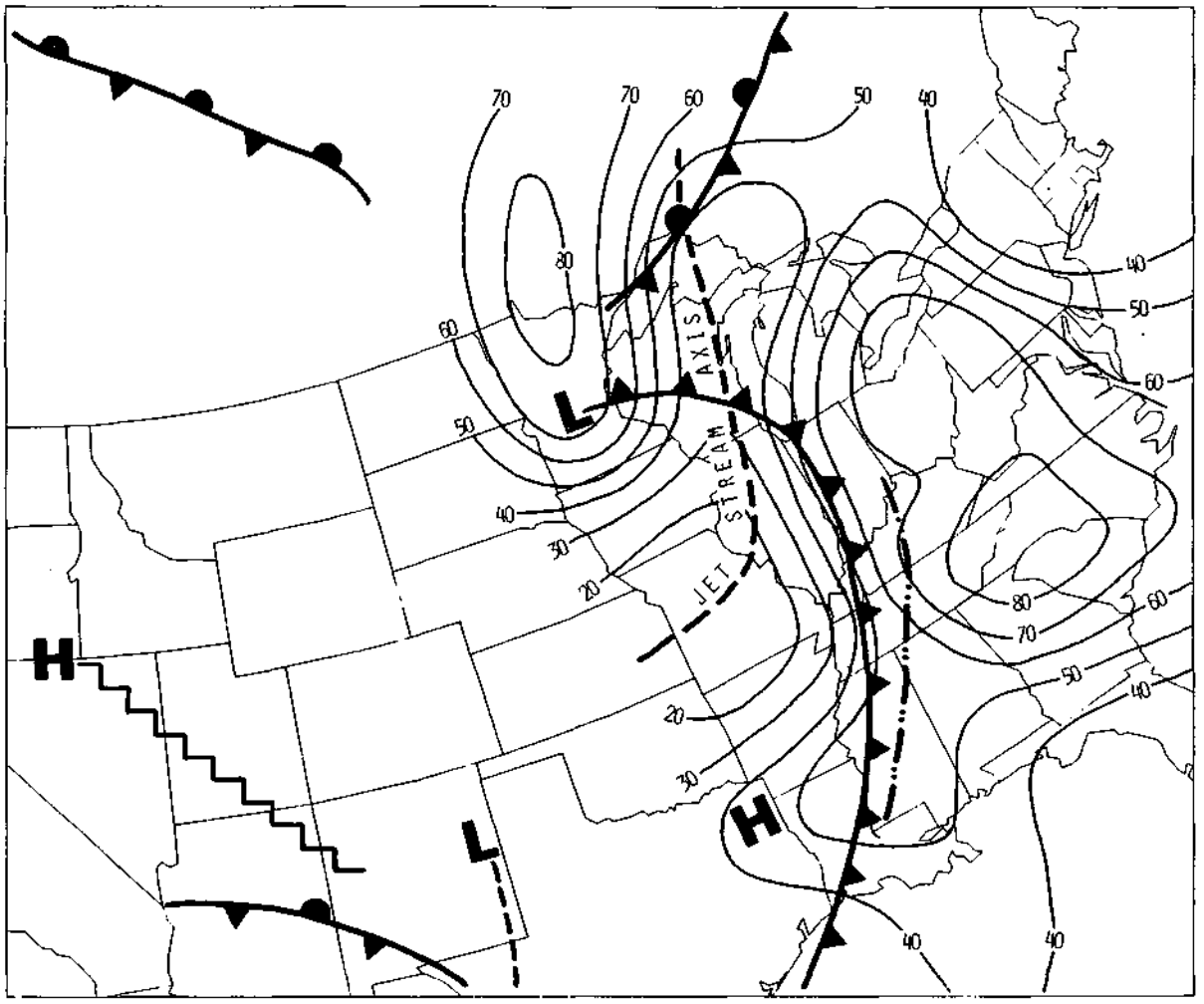

Figure 24. Relative humidity at 600 mb for 12 GMT 13 April 1964.

significant precipitation was retarded and the minimum appeared in the prefrontal rainfall distribution as shown in figure 13.

The pattern recognition provided a crucial test of the realism of the variational analysis. Vertical motion patterns associated with the major cyclone and its frontal system differed from the 12 forcing function balanced omega vertical motion field (Krishnamurti, 1968) which had been used as the standard for comparison. The variational analysis gave a 4 cm s^{-1} vertical velocity north of the major cyclone as compared with an 8 cm s^{-1} vertical velocity for the balance model. However, approximately 50% of the balance vertical velocity was derived from the latent heat parameterization - a term neglected in the dry variational formulation. Ascent over Wisconsin and Michigan ahead of the front was replaced by subsidence in the variational model. Detailed analyses of the three-dimensional wind and relative humidity fields in relation to a schematic jet stream model support the hypotheses that the subsidence was physically realistic and was associated with the mid-tropospheric jet stream. Finally, the variational analysis introduced a center of strong rising motion along the prefrontal squall line. These vertical motions should be taken as representative of the net vertical mass displacements on the scale of the observations. Local vertical mass transports within the convective elements of the squall line cannot be estimated by this analysis.

The general conclusion is that the variational vertical velocity patterns are physically reasonable with regard to the scale of the observation network. The apparently anomalous patterns can be explained by known weather circulations. The variational model has provided spatial resolutions not apparent with the balance model.

7. Results: Tendency Term Formulation

This section addresses the question as to what role the tendency term subsidiary variational formulation plays in the final adjustment when quasi-geostrophic scale theory is violated. The results obtained from several tendency term formulations are summarized. All of these formulations produced fields of u, v, and a tendencies. Since no short range (0-3 h) verification tendencies were available for the 13 April 1964 case study, the following approaches were used to evaluate the performance of the tendency term formulations.

1) Pattern recognition techniques were used to compare adjusted u, v, and cr fields with the corresponding observed fields. Several of the tendency term formulations altered these fields in an unrealistic manner. Further, locations of tendency patterns and their signs with respect to the locations of the major storm and the jet stream were qualitatively revealing.

2) Tendency magnitudes were directly evaluated by orders of magnitude to address the question: Are the implied rates of change too large to be physically realistic?

3) Tendency term magnitudes were investigated for realistic changes in areas where the progression of meteorological events indicated little or no changes over a fairly long period of time. Thus there were some areas within the fields where the expected tendencies were approximately zero. These areas provided "local verification data."

The tendency term subsidiary variational formulation developed by Achtemeier (1975) serves to overcome two potentially serious drawbacks of the primary variational formulation. These are the problems of closure and explicit tendency term formulations. First, in a strong-constraint variational formulation such as proposed by Sasaki (1970), there can be a maximum of N-1 strong constraints to be satisfied exactly for N variables to be adjusted.

The primitive equations form a closed set of five equations with five unknown variables. If the five variables are to be adjusted, then there must be only four primitive equation strong constraints. The remaining primitive equation must be carried as a weak constraint, which is satisfied approximately, or not carried at all. This equation would not be satisfied by the initial state; the forecast could become contaminated with high frequency oscillations.

Second, use of the primitive equations with their explicit representations for time variations of meteorological quantities in a variational initialization model requires an adequate formulation for the tendency terms in a manner consistent with spatial terms at the synoptic time. Most marked intensification of cyclones usually occurs within the space of 6 to 12 h which is barely detectable with a 12 h sampling frequency. Though the standard sampling frequency appears sufficient to give an overview of the evolution of a cyclone, it is not capable of giving acceptably accurate estimates for rates of development on a point-to-point basis.

Local tendencies can be incorporated into the variational analysis by fixing them and assuming that generated error will not appreciably contaminate the solution. But this ignores the fact that the tendency terms are of the same order of magnitude as the advection terms and that generated error undoubtedly will contaminate the solution, especially the error sensitive divergence calculations.

The tendency term subsidiary formulation incorporates the divergence equation as a strong constraint. The variables to be adjusted are the previously adjusted u, v, and $\dot{\sigma}$ obtained from the four primitive equation (primary) variational analysis. The divergence at each sigma-layer is computed and converted to vertical velocity by vertical integration of the divergence

theorem. Generally, the vertical velocity does not vanish at the top of the model - a boundary requirement if the divergence theorem is to be exactly satisfied. The velocity components are adjusted by a variational technique developed by O'Brien (1970) so that the vertical velocity does vanish at the top of the model. There remains a residual between the adjusted and previously adjusted velocity components that must be included in the primary variational model adjustments at the next cycle. This is accomplished if it is assumed that the residuals exist because the tendency terms in the forcing functions from which the adjusted velocity components were computed had been improperly specified. The residuals then are expressed as tendency corrections which are added to the tendencies carried in the forcing functions F_6, F_7, and F_8 (see (18)-(20)). When the primary variational model is run again, the new tendencies contribute to the adjusted velocity fields. This is a part of a cyclical process in which the two variational models are run until the solution stabilizes.

The subsidiary formulation completes closure and provides a means for calculating tendency terms as part of the variational balance. Since the tendencies are not included in the adjustment in a least squares formulation as are the observed variables (including vertical velocity), the tendencies may be free to assume unrealistic values which are necessary to bring about a balance between the observed variables but can be an accumulation of analysis discrepancies. Thus, in evaluating the overall performance of the variational initialization, it must be known how the tendency term subsidiary variational formulation contributes to the final solution under conditions of rapid cyclogenesis.

The quantitative description of the subsidiary variational formulation is as follows. Let

$$\frac{\partial \dot{\sigma}}{\partial \sigma} = -M_{4x} \tag{28}$$

where

$$M_{4x} = \frac{\partial u}{\partial x} + \frac{\partial v}{\partial y} + R_0^2 \frac{\omega_s}{P_s - P_u} - 2R_2(\varepsilon u + \delta v). \tag{29}$$

Integrating (28) along a grid column from the surface to the upper pressure level gives

$$\dot{\sigma}_K = \dot{\sigma}_s - \sum_{k=2}^{K} D_k \,, \tag{30}$$

where D_k is the mean divergence with the kth layer and is given by

$$D_k = \frac{\Delta\sigma}{2} [M_{4x_k} + M_{4x_{k-1}}]. \tag{31}$$

Note that $\dot{\sigma}_k$ derived from the continuity equation will be typically unequal to $\dot{\sigma}$ obtained from the energy equation. Since the layer integrated divergence seldom goes to zero at the top of the model, the vertical velocity $\dot{\sigma}_K \neq 0$. O'Brien's (1970) method leads to the solution for the divergence adjustment:

$$D_k' - D_k = [-\overline{\Pi}_{1k}^{-1} / \sum_{i=2}^{k} (\overline{\Pi}_{1i})^{-1}][\dot{\sigma}_K - \dot{\sigma}_s + \sum_{i=2}^{k} D_i] \,, \tag{32}$$

where $\overline{\Pi}_{1k} = \frac{1}{2} (\Pi_{1k} + \Pi_{1k-1})$ is the precision modulus which weights the divergence adjustment according to the measurement accuracy of the horizontal wind. The corresponding $\dot{\sigma}$ adjustment is

$$\dot{\sigma}_k' - \dot{\sigma}_k = [-\sum_{i=2}^{k} (\Pi_{1i})^{-1} / \sum_{i=2}^{k} (\overline{\Pi}_{1i})^{-1}](\dot{\sigma}_K - \dot{\sigma}_K') \tag{33}$$

where $\dot{\sigma}_K' \equiv 0$ is the upper boundary condition for the model.

After finding these adjusted quantities, they must be compared with the primitive equation variation. In accordance with the assumptions stated above, the specific volume tendency should be modified in such a way that when the energy equation is solved for $\dot{\sigma}$, (33) would be satisfied. Thus, at level k,

$$\frac{\partial \alpha'}{\partial t} = \frac{\partial \alpha}{\partial t} + \sigma_\sigma(\dot{\sigma}_k' - \dot{\sigma}). \tag{34}$$

The horizontal velocity component-adjusted tendencies are somewhat harder to find. From (31) the divergence adjustment is related to the weak constraint by

$$D'_k - D_k = \frac{\Delta\sigma}{2}\left[M'_{4x_k} - M_{4x_k} + M'_{4x_{k-1}} - M_{4x_{k-1}}\right]. \tag{35}$$

An adjustment velocity potential X_d, is defined as

$$\begin{aligned} u'_k - u_k &= u'_k - u = \frac{\partial \chi_d}{\partial x}, \\ v'_k - v_k &= v'_k - v = \frac{\partial \chi_d}{\partial y}, \end{aligned} \tag{36}$$

and the combination of (35) and (36) gives a second-order elliptic partial differential equation in X_d,

$$\nabla^2 \chi_d - 2R_2\left(\epsilon\frac{\partial \chi_d}{\partial x} + \delta\frac{\partial \chi_d}{\partial y}\right) = \frac{2}{\Delta\sigma}(D'_k - D_k) - F_{k-1}, \quad k = 2(1)\ k \tag{37}$$

where F_{k-1} has the same form as the left hand side of (37) except taken at the k-1 level. All quantities on the right hand side of (37) are known because the observed surface divergence is uncorrected, i.e., $\chi_{ds} = 0$ for all grid points and the solution sequence proceeds from the lower boundary upward. Equation (37) is solved by using standard successive over-relaxation methods. Lateral boundary conditions are $\chi_d = 0$; i.e., no velocity adjustment along the boundaries.

Modified velocity tendencies as obtained through the momentum equations are

$$\frac{\partial u'}{\partial t} = \frac{\partial u}{\partial t} + \frac{1}{R_0}\frac{\partial \chi_d}{\partial y}, \tag{38}$$

$$\frac{\partial v'}{\partial t} = \frac{\partial v}{\partial t} - \frac{1}{R_0}\frac{\partial \chi_d}{\partial x}. \tag{39}$$

This subsidiary formulation is not a mutual balance between the horizontal velocity components, u and v, and the vertical velocity $\dot{\sigma}$. Rather the divergence is adjusted (ultimately the velocity components are adjusted) so that the vertical velocity $\dot{\sigma}_K$, computed from the vertical integration of divergence, vanishes at the upper boundary. The subsidiary vertical velocity $\dot{\sigma}_k$ has not been adjusted with respect to the $\dot{\sigma}$ computed from the energy equation. The $\dot{\sigma}$ is set equal to $\dot{\sigma}_k$ and the residual is transferred to the specific volume tendency $\partial\alpha/\partial t$ through (34). This method forces the vertical velocity into a balance with the adjusted horizontal wind components. This approach is tractible since the mass field should be brought into adjustment with the wind field for small synoptic and subsynoptic motion scales (Washington, 1964). (It is

theoretically possible to variationally balance u, v, and $\dot{\sigma}$ through the divergence theorem. This was done as part of this study, however, this approach failed because there exists no practical way to derive $\dot{\sigma}$ in the absence of specifications for $\partial\alpha/\partial t$. This conclusion is based on a mutual adjustment for the 3 velocity components which produced unrealistic final vertical velocity fields as judged from pattern recognition.)

Several runs with the primary variational model showed that the solution sequence proceeded more smoothly if first guesses of the u and v tendencies were provided instead of setting the tendencies initially to zero. The method (Method 1) which provided first guess tendencies for the variational analyses discussed in the foregoing sections consisted of computing each term of the appropriate momentum equation from the initial objectively analyzed unadjusted data and determining the tendencies as residuals. The vertical velocity was set to zero.

Fields of u and v tendencies calculated at each sigma level by Method 1 were compared with the tendencies generated as part of the final variational balance. The subsidiary variational formulation permitted greater divergence adjustments at the upper levels where the standard errors of observation for the wind were larger (see Table 1). Differences between initial and final tendencies also were largest at these upper levels. Figures 25 and 26 show, respectively, the level 5 $\partial v/\partial t$ for the initial and the final analyses. Both fields so show evidence for small scale irregularities. These would be expected to generate inertio-gravitational oscillations if these variational fields were used for an initial state for a numerical weather forecast model.

No major adjustments in the patterns and magnitudes of the large scale features were brought about by the subsidiary formulation. Both figures show

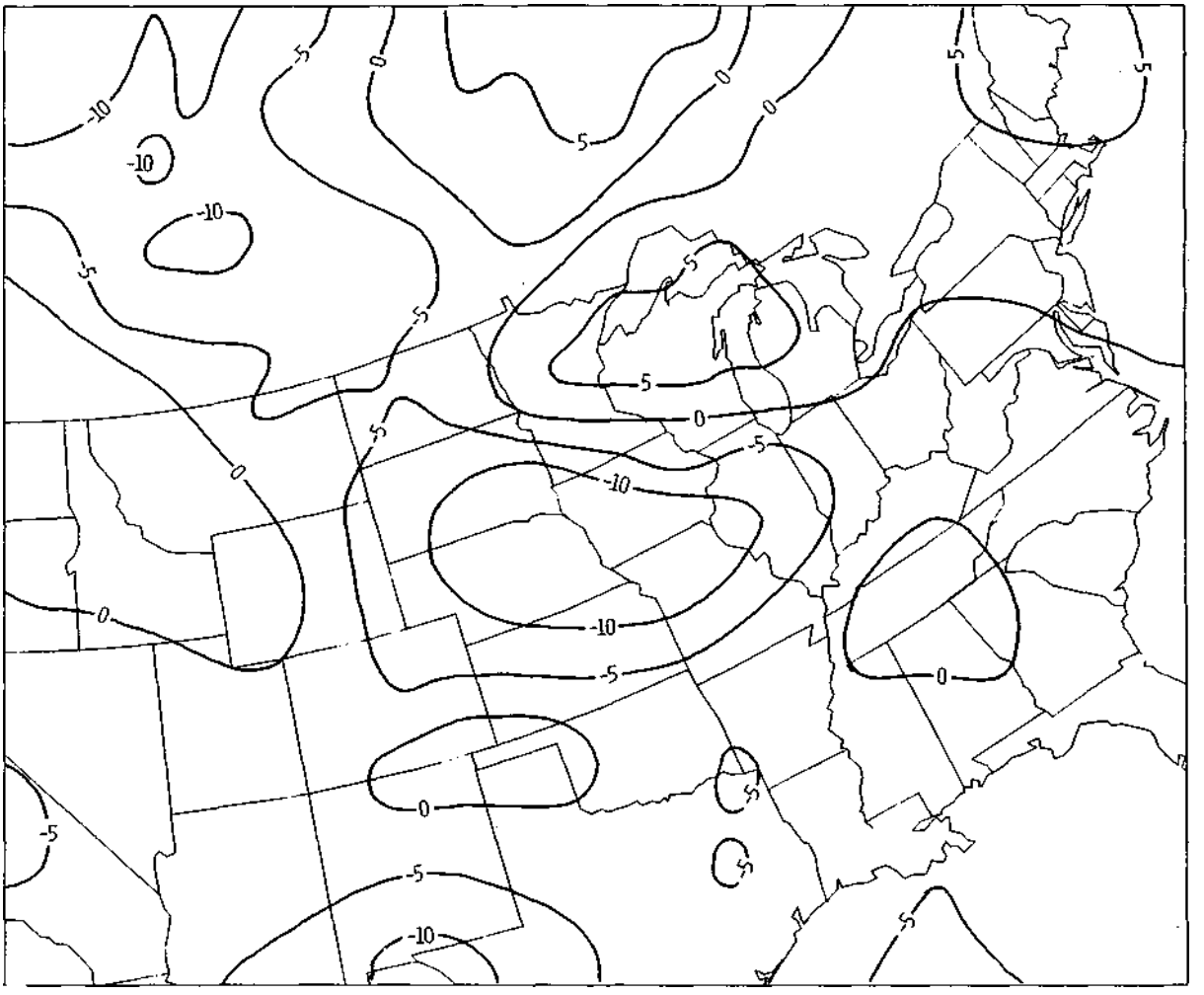

Figure 25. The level 5 $\partial v/\partial t$ Method 1 observed tendencies for 12 GMT 13 April 1964.

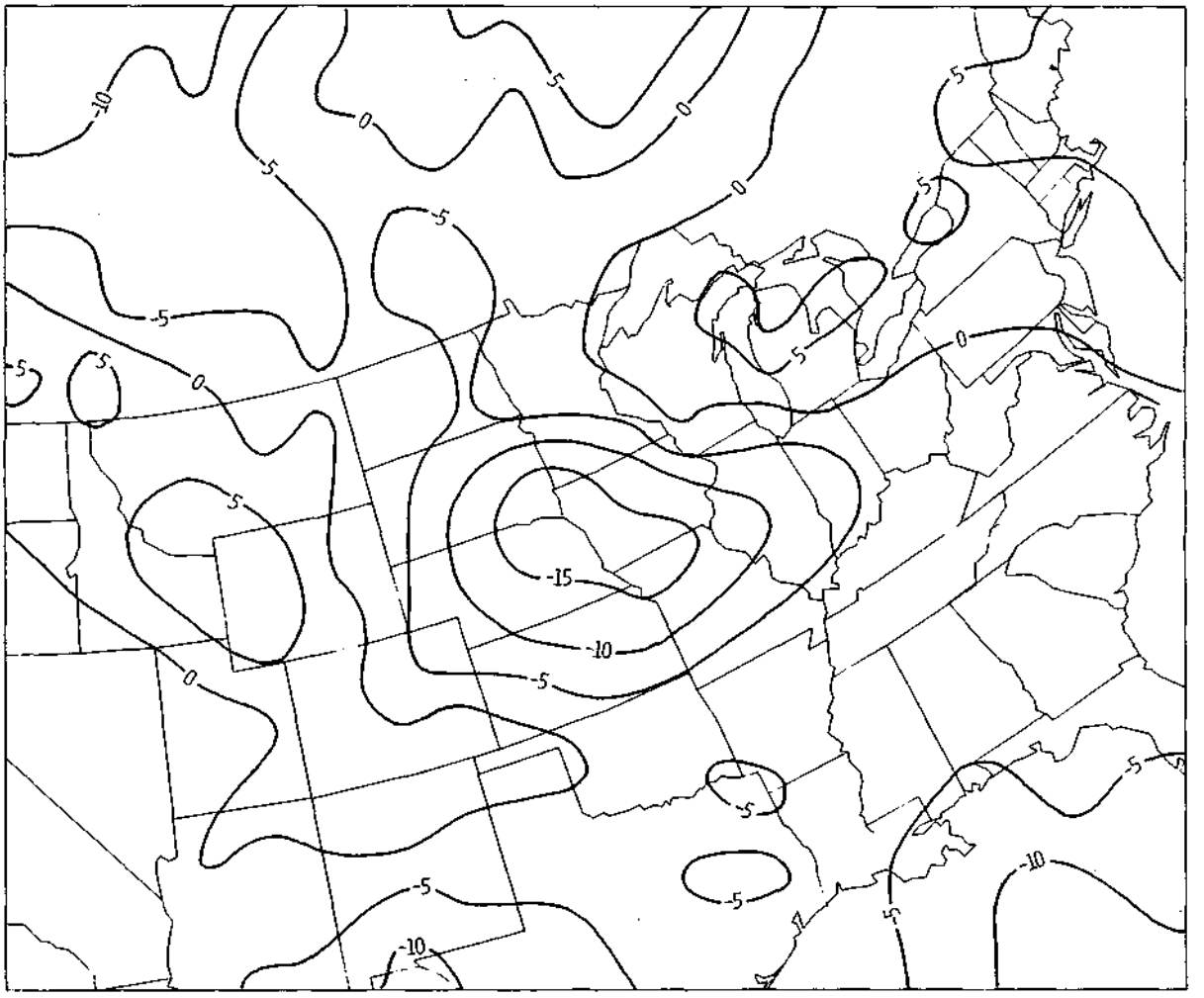

Figure 26. The level 5 $\partial v/\partial t$ Method 1 variational tendencies for 12 GMT 13 April 1964.

large negative tendencies from western Canada to Nebraska and Iowa. Large positive tendencies are found over the Great Lakes, New England, and the northwestern United States. Generally, the magnitudes are similar. According to quasi-geostrophic scale theory, the magnitudes of the tendency terms should be of the order one. However, as shown in both figures 25 and 26, the tendency magnitudes exceed 5 (order 10) over large areas.

Locally, the tendency terms could violate quasi-geostrophy within a strong rapidly developing cyclone. If such tendencies persisted for a long period of time very large changes in the wind field could result. For example, a nondimensional v-component tendency of 10 leads to a dimensional 12 h change in v of 43 m s^{-1}. A comparison between the 00 GMT 13 April and the 12 GMT 13 April level 5 wind fields revealed that maximum 12 h velocity component changes seldom exceeded 15 m s^{-1}. It is possible that such large tendencies operating over a shorter time period may have produced smaller, realistic component changes. Then it can be speculated that the tendencies became much smaller over the remainder of the period. For example, the $\partial v/\partial t = 10.0$ operating over a 3 h period would produce $\Delta v = 11$ m s^{-1}. Then a tendency of approximately $\partial v/\partial t = 1.0$ could account for the remainder of the change in v.

The pattern comparison method easily puts such speculations to flight even in the absence of direct tendency measurements. Portions of the wind component fields where the speeds were less than 5 m s^{-1} and where the progression of meteorological events was such that the wind field underwent little change in 12 h were sought out to establish that the local tendencies were small ($\partial v/\partial t \sim 1.0$). Method 1 initial tendencies and the variationally balanced tendencies were found to be an order of magnitude too large in some of these areas. Therefore it must be concluded that the Method 1 tendencies included

gross error locally. Further, since the variational adjusted tendencies did not depart greatly from the initial tendencies, but maintained these errors, the approach that led to the subsidiary variational formulation is placed in jeopardy. A critical analysis of the computer algorithms that generate the tendencies has thus far not led to the discovery of any errors in programming. Clearly more work is necessary to tie down the tendency term problem and to demonstrate that the variational approach as outlined in this paper is a worthwhile approach to the initialization of numerical weather prediction models.

Further investigation of the relationship between the wind field and the Method 1 tendency term formulation revealed that the first guess tendency magnitudes could be reduced by the inclusion of the vertical shear terms of (1) and (2) in the first guess tendencies. These terms are usually small but large vertical wind shears were found along the het stream. Some means for estimating the vertical velocity is required in order to specify the vertical shear terms. Call the new first guess tendency formulation Method 2.

Solve (3) for the specific volume tendency and the vertical velocity to find the residual RM_s.

$$RM_3 = -R_o \frac{\partial \alpha}{\partial t} + \dot{\sigma}\,\sigma_\sigma = R_o\left(u\frac{\partial \alpha}{\partial x} + v\frac{\partial \alpha}{\partial y}\right) + R_1\left(u\frac{\partial \alpha_T}{\partial x} + v\frac{\partial \alpha_T}{\partial y}\right)$$
$$+ R_o\,\dot{\sigma}\left(\frac{\partial x}{\partial \sigma} + \alpha\frac{p_s - p_u}{\gamma p}\right) + R_o\frac{\sigma_{\alpha_r} w_s}{\gamma p} + R_o R_2\frac{\sigma_{\alpha_T} w_s}{\gamma p}\,. \tag{40}$$

Initially, $\dot{\sigma}$ in the third right hand side term is set to zero. A first guess at $\dot{\sigma}$ is obtained from RM_3 via

$$\dot{\sigma} = \frac{RM_3}{2\sigma_\sigma}\,. \tag{41}$$

Here the residual has been partitioned equally between the specific volume tendency and the vertical velocity. The value of $\dot{\sigma}$ from (41) is substituted into term 3 of 40 and RM_3 calculated again. A second estimate for $\dot{\sigma}$ is obtained from (41) and is used for the calculation of the vertical shear terms in Method 2.

The variational model was rerun with first guess tendencies computed by Method 2. The tendency fields were also filtered to remove the small scale features. The final balanced $\partial v/\partial t$ at level 5 (fig. 27) should be compared with the Method 1 final tendencies in figure 26. The large positive tendencies that were found along the jet stream axis from Washington to Wyoming (fig. 5) were decreased in magnitude as were the large negative tendencies located over Nebraska and Iowa. Elsewhere, except for the removal of small scale wiggles, the tendency magnitudes were largely unchanged. Tendency magnitudes in areas of light wind speeds and small 12 h changes were an order of magnitude too large. Therefore the conclusions drawn with regard to the Method 1 tendencies apply to the Method 2 tendencies.

The use of Method 2 in place of Method 1 in the variational adjustment had little effect on the final adjustments of the observed variables u, v, a, (J) as shown in Table 3. Root-mean-square residuals between the variational analyses and the initial obj ective analyses for these variables were virtually identical for the two methods.

The use of Method 3 demonstrated that the variational analysis is sensitive to the specification of the tendency term formulation. In Method 3 the initial tendencies for u, v, and a were assigned to zero. Further, these tendencies were forced to remain zero through the first 4 cycles where the bulk of the variational adjustment is largely fixed. (Figure 10 shows that

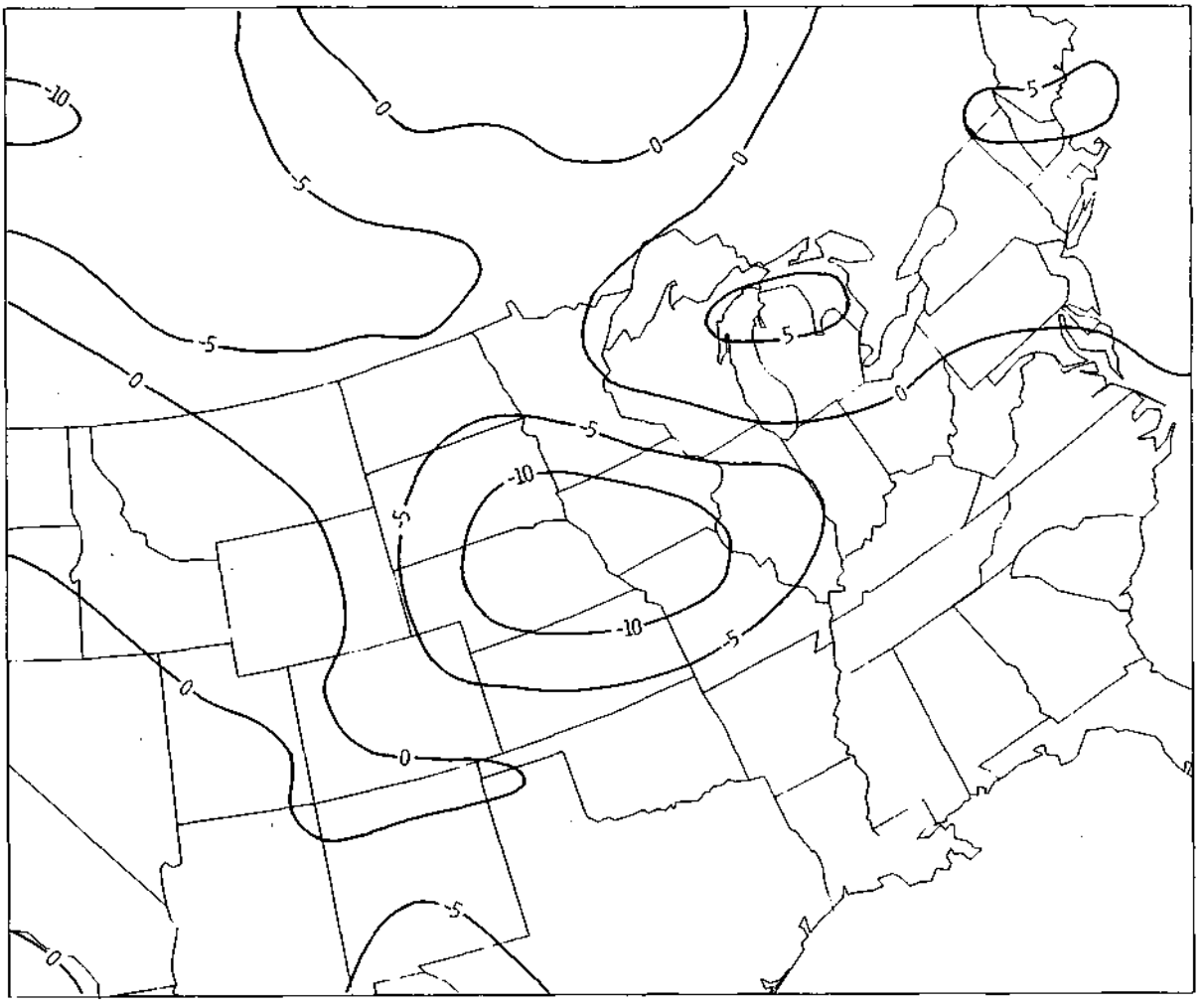

Figure 27. The level 5 $\partial v/\partial t$ Method 2 variational tendencies for 12 GMT 13 April 1964.

only minor rms variations from the fields established in the first few cycles are found.) The subsidiary variational formulation had no input to the adjustment until cycle 5. At cycle 5 the constraint on the tendencies was removed and the tendencies were modified to satisfy the divergence constraint.

A comparison of Method 3 level 5 (fig. 28) $\partial v/\partial t$ with the v-component tendencies in figures 25-27 shows a profound alteration brought about by requiring the tendencies to vanish through the first 4 cycles. Method 3 tendencies are much smaller than tendencies estimated by the first two methods. However, Method 3 tendency patterns do not occur on the scale of the weather systems found in the wind field (compare with fig. 5). The large area of negative tendencies that covers the middle of the analysis grid seems to have little correspondence with the major storm or the jet stream. Further, the rms residuals between the variational analysis and the initial analysis (Table 3) have been largely increased for the velocity components and the geopotential height. This means that the adjustment required to satisfy the primitive equation constraints was much larger when the tendency terms were forced to zero. Reasons for the rms decreases for the specific volume were not sought because the specific volume was accorded small relative weights in the adjustment.

The Method 3 alterations were clearly evident in the horizontal wind field and in the vertical velocity. For space saving purposes, only the vertical velocity patterns for level 5 are presented for pattern comparison. The magnitudes of the vertical velocity patterns (fig. 29) have been reduced. The 4 cm s^{-1} rise center associated with the storm over Minnesota (fig. 12) is only 2 cm s^{-1} in figure 29. The 6 cm s^{-1} rise center near the prefrontal squall line has been diminished to 2 cm s . Further, the axis of rising

Table 3. Rms Residuals between the Variational Analysis and Initial Objective Analysis of u, v, α, Ø for Three Methods used to Compute Tendency Terms.

	Method					
u-comp	1	2	3	2a	2b	2c
2	.11	.14	.43	.13	.14	.09
3	.12	.14	.30	.12	.12	.13
4	.18	.18	.36	.14	.14	.19
5	.28	.28	.44	.20	.20	.30
6	.30	.27	.52	.23	.23	.35
v-comp						
2	.12	.15	.35	.11	.13	.09
3	.12	.12	.25	.09	.10	.16
4	.19	.18	.31	.13	.14	.25
5	.26	.26	.47	.20	.22	.32
6	.32	.32	.57	.27	.26	.45
Specific Volume						
2	1.32	1.29	.84	1.24	1.30	.56
3	1.20	1.18	.72	1.33	1.33	.60
4	2.60	2.56	1.36	2.64	2.65	.72
5	2.68	2.70	1.49	2.57	2.41	1.07
6	2.77	2.83	2.34	2.99	2.93	1.90
Height						
2	.10	.09	.11	.06	.06	.07
3	.11	.11	.16	.08	.05	.10
4	.14	.15	.19	.10	.06	.16
5	.21	.21	.25	.11	.08	.20
6	.26	.26	.29	.17	.10	.27

motion has been shifted to behind the front and has been located from Iowa through Missouri and Arkansas. Rising motion over Missouri replaces centers of sinking motion greater than -3 cm s^{-1} evident in both the Method 1 variational analysis and in Krishnamurti's 12 forcing function balance model. Thus, since the Method 1 patterns are physically realistic with respect to the meteorological disturbances discussed in Section 6, it must be concluded that the Method 3 patterns are physically unrealistic and Method 3 should be discarded as a tendency term formulation.

The tendency term subsidiary variational formulation affects the final adjusted fields through the magnitudes of the tendencies and the method by which the tendency calculations are controled. Method 1 and Method 2 led to physical realism that was as good as could be determined from pattern recognition techniques. However tendencies found by both methods were an order of magnitude too large in areas where the progression of weather events required small tendencies over a 12 h period. It is expected that the use of such fields in a numerical weather prediction model would lead to degenerative results. Method 3 led to smaller tendency magnitudes but failed the test of physical realism. Thus a method that retains physical realism in the variational initial state of the model described in this paper and develops tendency terms that are realistic from the standpoint of scale analysis has not yet been found.

8. The Moisture Parameterization for Large Scale Stable Precipitation

Precipitation processes were neglected from the original variational model for matters of convenience. A dry model simplifies the task of evaluating convergence and magnitude of adjustment from observed fields for the expected

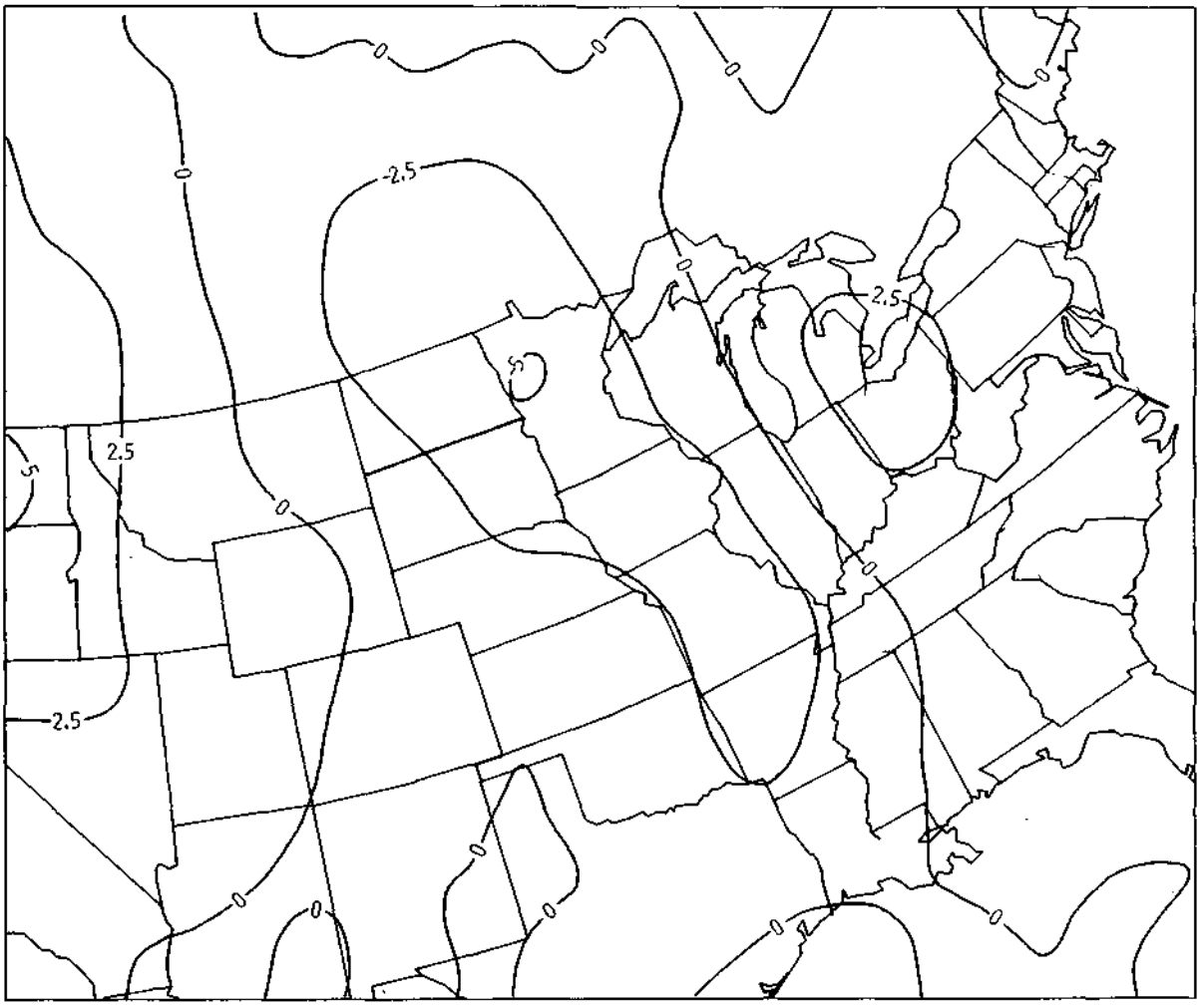

Figure 28. The level 5 $\partial v/\partial t$ Method 3 variational tendencies for 12 GMT 13 April 1964.

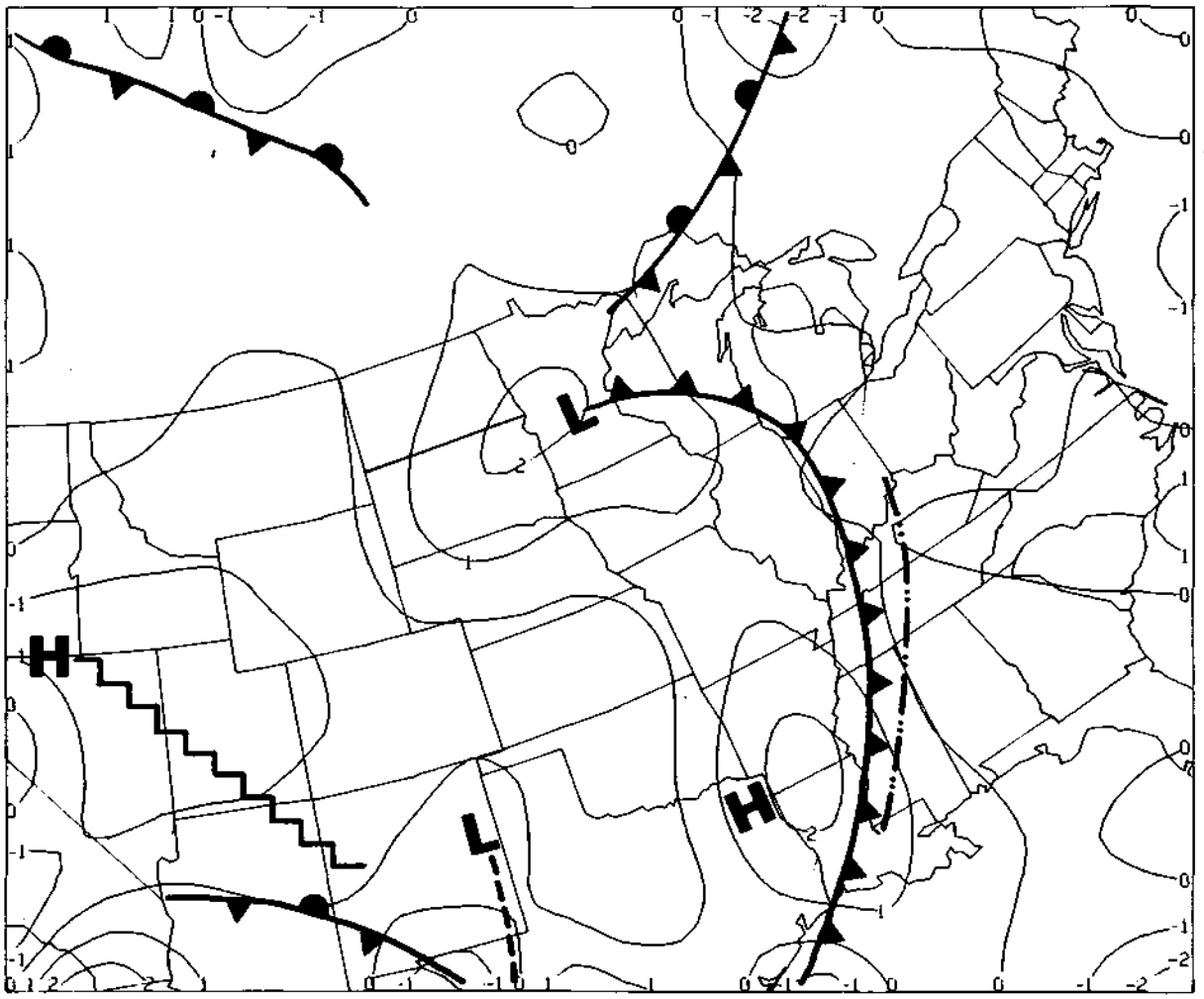

Figure 29. Sigma level 5 (455 mb) vertical velocity (cm s^{-1}) from the variational analysis with tendencies determined by Method 3.

range of meteorological systems. These evaluations have covered an instance of weak cyclogenesis (Achtemeier, 1975) and the case of intense cyclogenesis discussed in this paper. The inclusion of precipitation processes was not expected to change the conclusions regarding the tendency term formulation discussed in the previous section; the precipitation was confined to relatively small areas within the analysis grid.

The diabatic term that corresponds to the dimensionless form of the energy equation (3) is

$$DIA = \left[\frac{R_o^2\ PL}{Cg\ HF}\right] \frac{\alpha}{c_p T} \frac{dQ}{dt} \quad . \tag{42}$$

Aside from the Rossby number, the letters in brackets represent characteristic scales and are defined as follows:

P ~ 1000 mb characteristic pressure,
L ~ 10^6 m characteristic length,
C ~ 10 m s^{-1} characteristic velocity,
H ~ 10^4 m characteristic height,
g ~ 10 m s^{-2} gravitational acceleration,
F ~ 10^{-3} Froude number.

For stable precipitation

$$\frac{dQ}{dt} = \ell \dot{\sigma} \frac{\partial q_s}{\partial \sigma} \tag{43}$$

where *Si* is the latent heat of condensation and q_s is the saturation mixing ratio. Substituting the equation of state, (42) becomes

$$DIA = \left[\frac{R_o^2\ PL}{Cg\ HF}\right] \frac{R\ell}{c_p} \frac{\dot{\sigma}}{p} \frac{\partial q_s}{\partial \sigma} \quad . \tag{44}$$

The characteristic scale for q_s is 10^{-2} gm/gm and $\dot{\sigma} \sim R_o \frac{C}{L} \dot{\sigma}'$ (Achtemeier, 1972). Therefore

$$DIA = \left[\frac{10^{-2} R_o^3}{gHF}\right] \frac{R\ell}{c_p} \frac{\dot{\sigma}'}{p'} \frac{\partial q_s'}{\partial \sigma'} . \qquad (45)$$

With $\ell = 600$ cal/gm, the term $R\ell/c_p = 7.2$ gH. Thus the diabatic heating term is given by

$$DIA = .72 R_o \frac{\dot{\sigma}}{p} \frac{\partial q_s}{\partial \sigma} \qquad (46)$$

where the primes have been dropped. Thus the diabatic heating term is one order of magnitude less than the static stability σ_σ in (3).

The release of latent heat due to stable precipitation was calculated where 1) the vertical motion was upward, and 2) the relative humidity was greater than 65%. The low value of relative humidity was chosen when it was found that the objective interpolation had smoothed out local relative humidity maxima. Once the latent heat was released, the precipitation fell out without affecting the moisture or heating at any other layer.

Since the subsidiary tendency term formulation forced the vertical velocity into balance with the adjusted horizontal wind field, the latent heating made no direct contribution to the vertical motion as it did in Krishnamurti's method. Instead, the latent heating was carried by the specific volume tendency. Thus the effect of the stable precipitation parameterization would be manifest in time as a local increase in temperature (specific volume) which would lead to an increase in the thickness of the layer and finally to a modification of the 3-dimensional velocity field. All this would occur in the process of time integration. For the initial fields, only the specific volume tendency was

changed by the inclusion of this term and these changes were confined to the ascent center located north of the major cyclone.

9. Additional Tests

a. Reweighted Precision Moduli

Tests to determine the sensitivity of the variational analysis to variations in the precision moduli that weight the observations in the adjustment yielded confusing results. It was expected that the increasing of the weight accorded to one of the observed variables would result in smaller adjustments from the observed fields for that variable and larger adjustments for the remaining variables. This was apparently not the case. Table 3 shows the rms residuals between the variational analyses and the initial objective analyses for the 3 tendency term subsidiary formulations. In addition, two analyses using reweighted precision moduli were run with Method 2. For run 2a, the precision modulus for the observed wind components, PI1, was increased by a factor of 10. The other precision moduli were not changed. A comparison of Method 2a with Method 2 rms residuals shows that the adjustments from the observed fields for u, v, and Ø have been decreased at all levels.

Next, the precision modulus weights for the geopotential height were increased by a factor of 10 and the other weights left unchanged. In comparison with Method 2, it was expected that the adjustments from the observed fields for the geopotential would decrease and the adjustments for the wind components would increase. The wind component rms residuals shown in Table 3 under Method 2b are essentially unchanged from run 2a while there has been a slight reduction of the rms residuals for the geopotential. Thus both test runs produced smaller adjustments from the observed fields than did the run for which the precision

moduli had been determined from realistic estimates for the standard observation error (see Table 1). No explanation for there findings has yet been found.

b. Specific Volume Correction

Systematic errors in the specific volume arose from using the hydrostatic equation as the constraint in place of the hypsometric equation. These errors were removed in the mean by adding a temperature correction for each level. The rms residuals for run 2c are summarized in Table 3. There is an obvious decrease in the specific volume rms residuals for the five adjustable levels. However the rms values for the velocity components increased above the values calculated for Method 2. The geopotential height rms values were essentially unchanged. These results indicate that the hydrostatic errors are functions of the spatial distribution of stability and cannot be removed from the analysis by a mean temperature error correction.

10. Vertical Velocity History for the Developing Storm: 00 GMT 12 April - 00 GMT 13 April 1964

The Method 2 variational analysis was run for the synoptic observations for the 36 h period prior to 12 GMT 13 April 1964 - the time of maximum intensity of the major cyclone. The purpose of this section is to document the evolution of the vertical velocity patterns with respect to the position of the mid-tropospheric jet stream, pressure centers, frontal zones, and precipitation patterns. This information has been extracted from other charts and presented in condensed form in the following figures. The fronts were located from detailed surface analyses and some disparity between these and the vertical motion fields calculated variationally from synoptic observations should be expected.

Figure 30 summarizes the weather events for 00 GMT 12 April 1964. There were three major weather disturbances over the analysis area at this time. A 993 mb low pressure center associated with a rapidly moving mid-tropospheric short wave was located along an arctic cold front north of Minnesota. The variational analysis developed a 3 cm s^{-1} ascent center for this system. This vertical motion pattern connected with the ascent center associated with the incipient major cyclone which was entering the analysis area over Nevada. Its accompanying surface frontal pattern extended from a weak 999 mb surface low over southern Montana to Nevada. The nose of the mid-tropospheric jet stream over Nevada separated rising motions on the cyclonic shear side from sinking motions on the anticyclonic shear side. Maximum vertical velocities in excess of 4 cm s^{-1} were found over Nevada and Utah.

The third weather disturbance was a weak upper level short wave located over the lower Mississippi valley. Maximum vertical motions exceeded 2 cm s^{-1} with this system. This system differed from the first two disturbances in that its vertical velocity center was located 600 km ahead of the surface low pressure center and its associated frontal system. This low was located under an area of subsidence according to the variational analysis. The upper level disturbance had moved ahead of the surface low, the low was dissipating and, after 00 GMT, it was no longer present in the surface pressure field.

The precipitation patterns (shaded areas in fig. 30) developed where there was sufficient moisture within areas of rising motion. The shaded areas enclose those stations reporting precipitation sometime during the 12 h period centered about 00 GMT. Precipitation amounts in the west were light with mostly trace amounts reported in Montana and Idaho. Light amounts were also reported over North Dakota, Wisconsin, and southern Canada. The disturbance in the

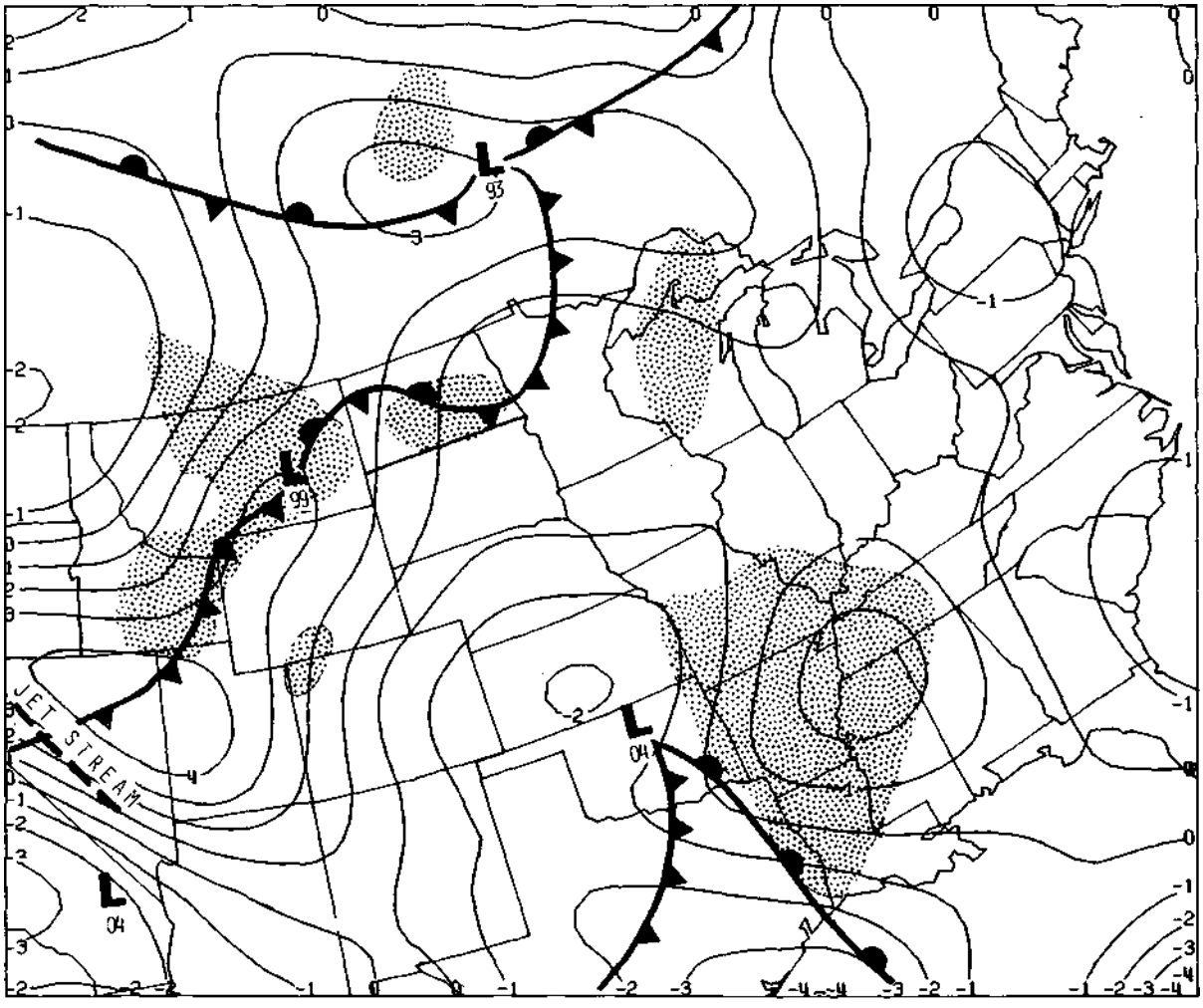

Figure 30. Summary of variational vertical velocity patterns, precipitation patterns (shaded) and the positions of low pressure centers and fronts for 00 GMT 12 April 1964.

south had been drawing upon ample moisture from the Gulf of Mexico. Though weaker than the storms to the west, it contained more moisture and amounts upto 0.5 in fell over Arkansas and Mississippi during the 12 h period.

By 12 GMT 12 April (fig. 31) the major storm had pushed to the high plains. Its elongated vertical velocity pattern extended from North Dakota to Northern Texas and eastward to merge with the weak disturbance over the lower Mississippi valley. A 995 mb low over South Dakota and a 994 mb low over southeast Colorado were connected by a cold front that extended southwestward into Arizona. Strong subsidence (-5 cm s^{-1}) over Utah was located beneath the intensifying mid-tropospheric jet stream. Precipitation associated with the major storm remained light with amounts generally less than 0.10 inch scattered through the central and northern plains. Amounts in excess of 1.00 inch fell over Mississippi in association with the weak mid-level disturbance. Much of this precipitation was convective in origin and the variational vertical motions under-estimate the magnitude of the vertical moisture transport. No precipitation was reported in conjunction with the lobe of vertical motion in excess of 3 cm s^{-1} over Oklahoma. Figure 30 shows that this rise center replaced a subsidence center of -2 cm s^{-1} located over the same area 12 h earlier. The objectively analyzed relative humidity fields showed that the relative humidity over Oklahoma and Texas increased from 20% to 40% - still much too dry to support precipitation.

Frontal positions, pressure centers, vertical motion, and precipitation patterns for 00 GMT 13 April are summarized in figure 32. During the previous 12 h period, the low pressure center located over southeastern Colorado moved to southeastern Nebraska and deepened by 2 mb. During the next 12 h this low will move to southern Minnesota and deepen 18 mb to a 974 mb central pressure.

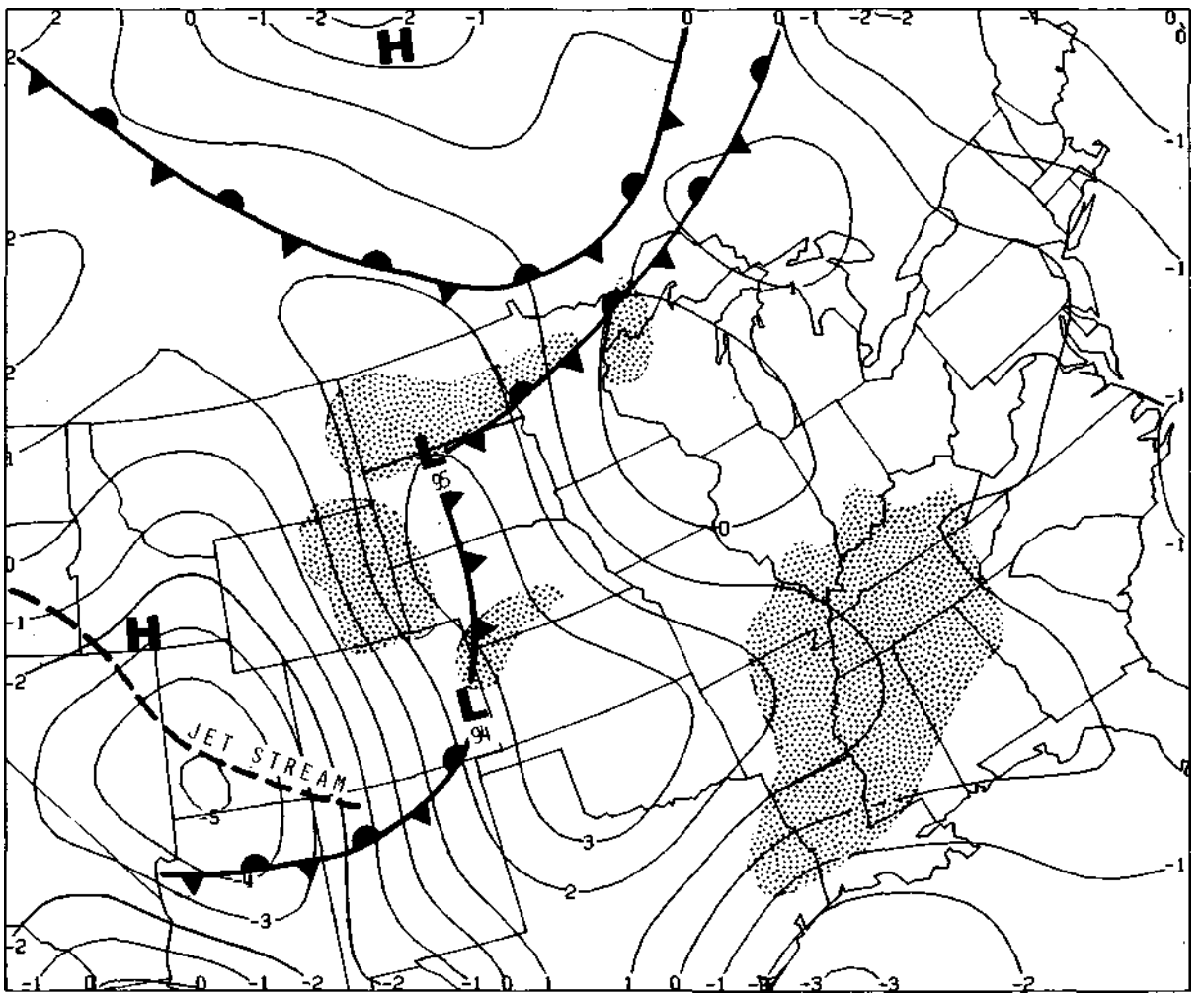

Figure 31. Same as in figure 29 except for 12 GMT 12 April 1964.

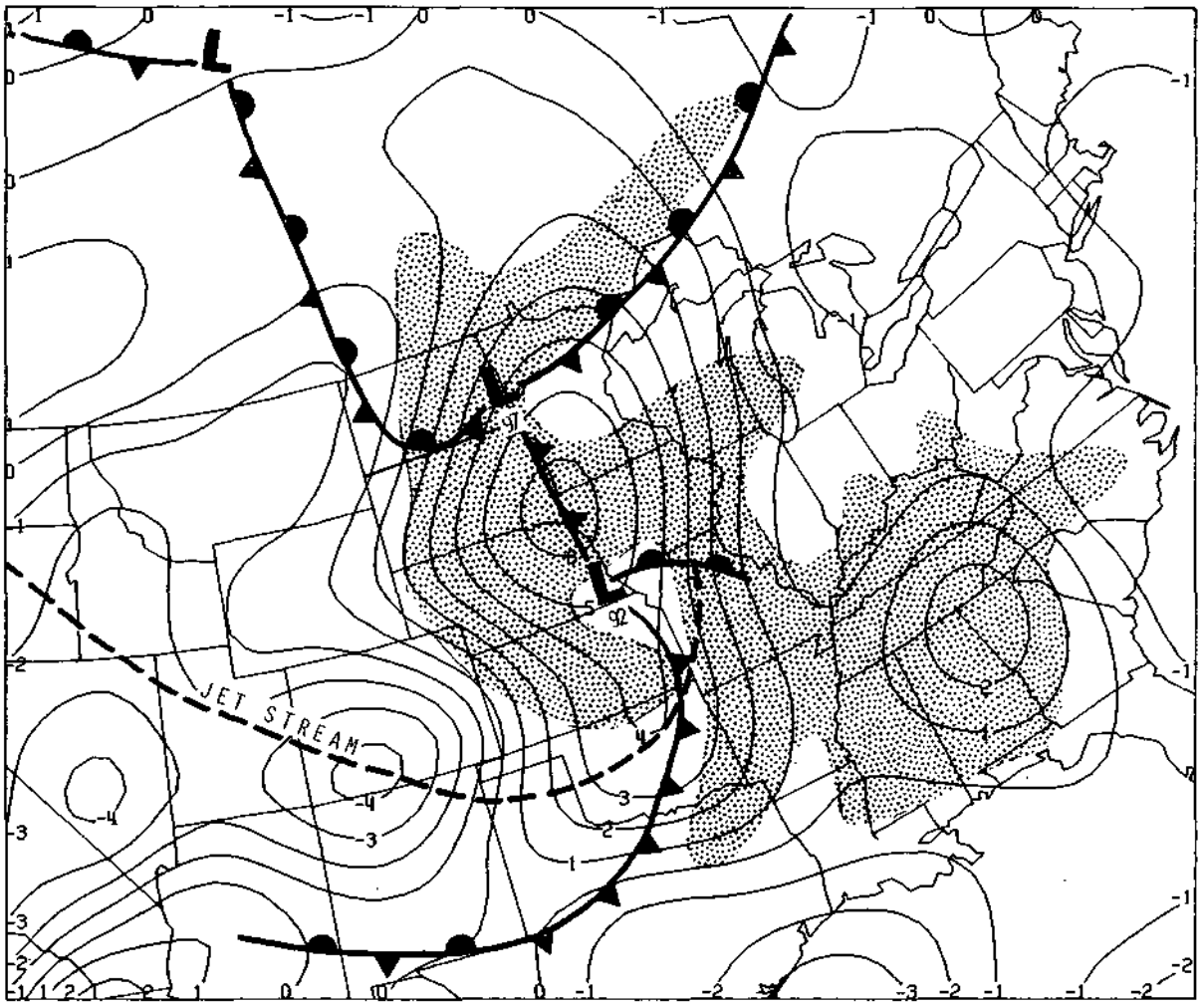

Figure 32. Same as in figure 30 except for 00 GMT 13 April 1964.

Figure 32 shows that the jet stream had reached the axis of the mid-level trough and was curving to the northeast. This combination of cyclonic curvature and strong cyclonic wind shear often leads to explosive cyclogenesis. The variational analysis placed a 6 cm s^{-1} ascent center just north of the surface low position. This was the largest vertical velocity associated with the storm center for all analysis times, including 12 GMT, 13 April and may be representative of the increase in vertical motion as part of the intense cyclogenesis.

Subsidence exceeding -4 cm s^{-1} found along and to the anticyclonic shear side of the mid-tropospheric jet stream from Oregon to New Mexico is in agreement with the modeled jet stream vertical motions as simulated in Section 6. The jet stream is embedded within rising motions along the remainder of its course from Texas to Missouri. This underlines the difficulty in interpretating the vertical motion fields when the jet stream motion field is superimposed upon the stronger vertical motion field of some other system. The ascent pattern over Kansas and Oklahoma has apparently been decreased in magnitude and areal coverage by the intrusion of subsidence from Colorado. The pattern shape contrasts with the vertical motion pattern 12 h earlier for which maximum areal coverage and magnitude were located over Oklahoma. During the 12 h following 00 GMT 13 April, the jet stream apparently split the ascent center and one center moved southeastward with the prefrontal squall line while the other moved northward with the developing cyclone.

The evolution of the precipitation patterns for the 12 h period was quite complex and is best viewed from figures 33 and 34 which show precipitation amounts for the 6 h periods ending at 00 GMT and 06 GMT 13 April 1964. The frontal patterns at these times are included also. Figure 33 shows that

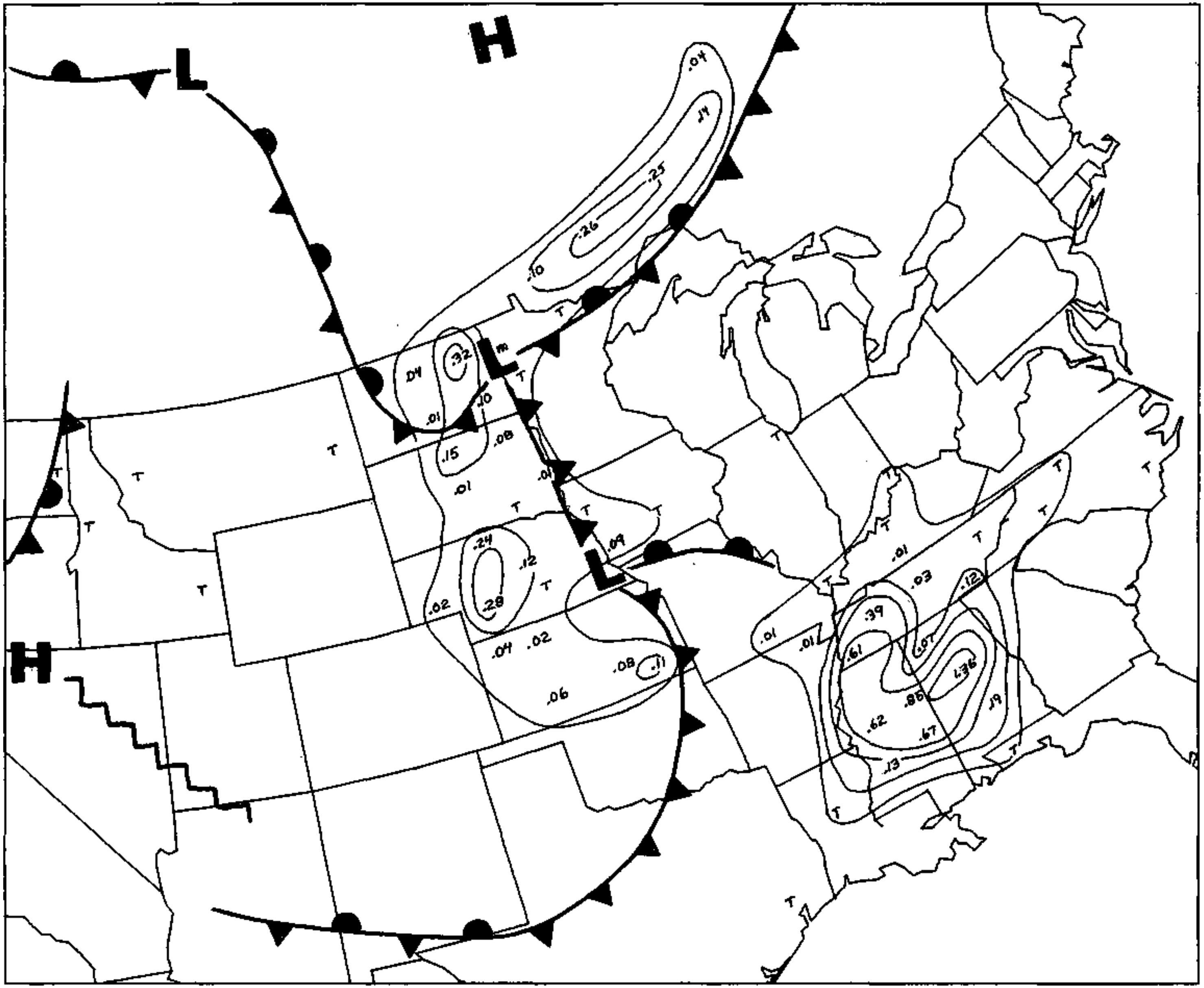

Figure 33. Fronts, pressure centers and 6 h rainfall for 00 GMT 13 April 1964.

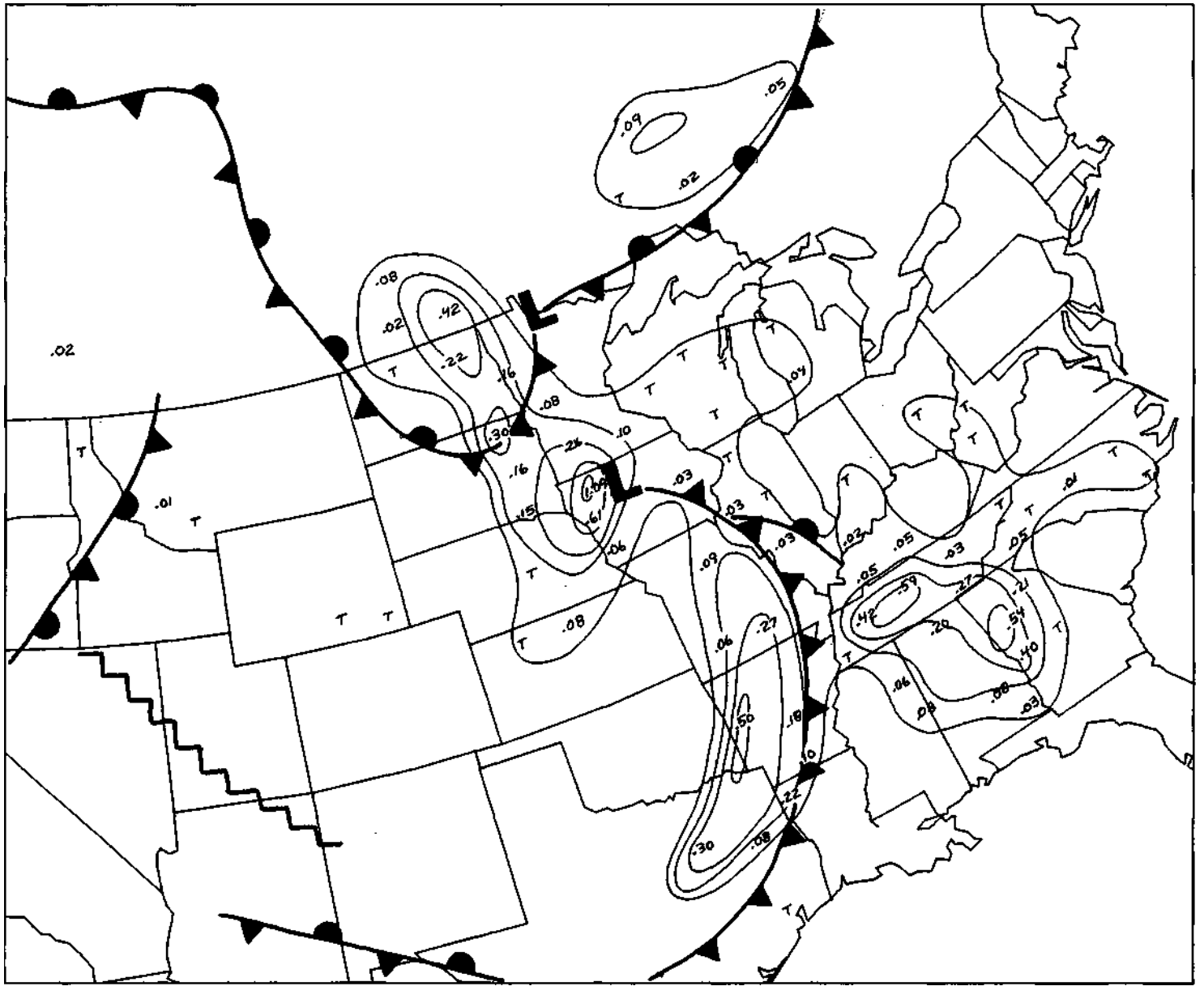

Figure 34. Fronts, pressure centers and 6 h rainfall for 06 GMT 13 April 1964.

precipitation was associated primarily with the incipient cyclone and with the dissipating short wave over the southern states. Copious amounts of rain fell with this convective disturbance. Lesser, but increasing, rainfall amounts were reported with the developing storm. It is noted that, during the 6 h period ending at 00 GMT 13 April, the frontal system had moved from the central Dakotas and Nebraska to the eastern parts of those states. Therefore the precipitation may have fallen along or slightly behind the front.

Between 00-06 GMT (fig. 34) heavy precipitation broke out in northwestern Iowa near the center of maximum vertical velocity calculated by the variational analysis. A second area of rainfall that broke out along the cold front from Missouri to Texas was the precursor to the prefrontal squall line observed at 12 GMT 13 April. A distinct minimum of precipitation between the two rainfall areas was found along the axis of the mid-tropospheric jet stream. A possible senario for the development of the vertical motion patterns for 12 GMT 13 April (fig. 12) is that the subsidence within the jet stream gradually dominated the rising motions over Missouri and Oklahoma (fig. 32) and the large ascent center associated with the major storm was split; one half continued northward with the major cyclone and the other half moved southeastward with the cold front and eventually with the prefrontal squall line.

The variational analyses presented for 00 GMT 12 April to 00 GMT 13 April 1964 reveal vertical motion fields that were consistent with the low pressure centers, frontal systems and precipitation patterns. These variationally derived motion fields are judged as realistic within the limitations of pattern recognition techniques. Further, the variational method is shown applicable to differing meteorological conditions.

11. Summary of the Performance of the Variational Model

This variational initialization model was developed by Achtemeier (1975) and applied to a case of weak cyclogenesis and slow movement of weather patterns. The versatility of the solution method which was based upon the expansion of terms of the constraining equations in powers of the Rossby number and treating the higher order terms as forcing functions was not determined by this case. Likewise, the effect of the tendency term subsidiary formulation upon the final balance was essentially unknown. Therefore, the study presented in this report was initiated to address these and other problem areas.

First, there were reservations as to whether the variational method would converge to a solution under conditions of rapid cyclogenesis that would cause the quasi-geostrophic approximation to be invalidated over large areas. The intense cyclogenesis on 13 April 1964 was selected as the test case. Although several associated problems remain to be worked out, it was found that the variational analysis stabilized to a solution. With one exception the rms residuals for the constraining equations either decreased to truncation levels or stabilized after significant residual decreases. For the one exception the final residuals were essentially the same as the initial residuals. Further, the final adjustments were realistic with regard to the standard errors of observation.

Secondly, the variational analysis includes the observed winds directly. Thus it should be possible to determine net vertical mass transports associated with subsynoptic and large mesoscale convective systems. Other static initialization techniques have largely failed to detect these vertical motions. A center of strong rising motion located over the position of the prefrontal squall line was produced by the variational analysis. Furthermore, the

variational analysis resolved subsynoptic scale vertical motions associated with the mid-tropospheric jet stream.

Thirdly, the effect of the tendency term subsidiary formulation was investigated with several subsidiary formulations. These results were largely unrealistic as determined by specified evaluation criteria. The subsidiary formulations were found to substantially influence the final balanced wind fields, particularly the error sensitive vertical velocity fields. The formulations that gave physically realistic vertical velocity fields also gave unrealistically large tendencies. The formulation that gave smaller tendencies also gave physically unrealistic vertical motion fields.

Since the tendency terms give the wind field trends for the first steps of a numerical integration, it can be asserted that the unrealistically large tendencies found from this study would lead to large spurious oscillations in the forecast. Further, as revealed by this study, these errors raise serious questions about the usefulness of this variational formulation as an initialization method. Clearly the role of the tendency term formulations and the origin of the large tendencies should be the subject of further investigation.

APPENDIX: Variational Objective Analysis

1. Introduction

A second part of the variational study, conducted independently of the model evaluation described in the body of this report, was devoted to the development of a variational objective analysis of the surface wind field. This phase looked forward to the eventual meshing of the dense surface observation network with the synoptic network in a consistent manner. Since the variational adjustment was known to be sensitive to the wind field, a method was sought that could reduce objective analysis error yet preserve the detail and magnitude of known wind field disturbances. The method also was designed for use with small data sets and is presented in this context.

As part of the METROpolitan Meteorological Experiment (METROMEX) the Illinois State Water Survey has acquired a large quantity of diverse meteorological data near St. Louis. Included are small mesoscale wind measurements from surface sites, rawinsondes, pibals, and aircraft. Ackerman (1977) has analyzed the wind field for the lowest 1.5 km over the meso-region surrounding St. Louis. The winds were obtained from single theodolite pilot-balloon measurements taken from 11 stations in an area within about 40 km from downtown St. Louis.

The relationship between precipitation and wind field perturbations over a large mesoscale network of surface stations has been investigated by Achtemeier and Morgan (1975). Twelve stations located in Illinois and parts of Indiana, Iowa and Missouri provided the wind data.

These studies have found that many important meteorological phenomena such as frontal zones, mesoscale convergence areas, and mesoscale wind maxima

often form along step-like mass and momentum boundaries between synoptic scale airmasses or form over known mesoscale perturbation sources such as the St. Louis urban area. The station densities are often insufficient to allow the complete discription of these disturbances; however, their divergence and vorticity fields can be detected and the locations, signs, and estimates of magnitudes relative to other disturbances can be roughly determined.

These divergences and vorticities were calculated once the wind components were objectively interpolated to points on a regular mesh. However, it was difficult to place much confidence in the results. When the weight function was chosen to be insensitive to small motion scales, the perturbations were smoothed toward larger scales and the spatial sensitivity of the analyses was lost. Further, the perturbations retained tended to be phase shifted toward the grid boundaries. If the weight function was chosen to be sensitive to small scales, spurious gradients between observations were generated and the suspected meteorological perturbations lost in these.

A method to eliminate spurious wind field gradients and yet retain the spatial resolution of the wind field perturbations is the subject of this paper. Two objective analysis methods with differing error characteristics are combined through a variational interface to produce a third analysis method that is designed to minimize independent analysis errors generated by the two original methods. To the extent that this is done, the analysis may be improved locally.

2. The Two-Analysis Method

Consider two objective interpolation methods. When applied to a data set, the first generates grid point values which, at an arbitrary point, the value F can be expressed by

$$F_1 = M + E_1 \ . \qquad (1)$$

The M is the "true" meteorological value. To it is added E_1, the sum of the errors of measurement (instrument calibration, exposure, observation, etc.) and of spatial modification by the analysis (smoothing, aliasing, phase shifting, amplification of short waves, etc.). The second objective analysis method generates at the same grid point the value

$$F_2 = M + E_2 \ . \qquad (2)$$

Here the value E_2 represents the errors characteristic of the second objective analysis method. To the extent that E, and E_2 are uncorrelated we may say that F_1, and F_2 are independent estimates of M at the grid point.

Given independent estimates of M, Sasaki's (1958) method of variational analysis can be used to produce a new estimate of M such that the adjustments from F_1 and F_2 are weighted according to the prescribed accuracies of the two techniques and are subject to some quantitative constraint between them. Moreover, the error characteristics should be such that the adjusted values will tend toward M. In the event that the errors are not independent ($E_1 = E_2$), there would be no adjustment.

Two very different wind field analysis methods are the successive-corrections (SC) method (Bergthorsson and Doos, 1955) and the line-integral (LI) method (Cecelski and Sapp, 1975). The SC method interpolates wind components according to some function of the relative distances of the observation sites from the grid points. The divergence and vorticity are computed directly from the grid point wind components by finite differences.

The LI method derives the wind field from fields of its gradients. Point values of vorticity and divergence are given at centroids of triangles defined

by neighboring wind observations through the application of line integrals around the triangles (Bellamy, 1949). Divergence and vorticity are presented at points on a regular mesh by the SC method. The fields of wind components are derived from the stream function and the velocity potential relaxed from the vorticity and divergence fields.

The LI method has the advantage of explicitly defining perturbations in the velocity field. One of its disadvantages is that the velocity fields constructed from the gradient fields are not constrained to return the observed velocities. Errors between observed and analyzed velocities can become quite large depending upon the inaccuracies in the line integral and the objective interpolation steps. Other disadvantages are that the magnitude of the divergence is a direct function of the station spacing, the wind changes between the triangle vertices are assumed to be linear, and the divergence and vorticity are sensitive to the shape of the triangle and its orientation with respect to wind direction.

By contrast, the SC method has the advantage of restoring the magnitudes of the original observations and the stability of developing the interpolated fields directly from the observations instead of from derivatives. Some disadvantages are that aliasing can generate spurious waves that increase the noise in the derivative fields and that the divergence and vorticity magnitudes are dependent upon the subjective choice of the weighting functions.

The error characteristics of the LI method should differ from the error characteristics of the SC method. The LI data points are located at the centroids of the triangles formed from surrounding wind observations. Thus any aliased short waves from the objective interpolation phase will not coincide with short waves built up by the SC method used directly on the wind field. The areas of triangles formed across data voids are larger than

the areas of triangles constructed within data dense areas. Since the divergence is inversely proportional to the area of the triangle, the LI method will tend to underestimate the magnitude of the divergence in data void areas. The SC method concentrates wind speed gradients in data void regions and the strength of these gradients increases with the variability of the wind speeds. Moreover, LI method triangle centroids concentrate within data void areas. Extremes calculated at any one centroid tend to be averaged out in the objective analysis phase.

Analyses by these two methods of the 1600 meter wind field of 26 July 1973 on a 70 x 75 km (5 km grid spacing) grid centered over St. Louis are shown in figure 1. The differing error characteristics are apparent because there is large variability in wind speeds from site to site. Further, missing stations have combined with balloon trajectories within a highly variable strong wind field to produce a non-uniform data distribution.

Figure la shows objective streamlines and isotachs of the wind field obtained by the SC method. We used an isotropic exponential weighting function similar to that used by Barnes (1964). The weight function constants were chosen so that the analysis would be sensitive to small scale wind features. The continuum response showed that about 50% of the minimum resolvable wavelength would be retained. However, Stephens and Polan (1971) show that, for discreet sampling, the continuum response will not give an adequate measure of the filtering for waves comparable to the shortest definable wave. Areas where aliasing is suspected are identified by A and B.

At A, the use of the isotropic weight function has led to the establishment of the fast wind speeds of station 1 into the interior of the field. Since there are no special "rules" governing mesoscale streamline-isotach patterns,

the "goodness," or acceptability, of the analysis may become a matter of subjectivity. An analyst experienced with quasi-non-divergent synoptic scale systems might prefer to reanalyze the field at A to make the isotachs more nearly parallel with the streamlines. One with experience with wave phenomena might prefer to amplify the feature.

The SC divergence is shown in figure lb. At A there has developed a divergence-convergence dipole, a pattern of strong divergence upwind from A and a pattern of strong convergence downwind from A. An area of strong convergence is found within the concentrated wind speed gradient at B. Thus the large amplitude centers shown in figure lb are largely caused by aliasing in the wind field analysis.

The vorticity field (fig. 1c) also shows large amplitude features of both signs. The -600×10^{-6} sec^{-1} center near point A may reasonably show the magnitude of the anticyclonic shear there. The 400×10^{-6} sec^{-1} cyclonic center to the upper left of point B has been introduced largely by the extrapolation of fast speeds from station 5 into the data void at B.

The LI method divergence and vorticity are found at the triangle centroids by

$$D = \frac{1}{A_T} \vec{V} \cdot \hat{n} ds \ , \tag{3}$$

$$\xi = \frac{1}{A_T} \vec{V} \cdot \hat{s} ds \ , \tag{4}$$

where n and s are, respectively, the unit vectors normal and tangent to the line increment ds, and A_T is the area of the triangle. The centroid divergence and vorticity was then interpolated to the grid points by the SC method. Then

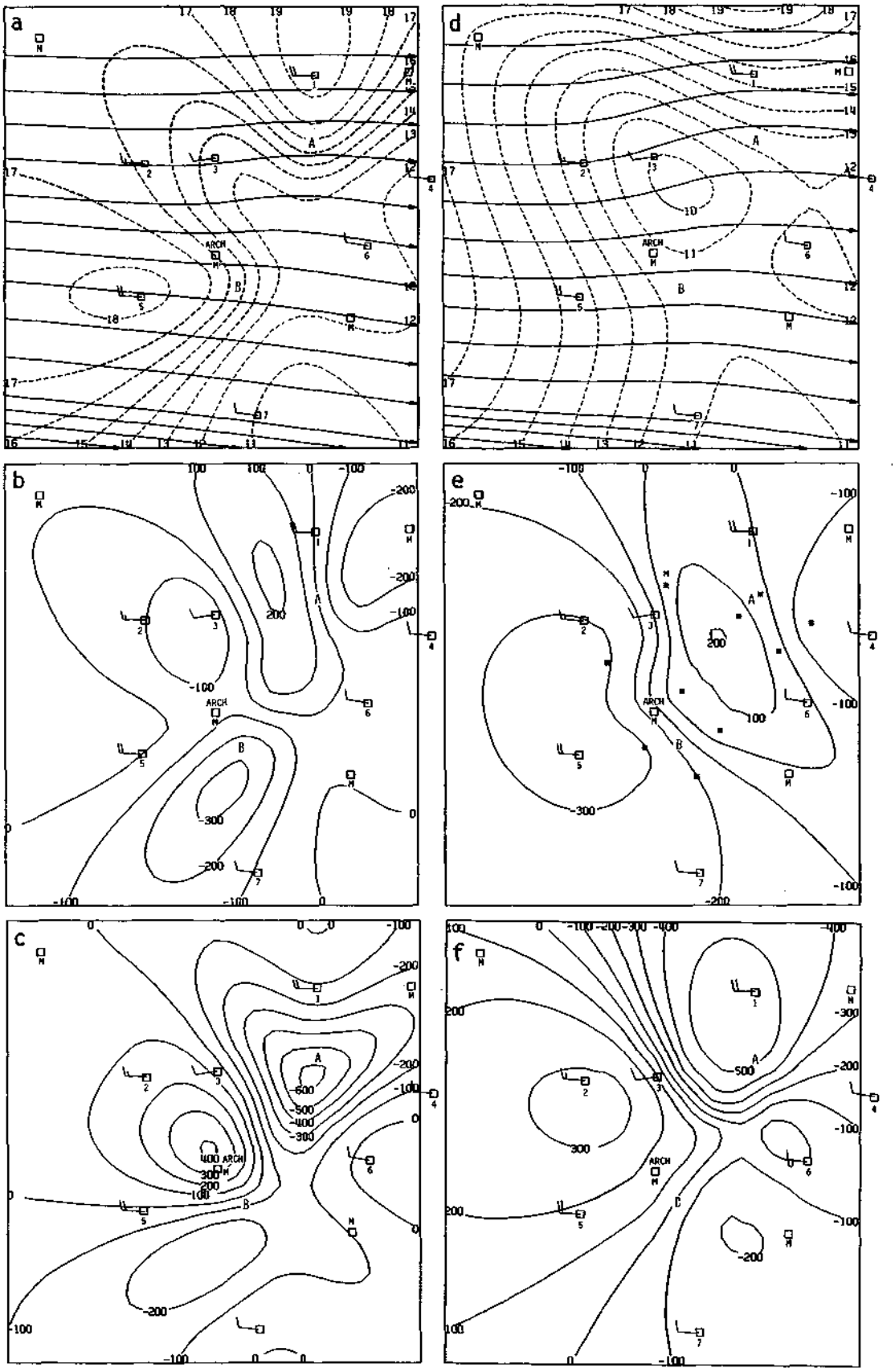

Figure 1. a) SC streamlines and isotachs, b) SC divergence, c) SC vorticity, d) LI streamlines and isotachs, e) LI divergence, and £) LI vorticity for the St. Louis area at 1600 m MSL, 1600 CST, 26 July 1973. Units are m sec^{-1} for isotachs and 10^{-6} sec^{-1} for divergence and vorticity.

the u and v wind components were found from the stream function and velocity potential as follows:

$$u = -\frac{\partial \Psi}{\partial y} + \frac{\partial \chi}{\partial x} \quad ,$$

$$v = \frac{\partial \Psi}{\partial x} + \frac{\partial \chi}{\partial y} \quad , \tag{5}$$

where

$$\nabla^2 \Psi = \zeta \quad ,$$

$$\nabla^2 \chi = D \quad . \tag{6}$$

The LI wind, divergence, and vorticity field are shown in figures 1d, 1e, and 1f. Since the LI winds are derived from the divergence and vorticity, the discussion of these three figures begins with figure le. The triangle centroids, denoted by the asterisks, cover only a small portion of the analysis grid. This was because several of the outlying wind observations were missing. The point M in figure le marks the centroid of a highly oblique triangle that gave questionable divergence and vorticity values. This data point was dropped from the LI analysis. All values outside of the network of triangle centroids arise from extrapolation.

Figure le shows that much of the divergence-convergence dipole near A has been retained in the LI analysis. The convergence center at B is not to be found. Instead, two convergence values are merged to produce a single (mostly extrapolated) -300×10^{-6} sec^{-1} center toward the left side of the grid. Figure 1f shows that the SC and LI vorticity fields are essentially identical with the exception of minor shifts in the positions of centers. The anticyclonic

center has been pushed above A and the cyclonic center has been weakened and shifted further to the upper left of B.

Streamlines and isotachs of the LI wind field constructed from (5) by using the SC wind field analysis for boundary conditions are shown in figure 1d. Comparison with the SC analysis in figure la reveals that the two analyses produced lighter winds in the central and lower right-hand parts of the grid. Both analyses placed stronger winds in the upper and left-hand portions of the grid. The intense wind gradients found at A and B in the SC analysis are not to be found in the LI analysis. The gradient reduction has been accomplished mostly by the smoothing of the high wind speeds at stations 1 and 5. The extent of reduction can be seen qualitatively by comparing the analyzed streamlines and isotachs at the station locations with the observed speeds and directions that have been superimposed.

Table 1 shows the departures between the analyzed and observed wind speeds. The SC method has restored wind speeds to within 1.0 m sec^{-1} of the observed values with a standard deviation of r = 0.2 m sec^{-1}. The standard deviation for the LI method is 2.3 m sec^{-1}. The LI method underestimated wind speeds by more than 4.0 m sec^{-1} at three sites. These are reductions of up to 26% of the observed values.

3. A Variational Method

In the last section, it was suggested that the error characteristics of the two methods were such that variationally adjusted values might tend toward the meteorological value M provided that a quantitative constraint between the two methods is found. The variables to be adjusted are u and v from the SC method and D and ζ from the LI method. These variables can be constrained through their divergence and vorticity relations,

$$D - \frac{\partial u}{\partial x} + \frac{\partial v}{\partial y} = 0 \ ,$$

$$\zeta - \frac{\partial v}{\partial x} - \frac{\partial u}{\partial y} = 0 \ . \tag{7}$$

The observations are meshed with the dynamic constraints (7) through Sasaki's (1958) variational formulation. The adjustment functional is

$$F = \int_x \int_y I \, dydx \ , \tag{8}$$

where I is given by

$$I = \Pi_1 (u-u^o)^2 + \Pi_1 (v-v^o)^2 + \Pi_2 (D-D^o)^2 + \Pi_3 (\zeta-\zeta^o)^2$$

$$\lambda_1 (D - \frac{\partial u}{\partial x} - \frac{\partial v}{\partial y}) + \lambda_2 (\zeta - \frac{\partial v}{\partial x} + \frac{\partial u}{\partial y}) \ . \tag{9}$$

The weights, Π_i, $i=1,3$ are Gauss' precision moduli (Whittaker and Robinson, 1926). The observed quantities u^o, v^o, D^o, ζ^o, enter in a least squares formulation so that departures from observed values will be minimized and receive precision modulus weights according to their relative analysis accuracies.

The objectively modified variables ($f_i = u, v, D, \zeta$) are determined by requiring the first variation on F to vanish. A necessary condition for the existence of a stationary set is that the functions are determined from the domain of admissible functions as solutions of the Euler-Lagrange equations,

$$\frac{-\partial}{\partial x_j} \left\{ \partial \left[\frac{\partial I}{\partial f_i / \partial x_j} \right] \right\} + \frac{\partial I}{\partial f_i} = 0 \ , \tag{10}$$

for each variable, i. Repeated indices, j, imply summation. Subjecting (9) to the operations specified by (10) yields the variations on the velocity components and line integral quantities.

$$2\Pi_1 \ (u-u^o) + \frac{\partial \lambda_1}{\partial x} - \frac{\partial \lambda_2}{\partial y} = 0 \ , \tag{11}$$

$$2\Pi_1 \ (v-v^o) + \frac{\partial \lambda_1}{\partial y} + \frac{\partial \lambda_2}{\partial x} = 0 \ , \tag{12}$$

$$2\Pi_2 \ (D-D^o) + \lambda_1 = 0 \ , \tag{13}$$

$$2\Pi_3 \ (\zeta-\zeta^o) + \lambda_2 = 0 \ . \tag{14}$$

Variation on the Lagrangian multipliers, λ_1, λ_2, restores the constraints (7). The Euler-Lagrange equations take the form of a 6-equation closed set of simple algebraic or linear partial differential equations. Variables may be easily eliminated to reduce the number of equations. The constraints (7) may be substituted into (13) and (14), derivatives of the Lagrangian multipliers taken, and these results substituted into (11) and (12). It is convenient to set $II_3 = II_2$ and to define the ratio $II = II_1/II_2$. Solving (11) and (12) for the velocity components yields two convergent Helmholtz equations,

$$\nabla^2 u - \Pi u + (\Pi u^o - \frac{\partial D^o}{\partial x} + \frac{\partial \zeta^o}{\partial y}) = 0 \ , \tag{15}$$

$$\nabla^2 v - \Pi v + (\Pi v^o - \frac{\partial D^o}{\partial y} - \frac{\partial \zeta^o}{\partial x}) = 0 \ , \tag{16}$$

which are solved for the adjusted velocity components by the method of successive over-relaxation. Boundary conditions are satisfied by the observed velocity components.

The precision modulus ratio will vary spatially according to

$$\Pi = \Pi_1/\Pi_2 \; g(x,y) = \frac{\sigma_D^2}{\sigma_{u'}^2} \; g(x,y) \; . \tag{17}$$

The divergence error variance is related to the wind speed error variance by

$$\sigma_D^2 = \frac{2\sigma_u^2}{(\Delta s)^2} \tag{18}$$

(Achtemeier, 1972). The As is the average station separation.

The space function g(x,y) is included to increase the relative weight placed on the SC method in those grid areas where point values must be found by extrapolation. Of course, extrapolation is seldom desirable, but where necessary, it is prudent to extrapolate values of a variable rather than values of its derivatives.

The value taken by g(x,y) at any grid point varies from 1.0-10.0 depending upon the distance R between the grid point and the triangle centroids. A non-normalized distance dependent exponential weight assigned to each grid point is given by

$$W = \sum_{i=1}^{NOC} e^{-k \; R^2_i} \tag{19}$$

where NOC is the number of triangle centroids and the shape factor k is chosen so that the weight decreases to 0.1 at a distance of approximately 3 grid points from the nearest centroid. Then the space function is given by

$$g(x,y) = \begin{cases} 10.0 & (W \leq 0.1) \\ 1/W & (0.1 < W < 1.0) \\ 1.0 & (W \geq 1.0) \end{cases} , \qquad (20)$$

The space function used for this variational objective analysis is presented in figure 2.

The precision modulus ratios were incorporated into (15) and (16) which were solved for the variationally adjusted u and v wind components for the case presented in figure 1. The most notable differences between the variational wind field (figure 3a) and the SC wind field (figure la) is the relaxation of the strong gradients at A and B. This has been accomplished by a 2.0 m sec^{-1} reduction of the wind speed at station 1 and a 1.0 m sec^{-1} reduction at station 5. The departures from the observed wind speeds at the station locations are summarized in Table 1. The variational method standard deviation was only 0.4 m sec^{-1}.

Variational wind speed departures from the SC method wind speeds are shown in figure 3b for the u-component. Most of the significant changes were brought within the data void areas at A and B. These moderate adjustments are sufficient to reduce the large amplitude aliased divergence centers found in figure lb and replace them with well defined but less variable mesoscale perturbation patterns (figure 3c). The variational method reduced the convergence near B from -315 x 10^{-6} sec^{-1} to -205 x 10^{-6} sec^{-1} but left the convergence lobe to the upper left of B unchanged at -172 x 10^{-6} sec^{-1}. The divergence of 228 x 10^{-6} sec^{-1} to the left A was reduced to 107 x 10^{-6} sec^{-1} whereas the extension of divergence to the lower left of A was increased slightly from 140 x 10^{-6} sec^{-1} to 166 x 10^{-6} sec^{-1}.

The reduction of the anticyclonic vorticity center at A to -464 x 10^{-6} sec^{-1} (figure d) from the SC value of -604 x 10^{-6} sec^{-1} is commensurate with the

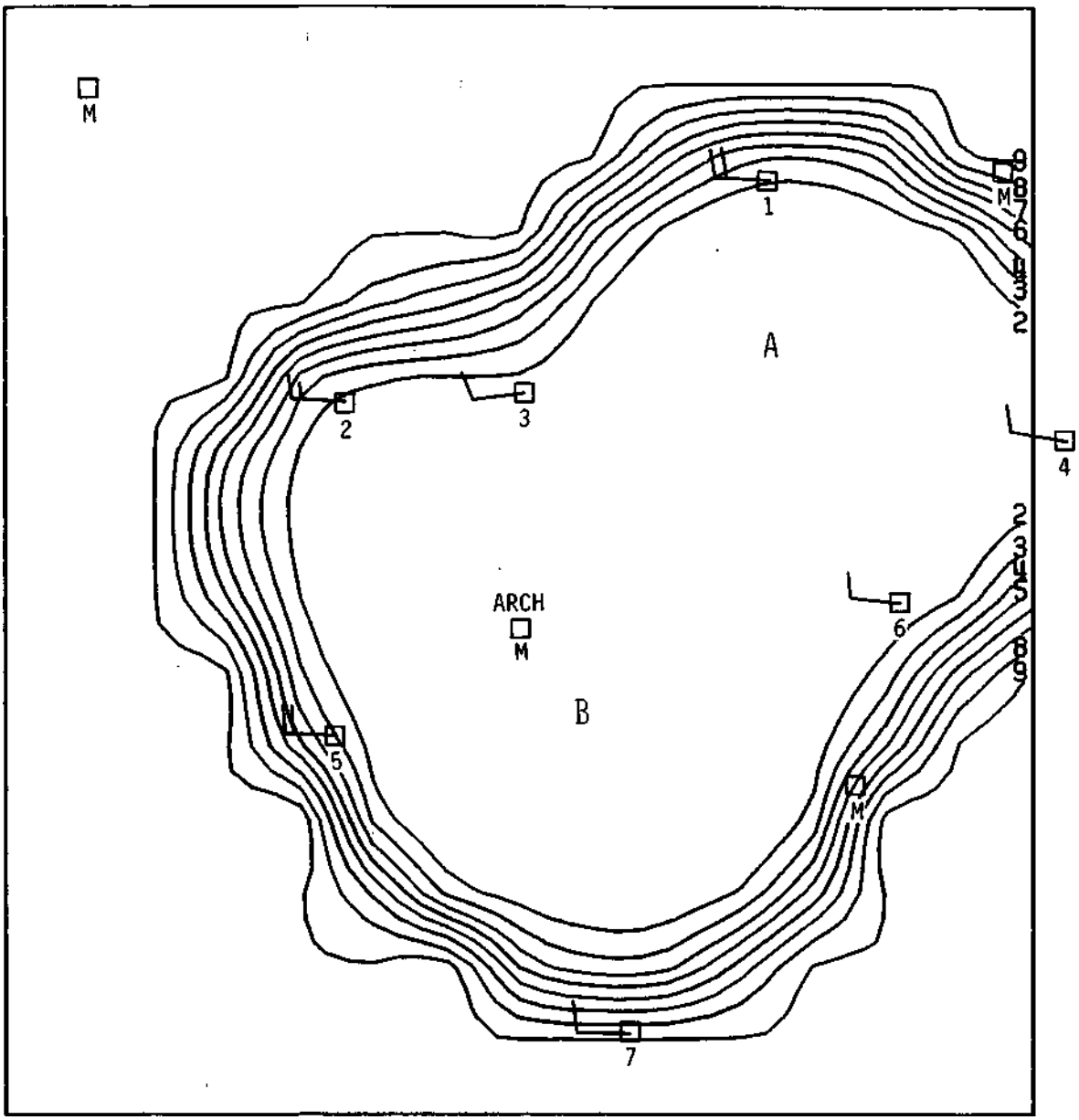

Figure 2. Distribution of the space function g(x,y) that weighted the SC and LI methods in the variational analysis.

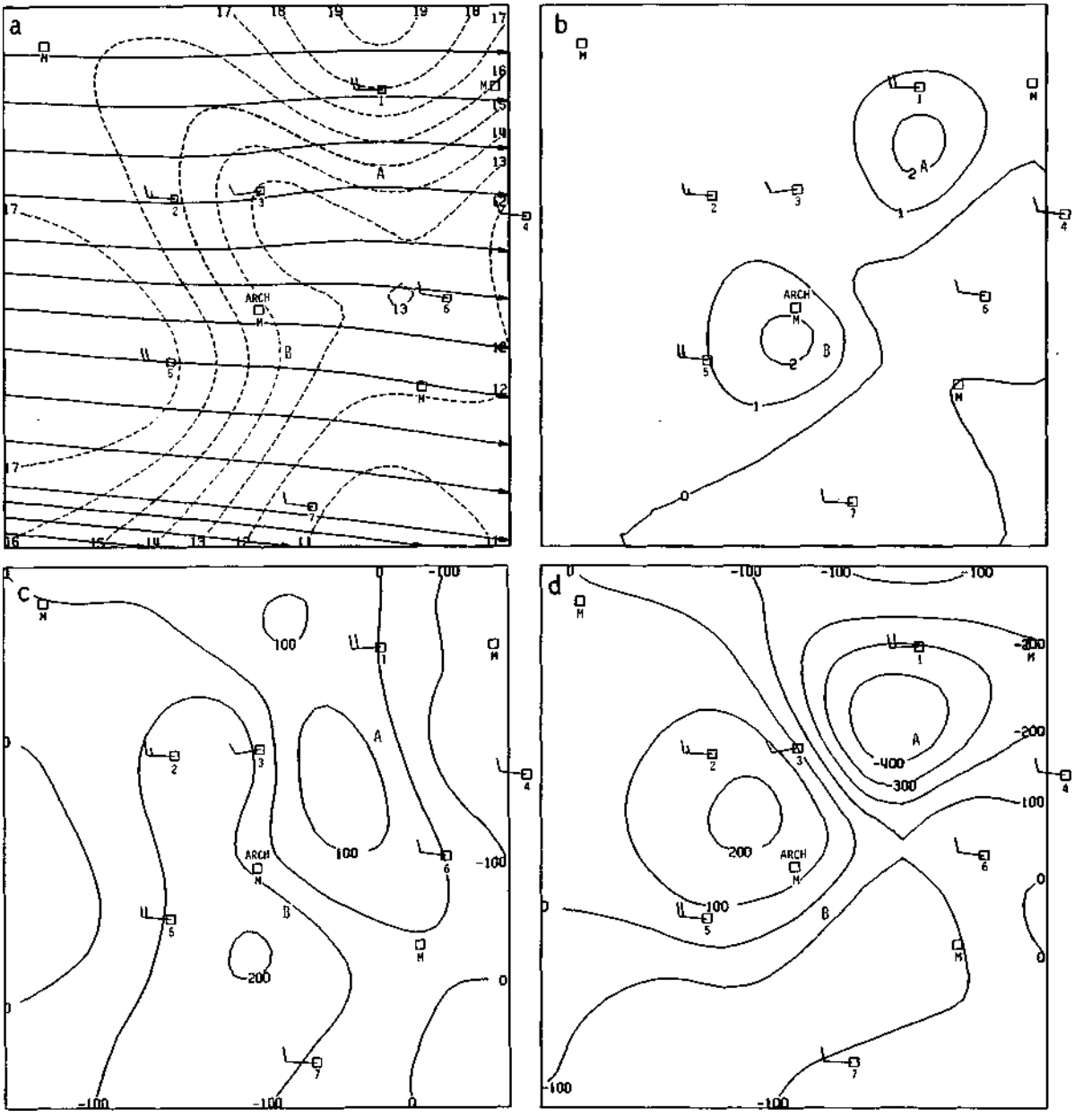

Figure 3. The variational analysis: a) streamlines and isotachs, b) SC minus variational u-component, c) divergence, and d) vorticity for the case of figure 1. Units are m sec^{-1} for wind speed and 10^{-6} sec^{-1} for divergence and vorticity.

Table 1. Differences between calculated and observed wind speeds at seven observations sites for the SC, LI, and variational objective analysis methods.

	V obs	V anal - V obs		
Station	m sec^{-1}	SC	LI	Variational
1	19.8	-0.5	-4.3	-2.0
2	16.6	-0.8	-4.3	-1.3
3	12.8	0.9	-2.5	0.1
4	11.3	0.5	0.5	0.7
5	18.3	0.1	-4.1	-1.0
6	12.5	-0.2	-0.5	0.0
7	10.8	0.3	0.3	0.4
std		0.2	2.3	0.4

reductlon of the wind speed gradient at A. The elimination of the outward protrusion of wind speed gradients at B has reduced the cyclonic center from 409×10^{-6} sec^{-1} to 223×10^{-6} sec^{-1}.

4. Concluding Remarks

In the foregoing analysis two objective interpolation methods with differing error characteristics have been variationally meshed with the aim to produce a hybrid objective analysis that eliminates undesirable features of any one method. The method when applied to a case with highly variable wind speeds and a non uniform data distribution gives good estimates of the wind speeds at the locations of the observations and retains wind field perturbations without smoothing the entire field. Some divergence patterns were retained without significant modification and some patterns were severely reduced in magnitude. These reductions occurred in data void areas where the SC method was known to suffer from aliasing and the LI method was known to underestimate the divergences.

It cannot be concluded that the unadjusted patterns were the meteorological signal because the error characteristics of the two methods were not fully known there. The variational analyses did reduce areas of known aliasing while it retained the remaining patterns with small adjustments from the observed fields. Applications of the method may lie in wind field analyses with small data sets and/or with known mesoscale perturbations that occur as step-like transitions between larger scale airmasses.

12. References

Achtemeier, G. L., 1972: Variational initialization of atmospheric fields—a quasi-geostrophic diagnostic model. Ph.D. Dissertation, Tallahassee, Florida State University, 211 pp.

_____, 1975: On the initialization problem - A variational adjustment method. MWR, 103, 1089-1103.

Ackerman, B., 1977: Mesoscale wind fields over St. Louis. Preprints 6th Conf. Planned and Inadv. Wea. Mod., AMS, Champaign, IL, 5-8.

Barnes, S. L., 1964: A technique for maximizing details in numerical weather map analysis. J. Appl. Meteor., 3, 396-409.

Bellamy, J. C., 1949: Objective calculations of divergence, vertical velocity and vorticity. Bull. Amer. Meteor. Soc, 30, 45-50.

Bergthorsson, P., and B. R. Dob's, 1955: Numerical weather map analysis. Tellus, 7, 329-340.

Charney, J. G., 1948: On the scale of atmospheric motion. Geofys. Publikas., 17, 1-17.

_____, 1962: Integration of the primitive and balance equations. Proc. Intern. Symp. Numerical Weather Prediction, Tokyo, Meteor. Soc., Japan, 131-152.

Cecelski, B., and L. Sapp, 1975: Objective wind field analysis using line integrals. Mon. Wea. Rev., 103, 89-100.

Dey, C., and R. McPherson, 1977: An experiment in global divergent initialization. Mon. Wea. Rev., 105, 1372-1383.

Endlich, R. M., and G. S. McLean, 1965: Jet-stream structure over the central United States determined from aircraft observations, J. Appl. Meteor., 4, 83-90.

Gerrity, J. F., Jr., 1977: The LFM Model - 1976: A Documentation. NOAA Tech. Memo. NWS NMC 60. 68 pp.

Glahn, H. R., and D. A. Lowry, 1972: The use of model output statistics (MOS) in objective weather forecasting. J. Appl. Meteor., 11, 1203-1211.

Haltiner, G. J., 1968: Numerical weather prediction. NWRF, 30-0768-142, Norfolk, Virginia, Naval Air Station, 88 pp.

Hayden, C. M., 1973: Experiments in the four-dimensional asimilation of Numbus 4 SIRS data. J. Appl. Meteor. 12, 425-436.

Hoke, J., and R. A. Anthes, 1976: The initialization of numerical models by a dynamic-initialization technique. Mon. Wea. Rev., 104, 1551-1556.

Houghton, D., D. Baumhefner, and W. Washington, 1971: On global initialization of the primitive equations: Part II. The divergent component of the horizontal wind. J. Appl. Meteor., 10, 626-634.

Hovermale, J. B., 1962: A comparison of data accuracy in the troposphere and in the stratosphere. Dept. of Meteorology, Penn. State Univ., Contract AF 19-(604)-6261, Report No. 2.

Kreitzberg, C. W., 1976: Interactive applications of satellite observations and mesoscale numerical models. Bull. Amer. Meteor. Soc, 57, 679-685.

Krishnamurti, T. N., 1968: A study of a developing wave cyclone. MWR, 96, 208-217.

Lorenz, E., 1969: Atmospheric predictability as revealed by naturally occurring analogues. J. Atmos. Sci., 26, 663-646.

Miyakoda, K., and R. M. Moyer, 1968: A method of initialization for dynamical weather forecasting. Tellus, 20, 115-130.

Nitta, T., 1969: Initialization and analysis for the primitive equation model. Proceeding of the WMO/IUGG Symposium on numerical Weather Prediction, Tokyo, Japan, Nov. 26-Dec. 4, 1968. pp. VI. 11-20; Japan Meteorological Agency, Tokyo, 1969.

Nitta, T., and J. B. Hovermale, 1969: A technique of objective analysis and initialization for the primitive forecast equations. MWR, 97, 652-658.

O'Brien, J. J., 1970: Alternative solutions to the classical vertical velocity problem. J. Appl. Meteor., 9, 197-203.

Ogura, Y., 1962: Dynamic Meteorology. (Unpublished manuscript).

Otto-Bliesner, B., D. P. Baumhefner, T. W. Schlatter, and R. Bleck, 1977: A comparison of several meteorological analysis schemes over a data-rich region. Mon. Wea. Rev., 105, 1083-1091.

Phillips, N. A., 1957: A coordinate system having some special advantages for numerical forecasting. J. Meteor., 14, 184-195.

_____, 1963: Geostrophic motion. Rev. Geophys., 1, 123-176.

Reiter, E., 1961: Jet Stream Meteorology. Univ. Chi. Press, 515 pp.

Riehl, H. , 1952: Forecasting in middle latitudes. Meteor. Monog., 5, Boston, 80 pp.

Sasaki, Y., 1958: An objective analysis based on the variational method. J. Meteor. Soc, Japan, 36, 77-88.

_____, 1970: Some basic formalisms in numerical variational analysis. MWR, 98, 875-883.

Stephens, J. J., 1965: A Variational Approach to Numerical Weather Analysis and Prediction. Ph.D. Dissertation, University of Texas, Austin.

_____, and A. L. Polan, 1971: Spectral modification by objective analysis. Mon. Wea. Rev., 99, 374-378.

Stuart, D. W., 1971: Specifications of Meso-scale Weather from Large-scale Dynamical Calculations. Final Rept. No. 71-4, Florida State University, 75 pp.

_____, and T. N. Krisbnamurti, 1970: Specifications of Meso-scale Weather from Large-scale Dynamical Calculations, Final Rept. 70-5, Florida State University, 79 pp.

Temperton, C., 1976: Dynamic initialization for barotropic and multi-level models. Quart. J. R. Met. Soc, 102, 297-311.

Vuorela, L. A., 1957: A study of vertical velocity distribution in some jet stream cases over Western Europe. Geophysica, 6, 68-90.

Warner, T. T., 1976: The initial growth of data-related errors in mesoscale numerical weather prediction models. 3rd Symposium on Atmos. Turb. Diffusion and Air Quality, AMS, Raleigh, NC, 74-81.

Washington, W., 1964: A note on the adjustment towards geostrophic equilibrium in a simple fluid system. Tellus, 16, 530-534.

Whittaker, E., and G. Robinson, 1926: The Calculus of Observations (2nd Edition) London, Blackie and Son, Ltd., p. 176.